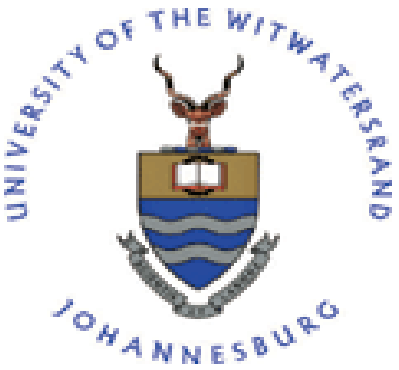

COMPARATIVE ANALYSIS OF SHOT AND LASER SHOCK PEENING IN 7075 ALUMINIUM ALLOY

Process Mechanics and Influence of Process Parameters

Kenosi Mokolobate

(Student number: 0412124J)

School of Mechanical Industrial and Aeronautical Engineering

University of the Witwatersrand

Johannesburg, South Africa.

Supervisors: Prof. Claudia Polese

A research report **proposal** submitted to the Faculty of Engineering and the Built Environment, University of the Witwatersrand, in fulfilment of the requirements for the degree of Masters in Engineering.

Date 2019-03-20

Declaration

I declare that this dissertation is my own, unaided work, except where otherwise acknowledged. It is being submitted for the degree of Master of Science in Engineering in the University of the Witwatersrand, Johannesburg. It has not been submitted before for any degree or examination at any other university.

Signed this 27th day of March 2019

KN Mokolobate

Acknowledgements

I would like to thank the following individuals for their invaluable support during the project:

- My supervisor, Prof. Claudia Polese of the University of the Witwatersrand, for her patience, dedication, guidance and wisdom at every stage of the project.
- Dr Daniel Glaser of the CSIR for his guidance and assistance with me the use of the laser.
- I would like to thank Ryan Farnham from SAAT for assisting me with the use of the shot peening machine at the SAAT and doing so free of charge.
- Prof. Joao Nobre of the University of the Witwatersrand for teaching me about incremental hole drilling.
- Mr Sean van Staden for teaching me all about incremental hole drilling.
- Dr Andrew Venter and Dr Deon Marais of NECSA for their assistance and hard work in performing Laboratory X-Ray Diffraction measurements.
- Mr Shadrack Moqabulane of the University of the Witwatersrand for access to and assistance with material preparation laboratories.
- Mr Ndivhuwo Brayner Nelwalani of the University of the Witwatersrand for operating the Scanning Electron Microscope.
- My wife Duduzile Emma Mokolobate and our lovely children for their support throughout this project.
- My other colleagues at the University of Witwatersrand, Mr Nicholas Stiekema, Mr Constantin Shulte-Brader, for the support and help during this project.

I would like to acknowledge the following institutions for their vital support:

- The South African Centre for Scientific and Industrial Research National Laser Centres (CSIR NLC) Rental Pool Program (RPP), funded by the Department of Science and Technology (DST).
- In addition, this work is based on the research supported in part by the National Research Foundation (NRF) of South Africa Incentive Funding for Rated Researchers (IFRR) for Prof. Claudia Polese (Grant Number: 109200).

Opinions, findings and conclusions or recommendations expressed in this work are those of the author and are not necessarily to be attributed to the to the NRF.

COMPARATIVE ANALYSIS OF SHOT AND LASER SHOCK PEENING IN AA7075 ALUMINIUM ALLOY

Table of Contents

List of Tables

Table Page

List of Figures

Figure Page

Abstract

Shot Peening (SP) is a widely used technique to improve the mechanical properties of metallic surfaces in the industry and is one of the most effective techniques of inducing residual compressive stresses into metal surfaces to enhance their fatigue performance. The SP processing is inexpensive. It has been used in different applications; however, the process has its limitations. The laser shock peening (LSP) process has been successfully used to introduce residual compressive stresses in metals. This process is an alternative surface processing technology to the SP. It has been used for medical implants, in nuclear power reactors, aircraft panel forming, and treatment of aircraft engine components. Whilst the SP and the LSP create residual stresses of similar magnitude, the LSP was found to induce residual stresses with greater depth into the metallic material. These residual stresses reached up to five times deeper and produced a uniform peening effect across the surface of the material compared to the SP making the LSP more appealing to the aviation industry.

This research was limited to residual stress, surface roughness, microstructure, and microhardness measurements on the SP and LSP-treated AA7075-T651 conventional aeronautical aluminium alloy. The incremental hole drilling technique was mostly used to analyse compressive residual stresses in the treated material and complimentary measurements on the surface were performed using the X-Ray Diffraction method.

It was found that the SP and the LSP processes produced compressive residual stresses (RS) in AA7075-T651. Compressive RS were found to be deeper in the LSP compared to those produced through SP. The surface roughness was higher in SP-treated samples compared to the LSP-treated samples. There were no appreciable changes to the microstructure of peened samples in both

conditions. Both the SP and the LSP resulted in hardened regions within the surface layer of the AA7075-T651; with LSP generating higher microhardness in comparison to SP.

CHAPTER ONE

1. Introduction

Shot Peening (SP) method is used to improve the mechanical properties of metallic surfaces in the aerospace industry. It was considered one of the most reliable techniques of inducing compressive residual stresses (RS) into the surface of the metallic material to improve their fatigue performance [1]. Shot Peening processing of material is inexpensive. The technology has been used in different applications, however, it has limitations [1]. Firstly, the process was semi-quantitative. An indication of the SP intensity can only be approximated by using the Almen type gauge. The Almen gauge correlates the surface curvature due to the peening process to the resultant intensity. Secondly, the SP method is unreliable, as it produces non-uniform SP intensity across the peened component [1]. Lastly, the compressive RS were not deep enough, usually not more than 0.25 mm in aluminium alloy and less in harder metallic material [2].

Shot Peening processing produced roughened metallic surfaces. This roughened surface finish was more pronounced in soft metals like aluminium [1]. These SP-treated metallic materials could not be used in wear applications unless the roughened layer was firstly removed. Removing the roughened surface inadvertently reduced the compressive layers; making the SP process less effective.

The laser shock peening (LSP) is considered as a substitute technique for surface processing of the metallic material. The technology has been successfully used to induce compressive RS into metals. Applications include aircraft panel forming, aircraft engine components, medical implants, and in nuclear power [3]. The LSP processing technique induces deeper compressive RS into metal surfaces of 4-5 times in depth [3]. The induced compressive RS had higher intensity and were uniform across the metallic surface. This resulted in a better surface finish when compared to SP.

CHAPTER TWO

2. Literature Review

2.1. Introduction

It has long been recognised that inducing residual compressive stresses using laser shock peening (LSP) or Shot Peening (SP) processing in metal components enhanced *inter alia* fatigue strength of the metallic material [4]. Several engineering components have been surface-treated with the LSP or the SP [5]. This resulted in the fatigue strength enhancement of the metallic material with associated surface hardening. Other mechanical surface treatment technique includes Cold-Rolling. This technique has also been used in industrial applications for enhancing mechanical properties of the metallic material; however, it has limitations. For example, cold-rolling could only be used for parts that were geometrically regular, thus limiting benefits derived from this process.

2.2. Shot Peening

Shot Peening is a cold-working surface treatment process [6]. It uses a high-speed stream of hard particles that are bombarded at the material from a uniform medium shown in Figure 2.1.

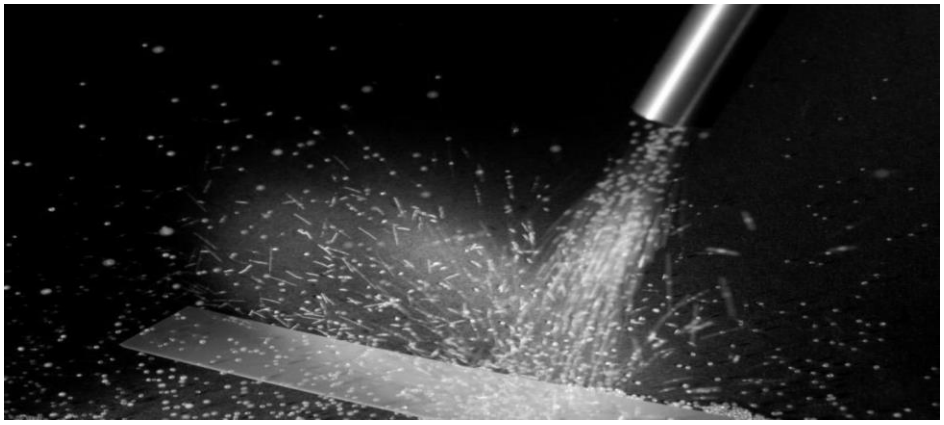

Figure 2-1. Shot Peening specimen **[7].**

The impact of the balls causes the metallic material to plastically deform on the surface. It also creates small indentations which produce roughened surfaces. A pictorial representation of shot peening and its effect are shown in Figure 2.2.

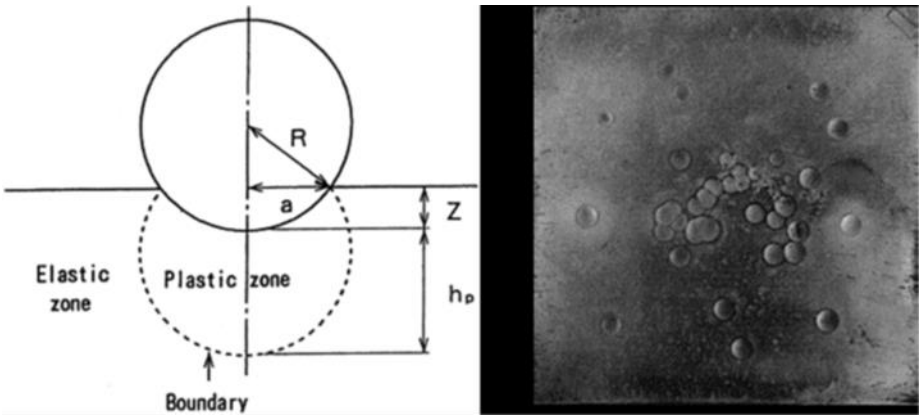

***Figure 2-2. Shot Peening mechanism (a) Elastic-plastic boundary (b) Indentations* [8].**

The process causes surface modifications which result in (a) near-surface strain hardening; (b) roughening of the surface and (c) the development of a characteristic profile of residual stresses [9-12]. The peak value of the compressive stress is reached at some depth below the surface. This peak value can reach 60% ultimate strength of the material [13, 14].

In metallic material, the resulting modifications caused a noticeable improvement in fatigue properties, and thus enhanced the service life of engineering components [15]. The SP technique was found to produce higher levels of compressive RS in metallic material that was under a pre-stress [13, 16, 17].

2.2.1. Shot Peening Technology

The SP technique uses an Almen strip to duplicate peening intensity that has already been established on the specified part. These strips have standard dimensions and are manufactured from steel of the carefully controlled structure and heat treated to ensure repeatability.

When the Almen strip is SP-treated, compressive RS induced causes the strip to bend or "arc" towards the peened side thereby producing an "arc height" [18]. The highest compressive RS are signified by the highest deflection point of the SP-treated sample. To measure the "arc height" an Almen gauge is used across the length of the Almen strip. A depiction of the test setup and the "arc height" is shown in Figure 2.3.

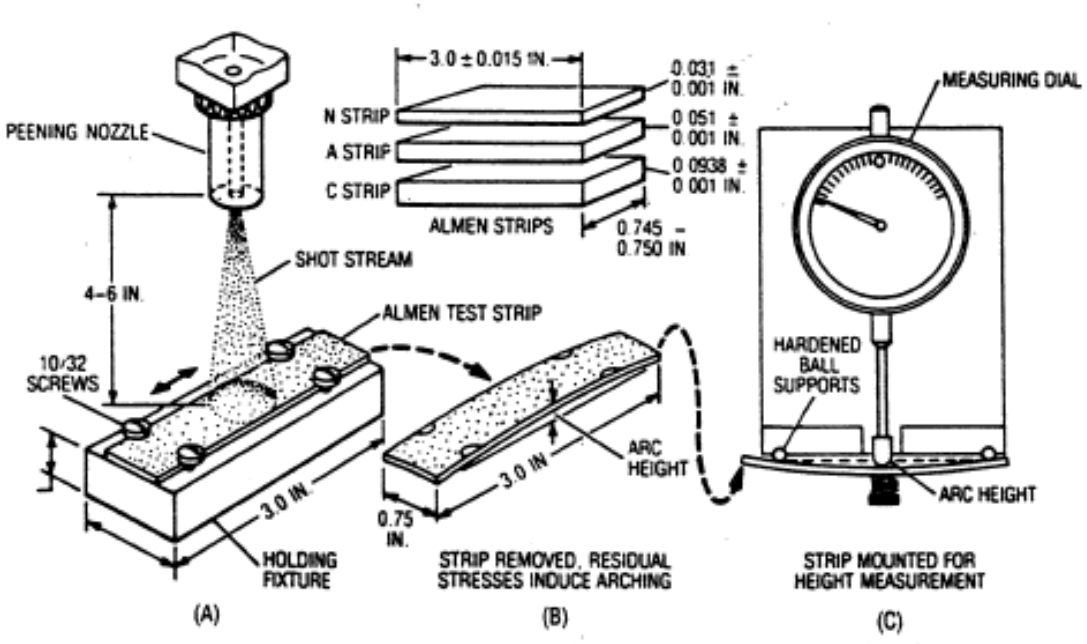

Figure 2-3. Measuring accessories for Shot Peening **[19].**

The Almen "arc height" is measured using predetermined points on the surface of the treated sample. This is done to approximate the radius of the curvature of the test specimen, and thus the results of the peening action. The arc height usually occurs in the middle of the SP-treated sample.

2.2.2. Saturation Curves for Shot Peening

This curvature/ or the "arc height" produced by the SP technique is a function of the shot hardness, the mass of shot, shot velocity, exposure time to the shot stream and angle of impingement. It represents the SP intensity and is a measure of the deflection of the test strip.

Several Almen test types are used to measure the "arc height", and thus the SP intensity of treated material in industry. There are different types of Almen strips used in industry, N, A or C type. The amount of peening intensity required determines the suitable Almen type. The Almen 'N' scale is used for the test piece of type N for measurement of low-intensity SP usually below 6A. Almen 'A' scale is used for the Almen test of type A, a measure of medium intensity of the SP usually between 6A to 24A. Lastly, the Almen 'C' scale is used for the test pieces of type C to measure a high intensity of the SP above 24A.

To measure the "arc height" an Almen test strip is usually peened on one side only. However, this Almen "arc height" is not properly termed intensity unless saturation is achieved. Saturation is a function of the energy of the shot stream. It creates the actual intensity for the specific SP machine set. The intensity curve is then developed from the SP treatment results and is used to measure the Almen saturation (Figure 2.4).

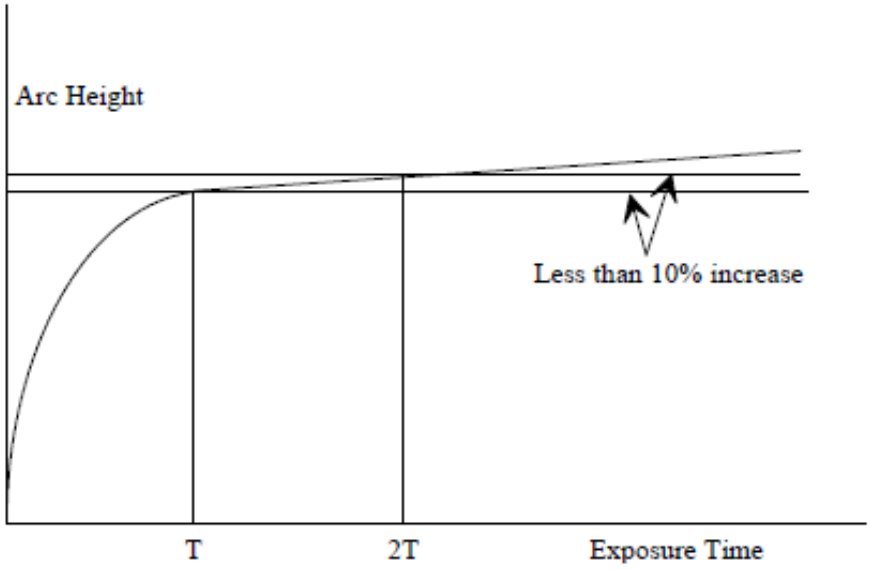

Figure 2-4. Shot Peening saturation curve theory **[19].**

Saturation is defined as the earliest point on the curve where doubling the exposure time produced no more than ten percent (10%) increase in “arc height”. In Figure 2.4, this point is reached at exposure time T.

2.2.3. Coverage for Shot Peening

In SP technique, coverage refers to the population of dimples on the surface of the SP-treated material. It is defined as a ratio of the indented surface to the total surface after SP-treatment and is expressed as coverage percentage [20]. For example, 100% coverage is achieved when the original surface of the treated specimen is destroyed entirely by overlapping peening dimples. For a 150% coverage, the specimen would have to be exposed to 1.5 times the time needed to achieve 100% coverage. The saturation and coverage of the SP-treated Almen strip are different. Neither will both necessarily occur at the same exposure time on peened parts.

2.3. Laser Shock Peening

The LSP technique was invented in the 1960s [21]. It used both continuous and pulsed lasers to produce shock waves. When the material is LSP-treated the exposed surface plastically deforms. It is this effect that has resulted in extensive studies [22-25].

The technique was initially used in fastener holes [26]. Several investigations have since been conducted on different metallic materials to determine the laser material interactions [21, 27, 28]. More systematic LSP studies have been carried out in France, China, and Japan [29, 30]. Its application and benefits have been shown in different engineering material such as steel [31-33], and aluminium alloys [34-37].

The LSP technique has been used for inducing residual compressive stresses in metallic material. It uses laser technology to generate short duration pulse, typically about 8-14 ns [34-37]. High

amplitude pressure pulse in the range of GW/cm^2 is applied on the target specimen surface to be treated. A thin-film of water, flowing on the surface of the sample, is used to contain the laser. This ensures that wave pressures are generated towards the depth of the specimen resulting in ionization of the target surface [38]. Shock waves that are produced are higher than the elastic yield strength of the metal causing the target surface to deform plastically at the edges [39]. As the material recovers, residual compressive stresses are produced at treated areas of the sample. This process is depicted in Figure 2.5.

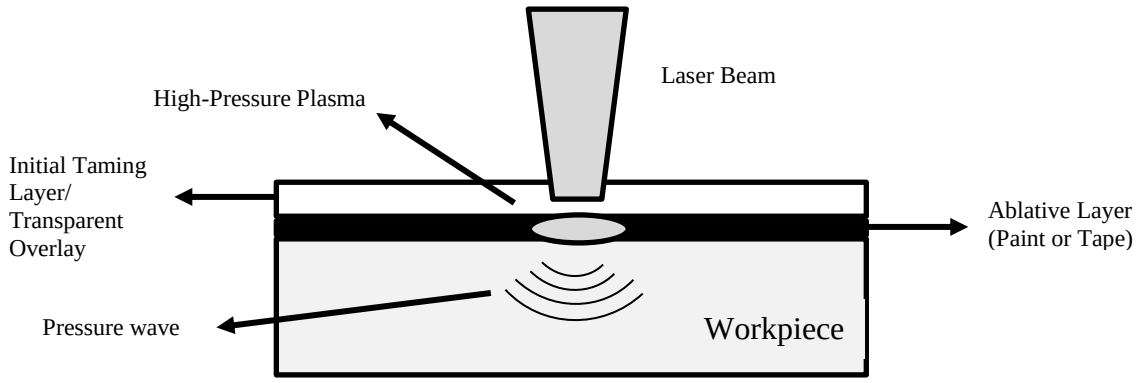

Figure 2-5. The Mechanism of Laser Shock Peening **[40].**

The LSP produces increased fatigue strength of the metallic material as a result induced compressive RS [41]. This results in the formation of other phases or twins, high-density arrays of dislocations increased yield strength and, strain hardness of the metallic material [42].

The distribution of RS produced across the laser treated surface is compressive and mostly even, it becomes tensile at the edges in thin metallic material [14]. However, large LSP-treated areas do not display tensile residual stresses at the edges [14]. In the industry, the LSP processing is seen as a replacement of the conventional SP treatment. This is owing to its residual compressive stresses which are produced in the metallic surface of the material; these reach about 10-times deeper into the material [43] and higher intensities across the metallic material [40].

Unlike, the SP technique which was difficult to apply to surfaces where access was limited, the LSP offered advantages and benefits in these hard to reach surfaces [44, 45].

2.3.1. Laser Technology

Laser emission technology originated from the theory of stimulated emission in 1917 [46]. It was only in the late 1940s and 50s that extensive work to realise a practical device based on the principle of stimulated emission was conducted. Towers and Schawlow [n.d.] constructed such a device using optical light. Two Soviet physicists also proposed related ideas independent of each other [46]. In 1960, the first laser was constructed by Theodore H. Maiman [46].

Laser technology was further enhanced by using an intense laser pulse to produce significant pressure on the surface of an irradiated target [46]. This was done by using the material that created a momentum impulse/ or pressure on the surface of the metallic material due to rapid evaporation, and thus creating laser shock peening.

2.3.2. Laser Operation

LASER amplifiers electromagnetic radiation of a specific frequency through a process of stimulated emission thereby forming a coherent light [47]. The light producing laser is different in character to that produced from an ordinary light bulb. The emitted radiation from the laser is made up of a beam of photons, with the same polarization and all in phase. A diagrammatic illustration of the laser process is given in Figure 2.6.

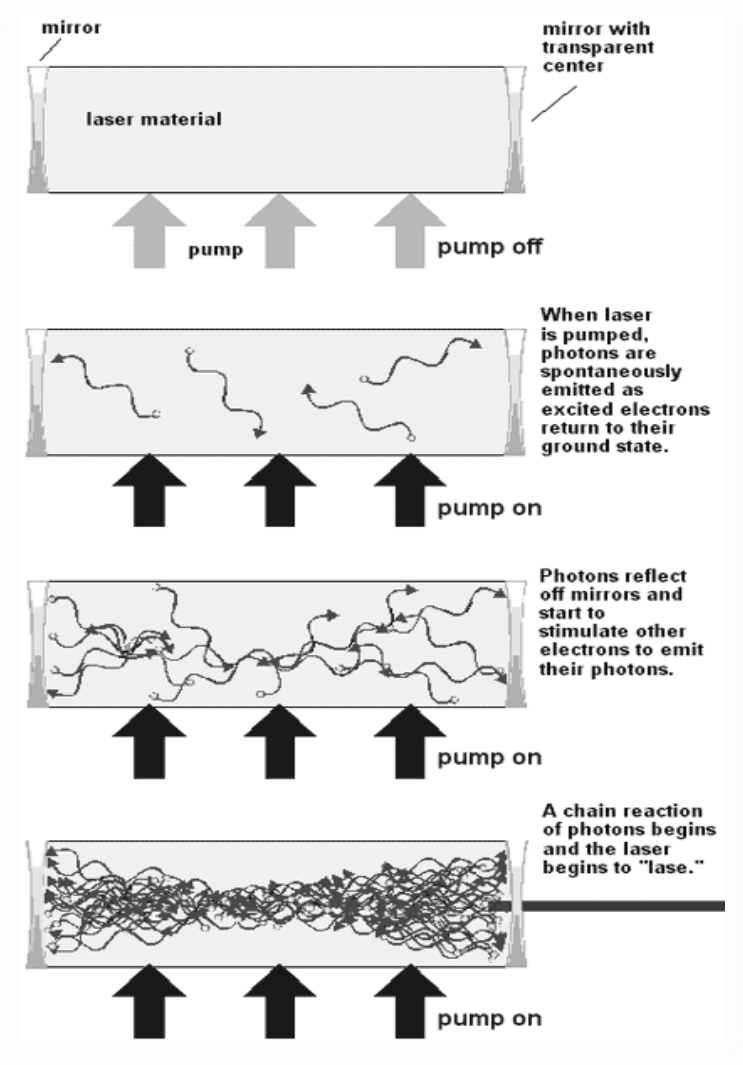

Figure 2-6. Laser Process **[47].**

In Figure 2.6, the laser is contained within a chamber wherein atoms of a medium energy are excited [47]. This brings these electrons into higher orbits with higher energy states. The electrons revert back to their lower energy state, thereby emitting extra energy, referred to as photons, in the process [47]. When these photons collide with other atoms, the photons, in turn, excite these atoms' electrons to jump down as well. These, in turn, emit further photons of the same frequency as the first [47]. This effect replicates further to produce more photons.

Mirrors are used at the end of the chamber to cause the beam to reflect back and forth. If a sufficient stream of atoms is maintained by an external source, coherent photons develop [47]. A partially transparent mirror allows the laser beam to exit from the end of the chamber thus forming the laser.

2.3.3. Conventional Laser Shock Peening

The conventional LSP with coating uses a Nd: glass laser. The laser has a near-infrared wavelength of $\lambda = 1.064\mu m$ and uses a protective coating or a sacrificial overlay on the material [22, 38]. This protective coating increases the efficiency of the laser absorption of the treated material. The protective layer prevents the plasma from expanding away off the surface thereby increasing intensity of the laser wave [3]. It also protects the metallic surface from damage or melting. Recent advances in laser material processing have yielded a multitude of innovative processes and applications in various fields. This has led to the discovery of laser shock peening without coating (LSPwC) technique [48].

2.3.4. Laser Shock Peening Without Coating (LSPwC)

The LSPwC has the same working principles as the conventional LSP [49]. Both techniques use a commercially sourced laser system [50]. The LSPwC has been used for preventative maintenance in Nuclear Power Plants (NPPs) [51]. Following this achievement, studies were initiated on the applicability of LSPwC for enhancing the fatigue strength of material [52]. The experiments revealed that the LSPwC also enhanced the fatigue strength of steels, aluminium alloys, and titanium alloys significantly [53]. However, this technique also resulted in the increased surface roughness of the metallic material. The roughened surface was attributed to direct irradiation of laser pulses on the material coating [53].

The applicability of LSPwC to aeronautical components has been studied [48]. Coupon tests for 7000 series aluminium alloys showed significant effects of LSPwC prolonging the fatigue lives of 7000 series aluminium alloys [54]. These effects were more pronounced in stress-concentrated areas such as fastener holes [48]; however, the LSPwC has its challenges. It suffers from a higher thermal effect which causes surface melting and re-solidification occurring a few microns on the surface of the metallic material [48].

2.3.5. Materials Laser Shock Peened in Literature

Research studies carried out in this field involved the effect of the LSP process on the RS profile. Other studies investigated the effect of the LSP treatment on a material microstructure, fatigue life, and stress corrosion cracking behaviour on fatigue life of the metallic materials [40]. Several studies conducted to understand laser parameters have also been undertaken. An extract of some of the completed studies is shown in Appendix A.

2.3.6. Application of Laser Shock Peening in the Aerospace Industry

Surface enhancement methods have been used in aerospace, automobiles, nuclear and manufacturing industries. This section explores the application of the LSP and SP in the aerospace industry and advances that have been made in the use of the LSP and SP techniques.

Aviation components, such as rotor components and turbine blades have been successfully treated with the LSP technique [55]. Other components include thin-walled airframe aluminium structures [56]. Fastener holes in aircraft skin structures have also been successfully treated with the LSP processing [48]. Despite these developments, debates about the advantages of the LSP over SP processing on the metallic material have not abated [57, 58]. The LSP has been found to have clear advantages over SP particularly on components of complex geometry [57]. For example, restoring

fastener holes in ageing aircraft where possible initiation of cracks are unnoticeable by normal inspection [41]. In this application, the LSP has been found to offer better results compared with SP [55]; however, these benefits were not pronounced in aircraft skin structures [59].

Other studies have demonstrated successful LSP applications in the shaping and forming of metals [40] and inspection of coatings [60]. Typical aircraft skins use thin sheets of aluminium alloy around a thickness of 1.6 mm [59]. When processed with the LSP technique, induced compressive RS were insufficient to retard fatigue growth [59]. This was attributed to the limited depth found in the aluminium sheet that was used [59].

2.4. Residual Stress Analysis

Different methods of measuring compressive RS induced on the surface of the metallic material have been used in literature. Ballard [30] formulated a model to analyse the surface residual stresses. This model was based on perfect elastic-plastic solution and assumed uniaxial strains [61]. However, this model was deficient due to the complex three-dimensional nature of the LSP shock wave propagation.

Other researchers have created simulation models using finite element models (FEM). For example, Braisted et al. [62] built a two-dimensional FEM to study the effect of the LSP on the metallic material. Peyre et al. [63] used the XRD technique to measure dynamic yield strength, pressure-loading and compressive RS to validate this model. Ding et al. [29], simulated single shot laser peening problem on thin specimens to advance the two-dimensional model to a three-dimensional model using quarter symmetric models. Ding et al. [29] observed the development of tensile stresses in the middle section of the specimens.

Other studies focused on the effect of different constitutive models for the laser peening simulation process [64]. The three-dimensional laser peening simulations were further used to consider the

effect of multiple LSP shots [65]. To do this, a single symmetric cell with overlapped laser shots was constructed [61]. This cell was used to simulate large laser peening problems and extrapolating the results obtained in a single cell to multiple cells. Other three-dimensional models have been used to devise parametric optimisation strategies to maximise the RS induced in the components [66].

Experimental prediction methods have also been used to measure compressive RS induced by the LSP processing; however, material restrictions and spatial resolution differed with the method used [67]. Some of RS measuring methods used destructive testing procedures which detrimentally altered tested components. A summary of other commonly used methods for measuring RS in the literature is in Appendix B.

In this study, the incremental hole drilling (IHD) and the X-Ray Diffraction residual testing methods have been selected for measuring compressive RS [68]. These techniques were used in several studies and were considered reliable and inexpensive compared to other RS testing methods in Appendix B [69].

2.4.1. Incremental Hole Drilling (IHD) Residual Stress Measurement

When a sample is treated with LSP, compressive RS will distribute at the surface and through the thickness of the metallic material. Such distribution of RS is not uniform, typically peak compressions are found closer to the surface of the treated metallic material [70]. These compressions gradually decrease with depth.

Measurement of the compressive RS is conducted in accordance with the ASTM E837-13 [71]. This standard defines material thickness according to the diameter of the strain rosette gauges used. The technique requires the following assumptions: the material is assumed to be thick [70]; the material is isotropic and elastically linear [72]. Furthermore, the stresses that are measured are

below the elastic limit of the metallic material [71]. Moreover, these stresses are constant, i.e., the average value is used [72]. Lastly, that the sizes of the strain gauge rosette, as provided by the manufacturers, are accurate [71].

The type of strain gauge rosette to be selected is dependent on the application. Figure 2.7 shows a visual representation of strain gauge rosette.

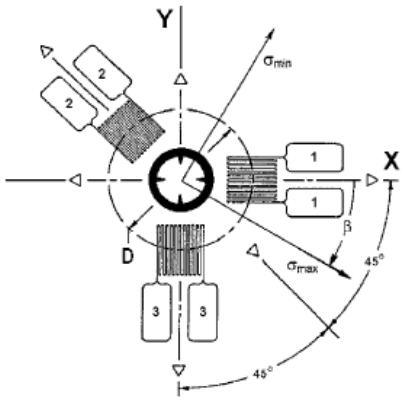

***Figure 2-7. Visual representation of a strain gauge rosette* [73].**

This type of strain rosette gauge has three sets of strain gauges that are set at a fixed predetermined angle from each other. Before drilling can commence, a strain gauge rosette is attached to the surface of the test material [71]. Thereafter, strain gauges are reset to zero. Once the strain gauge rosette has bonded to the LSP or SP-treated surface of the metallic material, the drilling mill is placed above the sample. A milling guide is used to accurately centre the drilling mill to the target spot on the strain gauge rosette. Figure. 2.8 shows the milling guide machine used for IHD.

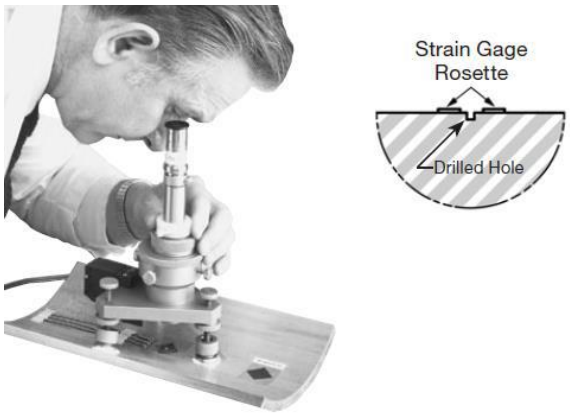

Figure 2-8. Example of hole drilling alignment through a monocular **[73].**

Strain measurements are obtained by drilling from the surface the metallic material through the centre of the strain gauge rosette [71]. At pre-set increments, the drill-bit stops, and strain measurements are recorded from the centre of the strain gauge rosette. Drilling process recommences again. From the measured strains, average values of principal stresses, σ_1 and σ_2 are computed using mathematical relations based on linear elastic theory in accordance with ASTM E837-13 [71]. This standard specifies a hole drilling procedure for determining RS for linear-elastic isotropic materials.

2.4.2. Experimental Limitations of the Incremental Hole Drilling Technique

The IHD technique suffers from several limitations, surface roughness, drilling angle, zero determination resulting in experimental errors [72] and flatness of the metallic material [74]. These are more pronounced in the thin metallic material. The IHD technique is a semi-destructive method, drilled samples cannot be reused to repeat the analysis [74]. Furthermore, the IHD is only sensitive to near-surface stresses; its sensitivity varies with depth. Moreover, it is susceptible to errors in depth, hole position, and concentricity [74]. Hole drilling results are valid only up to 50% of the yield strength of the metallic material [74].

For complementary measurements of surface compressive RS, due to the LSP and the SP-induced residual stress (RS), the XRD method will be used.

2.4.3. X-Ray Diffraction (XRD) Stress Measurement

The laboratory X-Ray Diffraction (XRD) is a non-destructive method for determining residual stresses closer to the surface of the metallic material. The method uses the $\sin^2\psi$-method to determine induced-residual stresses [75, 76]. To measure strain, linear elasticity is assumed to cause the distortion of the crystalline lattice structure. Considering a single plane of atoms, Ray **1** and **1a** strikes **K** and **P** and scatter in all directions shown in Figure. 2.9 [69].

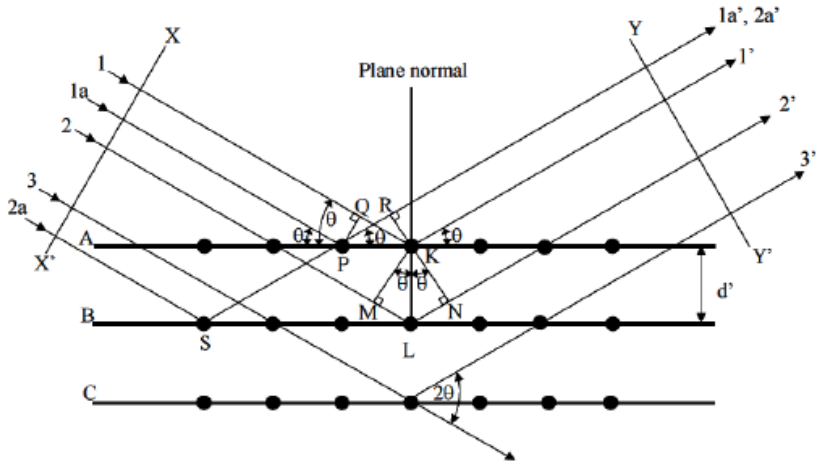

***Figure 2-9. Illustration of Braggs diffraction* [69].**

Directions **1'** and **1a'** are the dispersed beams in phase with each other, and thus constructively interfering with each other. Constructive interference is brought about due to the difference in path length between wave-fronts XX' and YY', it is equal to zero, i.e., (Equation 1),

$$QK - PR = PK\cos\theta = 0 \qquad (1)$$

Rays dispersed by atoms in the plane that are parallel to **1'**would also be in phase and contribute to the diffracted beam resulting in increased intensity. For constructive interference, rays are

dispersed by atoms in different planes, Ray **1** and **2** are dispersed by atoms **K** and **L**. Differences in the path for rays **1K1'** and **2L2** are stated as (Equation 2):

$$ML - LN = d'sin\,\theta + d'sin\,\theta \quad (2)$$

Dispersed rays **1'** and **2'** will only be in phase if the difference in the path is equal to a whole number, *n*, of wavelengths, i.e., if: (Equation 3)

$$d = \lambda/2sin\theta \quad (3)$$

Equation 3 is referred to as the Bragg's Law and is fundamental in XRD theory.

2.4.4. Experimental Limitations of the X-Ray Diffraction Technique

The laboratory XRD has limitations. It can only create an average stress field [66]. Local behaviour that considerably contributes to the fatigue strength of the metallic material is overlooked with this technique. The XRD method is limited to small components [74]. Unlike the IHD, typical laboratory XRD machines are limited to measurement of RS on the surface of the metallic material [71].

2.5. Effect of Shot Peening and Laser Shock Peening on Residual Stress

The SP and LSP techniques induce compressive RS as their key output. Using Inconel 718, literature has shown that in-depth compressive RS produced by the LSP processing was more superior to SP processing shown in Figure 2.10 [77].

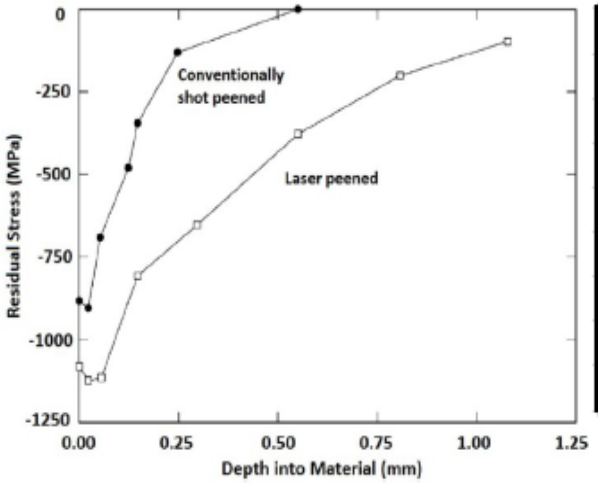

DEPTH	Shot Peened	Laser Shot Peened
0	-875	-1083
0.025	-900	-1150
0.0625	-720	-1125
0.125	-334	-850
0.3	-125	-667
0.5825	0	-350
0.875		-208
1.083		-167

***Figure 2-10. Inconel 718 RS profile induced by the SP and the LSP* [40].**

Dane et al. [40] further found that the compressive RS produced by the LSP processing extended deeper in the Inconel 718 material compared to those produced by the SP processing. Furthermore, SP results were found to produce limited fatigue strength which did not meet the fatigue life requirements [78].

Treating AA7075 aluminium alloy specimens with both the LSP and the SP resulted in increased magnitude and depth of residual stresses [79]. Rankin et al. [80] found comparable results when examining stress profiles produced by varying the SP and the LSP parameters shown in Figure 2.11.

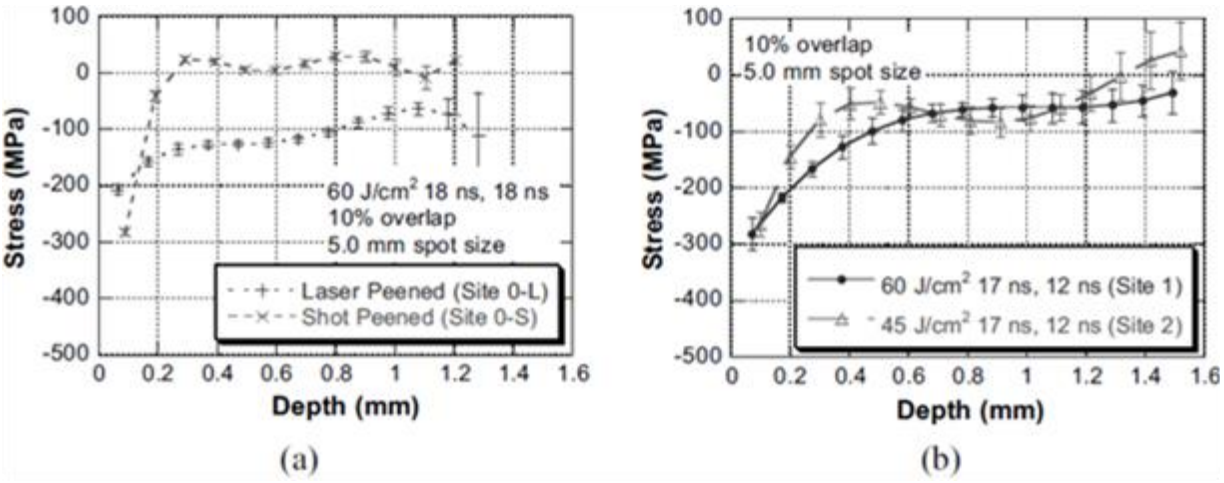

***Figure 2-11. Assessment of peening processes: (a) the LSP and the SP (b) energy density effect* [81].**

In Figure 2.11(a), the study found that compressive RS were deeper into the surface for LSP-treated material compared to SP treatment. Larger compressive RS produced by SP treatment were localised close to the surface. Furthermore, decreasing the laser beam width of the second-layer laser pulse from 8 to 12 ns [81], increased the near-surface RS to comparable magnitudes obtained with SP. Furthermore, dropping the laser fluence from 60 to 45 J/cm^2 [81] produced similar results as the SP. However, compressive RS rapidly reduced with increasing distances from the surface Figure 2.11(b). Figure 2.12 shows the RS profile of AA2024 alloy which was LSP-treated with 2500 pulses/cm^2.

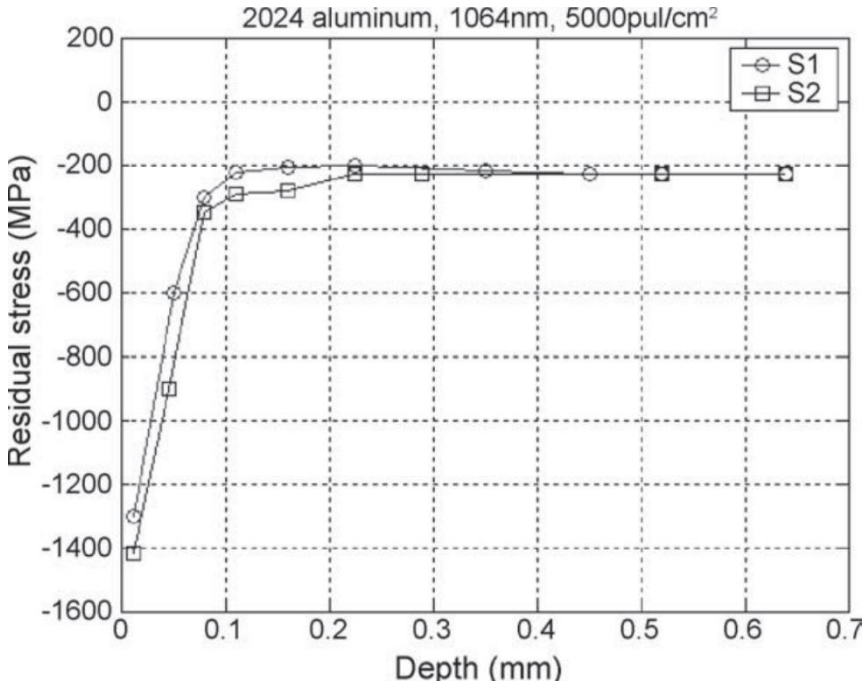

***Figure 2-12. Detailed RS profile of 2024 aluminium alloy sample processed with 2500 pulses/cm^2, where maximum and minimum mean principle stresses are represented by S1 and S2 respectively* [70].**

Using AA2024 samples, Rosas [82] again observed high-level compressive RS, of magnitudes of -1400 MPa closer to the metallic surface. These compressive RS were found to be localized closer to the surface, i.e., at depths less than 100 μm [70]. At depths greater than 100 μm, the residual compressive stresses reached maximum stresses between magnitudes of -100 MPa to -200 MPa [70]. Comparable results were observed in AA6061-T6 aluminium alloy [70].

Typical compressive stress profile versus depth in thick specimens is shown in Figure. 2.13.

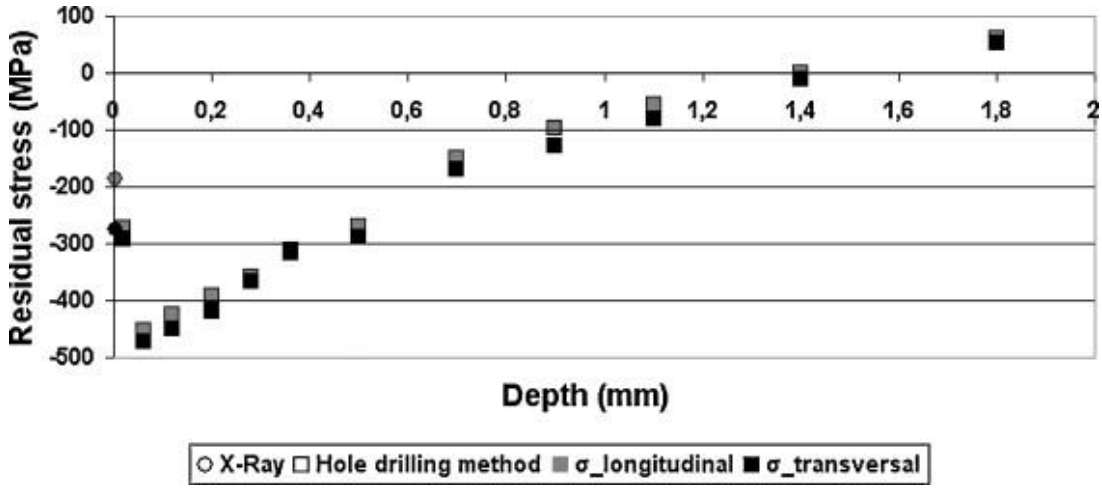

***Figure 2-13. RS calculated using X-Ray Diffraction compared with hole drilling results; where 9 mm thick specimen was laser treated using three impacts at 9 GW/cm^2 for 9 ns* [83].**

In this study, it was observed that hole drilling results were comparable to those obtained with the XRD method throughout the depth of the material [83]. Thus, these methods can be used to complement each other in determining compressive RS in the metallic material. They validate the results of compressive RS as determined in each case.

An interesting study of the effect of the SP and the LSP on the mechanical strength of AA7075-T7351 was conducted [8]. It was found that the LSP technique increased in-depth compressive RS in AA7075-T351 compared to the SP processing. It was further found that these residual stresses significantly improved fatigue performance of the metallic material [43, 77]. The LSP processing resulted in the strengthening of thin sections.

2.5.1. Effect of Coverage on Compressive Residual Stress using Shot Peening and Laser Shock Peening Techniques

Coverage is important when a uniform compressive RS in the surface layer of the SP-treated material is required. Peening procedure should stipulate coverage percentage required for a given engineered component that is being peened. In SP technique, coverage should never be less than

100% as fatigue and stress corrosion cracks can develop in the unpeened area, i.e., an area not covered in residual stress [20].

In the LSP process, successive shocks generate deeper compressive RS. The effect of successive laser shots was studied in LSP treatment of the Ti-6Al-4V Alloy [84]. The results of the study are shown in Figure 2.14.

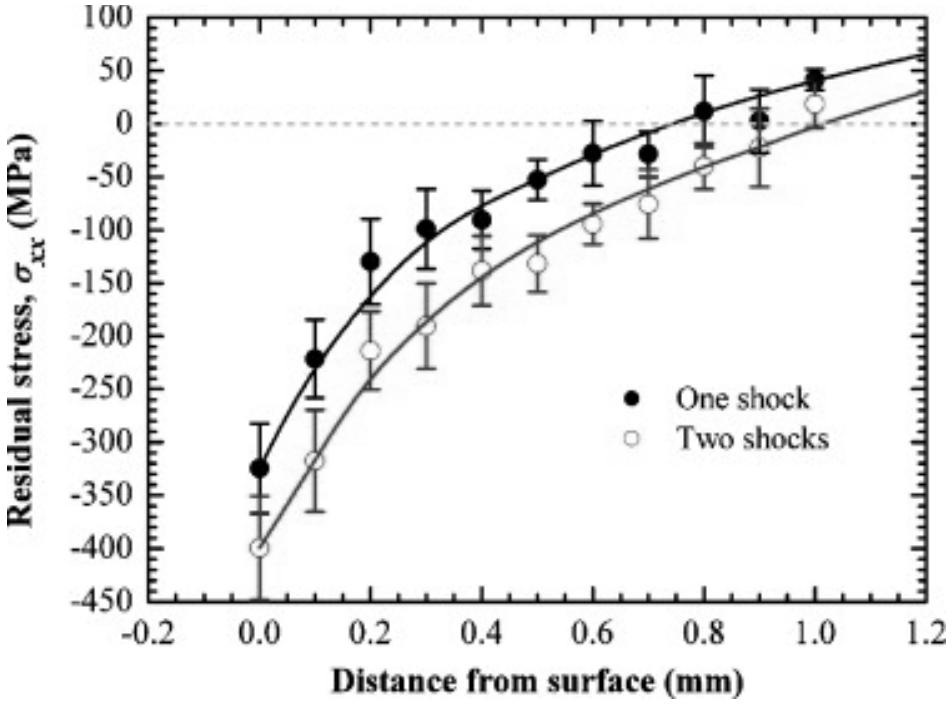

***Figure 2-14. Profile of the in-depth RS of the Ti-6Al-4V Alloy specimens* [84].**

Maximum residual stress values were found closer to the metallic surface of the test sample. The value of the residual stresses increased with increasing number of shocks [85, 86]. In another study, using AA7075 aluminium alloy, successive laser impacts increased surface compressive RS of the metallic material [87]. Using power intensity of 4 GW/cm^2, the LSP treatment produced compressive RS of -170 MPa at the first impact, -240 MPa at second impact and -340 MPa after the third impact [79]. Masse [88] recorded similar observations regarding increased magnitudes of the in-depth stresses due to repeated laser impacts.

2.5.2. Effect of Shot Peening and Laser Shock Peening Residual Stress on Thickness of the Material

It was found that the SP treatment was impractical for thin metallic sections [87]. In these applications, the use of the LSP treatment was considered more suitable [89]. Unlike in previous studies, it has been found that treating thin sections, of 1.5 mm thick 4340 steel, using an increase in the number of shocks did not produce increases in the in-depth compressive stresses [90]. The sheet was LSP-treated with one and five shots from both sides simultaneously and the residual stresses plotted [87]. It was found that the compressive RS decreased with increasing distance from the surface of the metallic material. Masse [88], further found that these residual stresses changed into tensile at some point within the metallic material. These compressive RS could distort the thin specimens [90].

However, on thick sections, there was no observable distortion of the specimen [40]. Increased compressive stress zones were attributed to increased plastic deformation brought by repeated laser impacts [40]. Comparable results were obtained using laser-treated 10mm thick AZ31B Mg alloy and subjecting it to one, two, and four laser impacts. The specimen also did not distort [86].

Cellard et al. [83] investigated the LSP-induced compressive RS in a nine-millimetre-thick specimen. They found that the LSP thickness layer varied from 5 μm to 1.8 mm [91]. They recorded compressive stress values of -690 MPa near the surface of the specimen. Compressive RS increased to -714 MPa at a depth of 200 μm due to the more severe laser impact condition [91].

Peyre et al. [45] studied compressive RS in AA7075-T351 using the LSP processing. They found that the maximum value of compressive RS increased with increasing number of laser shocks. They reported compressive RS of the order of -350 MPa near the surface of the AA7075-T7351 material and maximum depth of 0.85 mm [45].

Laser peening process has also been used to induce compressive RS in a relatively low strength, lightweight metal, Al7050-T451 [92]. A lower shock pressure of 2 GW/cm^2 to 4 GW/cm^2 was used to laser shock peen the metallic material [92]. Results obtained are shown in Figure 2.15.

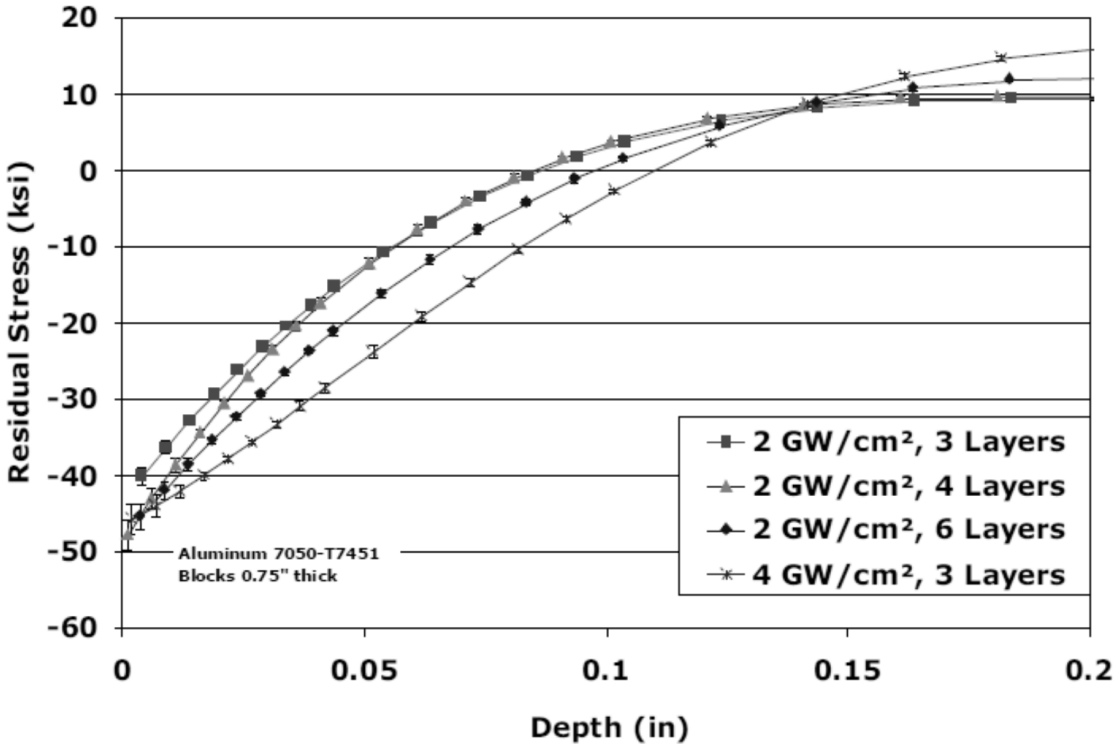

***Figure 2-15. RS versus depth data measured with the slitting method in AA7050-T7451 blocks are laser peened with various parameters* [92].**

The maximum compressive RS reported was -345 MPa using power at 4 GW/cm^2 and 3 successive LSP treatment with a maximum depth of approximately 3.8 mm [92]. In a similar research, Sanchez-Santana et al. [93] studied the effect of the LSP on AA6061 aluminium alloy. The results of the test are shown in Figure 2.16.

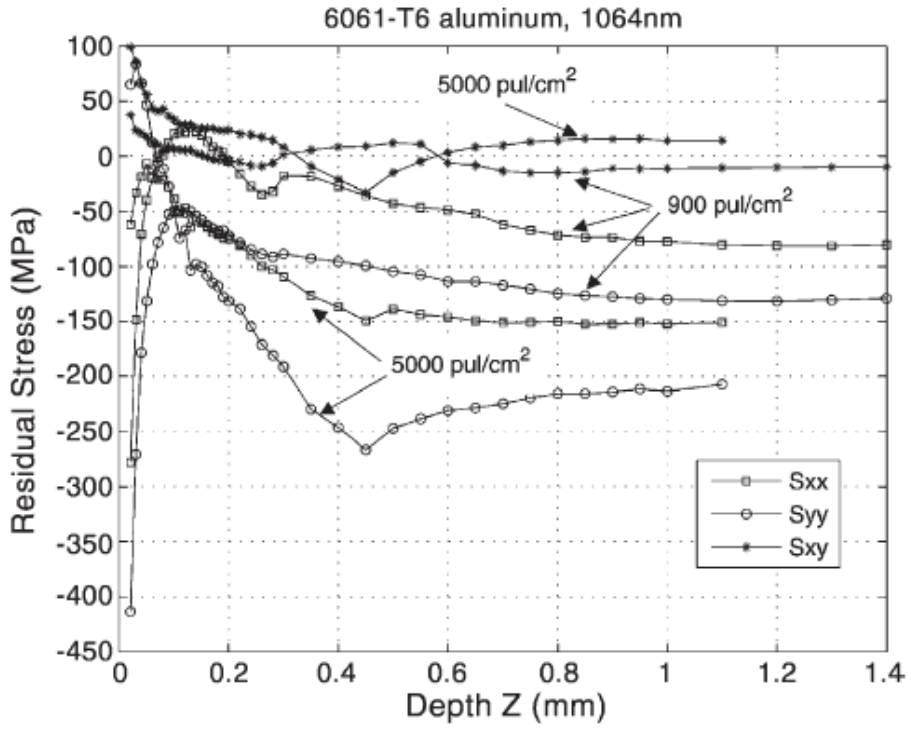

***Figure 2-16. Results of the LSP on AA6061-T6 aluminium alloy and the associated residual stress distribution* [93].**

It was found that higher pulse density produced greater compressive RS in the metallic material [93]. In this study, the S_{xx} depicted stress component along the swept direction of the LSP treatment. The S_{yy} is perpendicular to the S_{xx} direction while the shear stress is depicted by, S_{xy} [93]. There were no tensile stresses reported at greater depths in the material. Comparable results were reported in LSP-treated 304 stainless steel measured by XRD [94]. Results are shown in Figure 2.17.

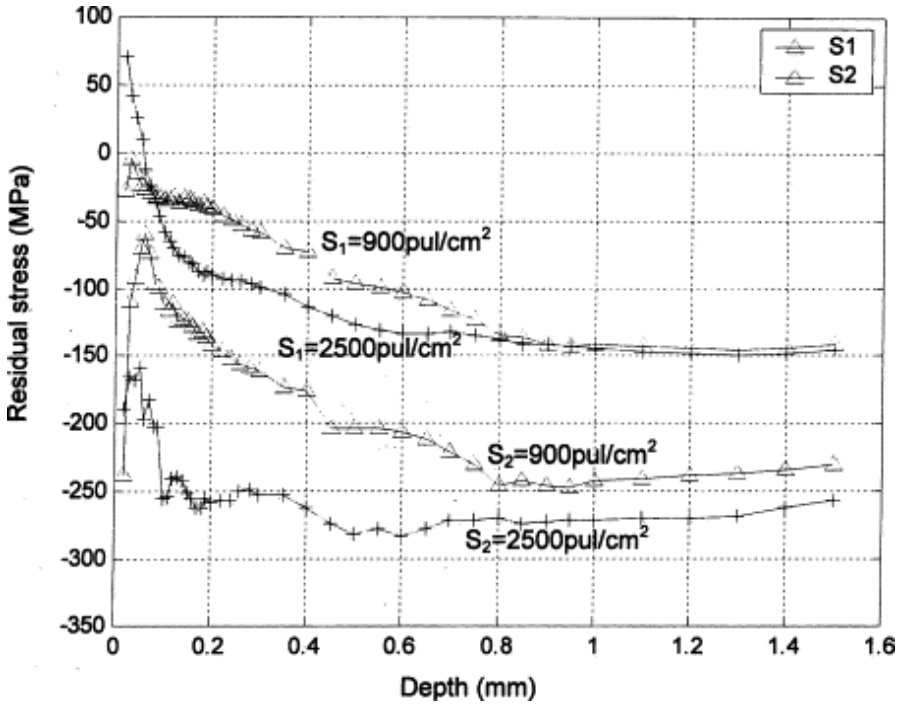

Figure 2-17. Results of RS distribution produced by the LSP treatment of 304 stainless steel **[95].**

In Figure 2.17, it was seen that higher pulse density produced larger the compressive RS, (S_2), which were normal to pulse swept direction. Compressive RS parallel to the pulse swept direction were depicted by S_1. Compressive stress component perpendicular to swept direction S_1 was found to be higher than S_2 [95].

2.5.3. Effect of Shot Peening and Laser Shock Peening Wavelength on Residual Stress

There are limited studies investigating the effect of wavelength on the RS profile. The literature on LSP studies using laser wavelengths of 355 nm, 532 nm and 1064 nm have previously been reported [96]. It was found that the laser wavelength influenced the magnitude of induced residual stresses in the material [40]. Other factors that had an influence on the magnitude of induced compressive RS included the laser type, power density and beam characteristics [96]. Figure 2.18 shows the results of varying pulse energy and wavelengths.

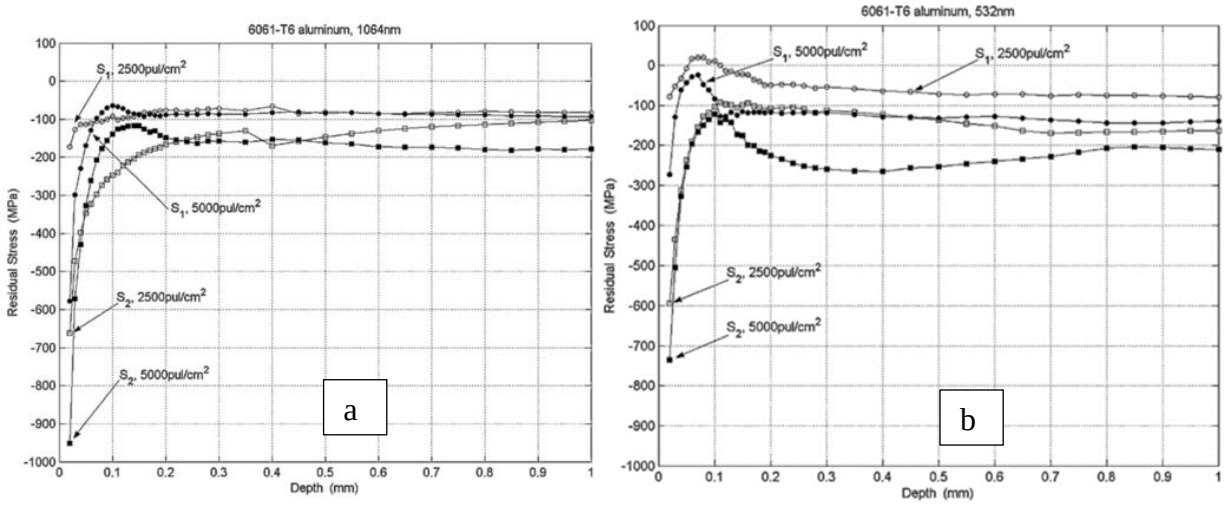

Figure 2-18. (a) RS profile of AA6061-T6 aluminium alloy produced using 1064 nm wavelength, (b) RS profile of AA6061-T6 aluminium alloy produced using 532 nm **[96].**

From the study, higher wavelengths and pulse energy results in residual stresses of the order of -950 MPa at 1064 nm and -750 MPa at 532 nm wavelengths respectively were found [96]. In both tests, the residual stresses are confined near the surface of the sample. The increase in residual stresses as a result of increased wavelengths was attributed to short pulse durations. Results of measured residual stresses on Ti-2.5 Cu, results are shown in Figure 2.19.

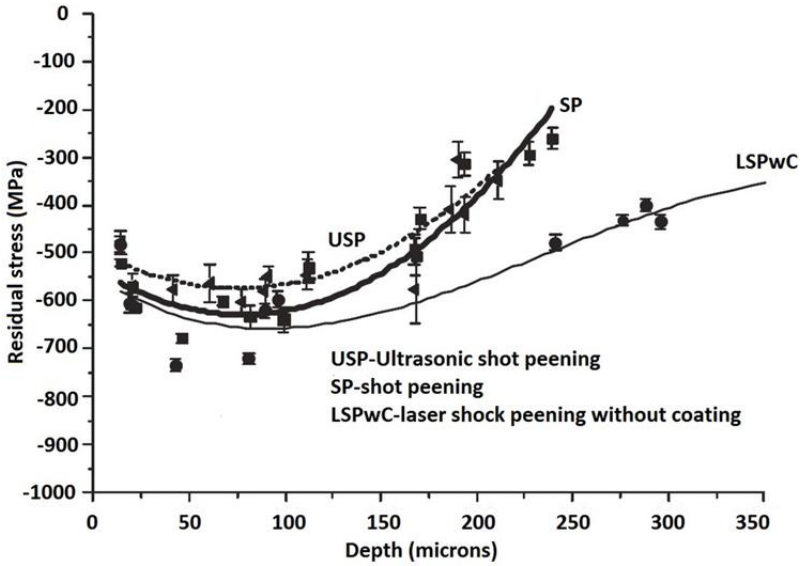

Figure 2-19. RS-depth profile in α-phase Ti-2.5Cu using SP, LSPwC and Ultrasonic shot processing **[97].**

Taking into account error bars, SP processing produced residual stresses of up to 250 μm [97]. Results exhibited higher and deeper compressive RS in LSPwC treated specimens compared to SP treatment. In AA2024-T3, Yang et al. [98] also found beneficial effects of the LSP treatment on fastener holes. Using XRD, they further found that the LSP produced high compressive RS of the order -384 MPa. Recent studies on wear resistance in AA2024-T3 aluminium alloy confirmed this observation [99]. Kadhim [99] found that the microhardness values increased with LSP pulse energy. Kadhim [99] attributed the increased microhardness to dislocation strengthening in the metallic material.

Tan et al. [100] studied the effect of the LSP on AA2024-T3. They found similar results about increased compressive RS in AA2024-T3 as shown in Figure 2.20.

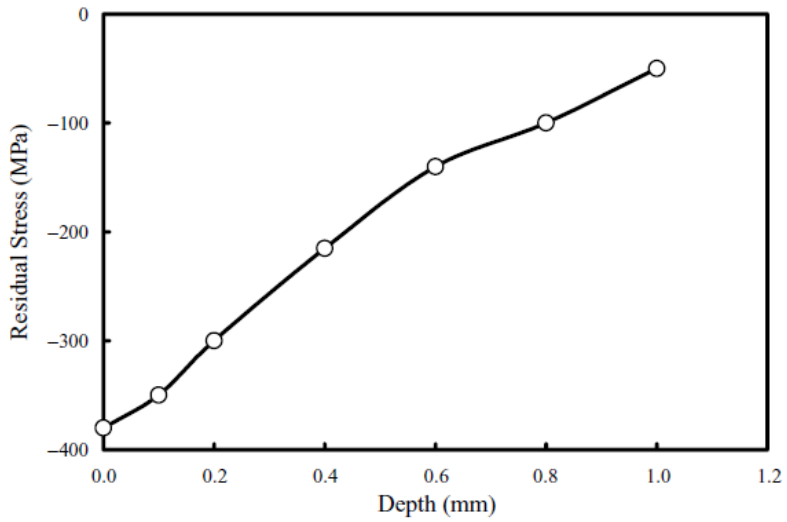

***Figure 2-20. In-depth RS of 2024-T3 Al after the LSP treatment* [100].**

Tan et al. [100] found that the highest compressive RS produced by the LSP was -380 MPa [100]. Furthermore, they found that the magnitude of RS decreased with increasing depth. Clauer [101] made similar observations regarding the compressive RS correlation through the depth of the material. The depth of penetration by the LSP was found to be more when compared to SP-treated

materials [100]. Furthermore, Tan et al. [100] found that microhardness varied with the thickness of the water layer above the target material at the pulse energy of 1 Joules.

2.5.4. Effect of Shot Peening and Laser Shock Peening Power Intensity on Residual Stresses

Using the same size shot mass of the SP process, increasing intensity means a higher impact speed. Lundberg [102] found that increasing the SP intensity had no influence in the thickness, but increased the subsurface compressive surface in ductile irons with higher yield strength. SP with a high intensity had an effect on the compressive RS depth profile. XiuQuan et al. [103] found that compressive RS increased with an increase in SP intensity in 7075 aluminium alloy; however, in another study, it was found that the SP intensity led to a lower surface stress [102]. Vielma et al. [104] found that the maximum compressive RS was not dependent on the SP intensity. They further found that high intensity SP treatments (>10A) provided worse results than 10A intensity SP treatment, despite producing a greater surface hardening in a much larger region due to high induced compressive RS [104]. They further found that high intensity SP treatments gave rise to increased surface hardening and deeper compressive RS due to surface damage; however, it gave rise to inferior fatigue performance.

In the LSP, compressive RS increased with increasing laser pressure; however, the power intensity of threshold had to be exceeded before the depth of these compressive RS could be increased [87]. Thus, the magnitude and depth of compressive RS were influenced by the laser power density [105]. Montross et al. [87] stated that a smaller spot diameter/ or spot size produced spherical shock wave expansion at the attenuated rate of $1/r^2$ while for larger spot diameters an attenuated rate of 1/r was observed. Montross et al. [87] contended that less attenuation behaviour resulted in further propagation into the material in large spot diameters. Furthermore, smaller spots produce

higher compressive stresses due to the inverse proportionality of power intensity and spot size given in Equation 4 [106]:

$$I\left(\frac{GW}{cm^2}\right) = \frac{P_{avg}}{f(pt)A} \quad (4)$$

where *I*, is the laser average intensity in GW/cm^2,

f is the laser frequency in Hz,

$p_{t,}$ is the pulse time in ns,

A is the laser spot area in cm^2, and

$P_{avg,}$ is the average power output in W.

The "Thin Lens Theory" is used to determine the laser spot area using Equation 5. Laser spot diameter for the circular beam is calculated in accordance with Winburn [107]:

$$d = 2.44\frac{Fx\lambda}{D} \quad (5)$$

To introduce defects such as microcracks, critical power density must be exceeded [40]. In AA7050 aluminium alloy internal cracking were observed [108]. These were attributed to laser power density. In that study, it was deduced that high power density had a major influence in the forming of internal cracks in the LSP-treated material.

2.6. Surface Roughness Analysis

Surface roughness has a great effect on the fatigue strength of the material [109]. Fatigue cracks generally initiate on the surface of the specimen. Fatigue is influenced by the circumferential direction of roughness normal to stress direction [110]. Taylor et al. [111] have compared the fatigue strength of AISI 4140 steel using different types of machined surfaces, grinding,

polishing, shaping, and milling. They found that the fatigue strength of polished samples was higher when compared to ground surfaces, i.e., the fatigue strength increased with decreasing surface roughness. However, milled surface samples produced opposite results, i.e., increasing surface roughness produced higher fatigue strength [109]. Surface roughness was the influential factor in short life regime of Ni-Cr-Mo steel. In a previous study, fatigue life was found to increase with decreasing surface roughness [109]. Arola and Williams [112] found that the high-cycle fatigue life of machined samples of AISI4130 steel was dependent on the texture of the surface. The fatigue strength increased with a decrease in surface roughness from two to six micrometres.

2.6.1. Measurement of Surface Roughness

Surface roughness measurement is carried out to approximate surface irregularities of the surface after processing or machining of a material [113]. This estimation of the roughness is carried out by dragging a measurement stylus across the surface of the sample being analysed. By calculating roughness heights of irregularities on the surface of the material, from the profile chart of the surface of the material, the surface roughness can be approximated. Figure 2.21 shows a schematic of the surface roughness tester and a depiction of the stylus travel and movement on the surface of the sample material.

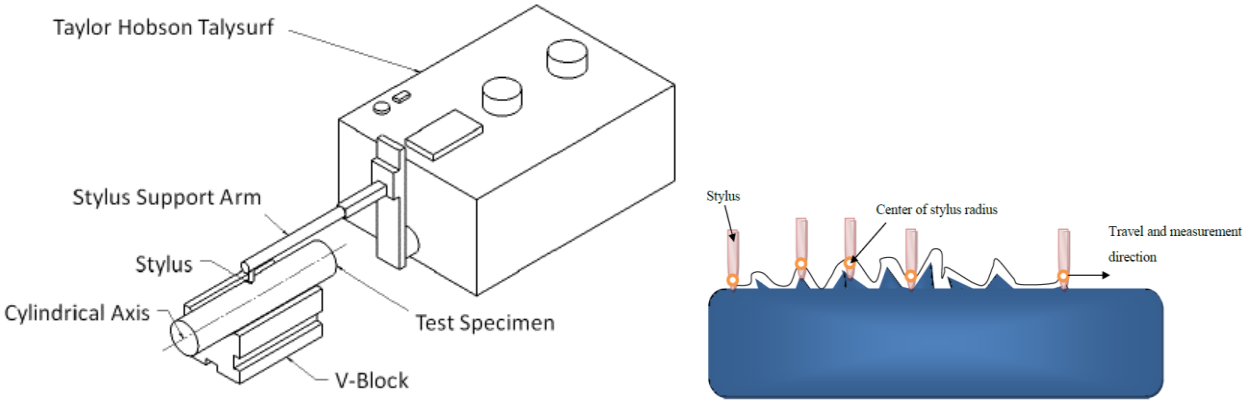

***Figure 2-21. Surface Roughness Measurement (a) Roughness Testing Machine. (b) Stylus shown traversing surface of the material* [113].**

A specimen is placed securely in a block to prevent it from moving during surface roughness measurement. The stylus is dragged across the surface of the material at a speed of 1mm/s. Measurements of surface irregularities are then recorded and analysed.

2.6.2. Arithmetical Mean Roughness (Ra)

Arithmetic mean roughness (Ra) is a measure commonly used to indicate the surface roughness of the material [113]. It is obtained by measuring the average length between "peaks and valleys" across a sampling length on the surface of the material. The deviation of "peaks and valleys" from the average line within the sampling length is then approximated. Figure 2.22 shows an illustration of the sample length.

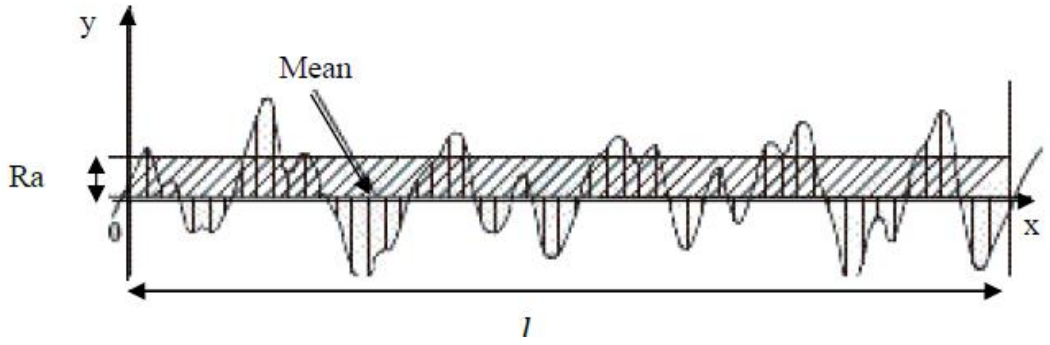

Figure 2-22. Sample length used to approximate Ra

The method to determine Ra averages all valleys and peaks to normalise the effect of extreme peaks in the sample length. Equation 6 is used to determine the Ra value [113]:

$$Ra = \frac{1}{l}\int_0^l \vdots f(x) \vdots dx \qquad (6)$$

2.6.3. Mean Roughness Depth (Rz)

Mean roughness depth is obtained by measuring the distance between heights and valleys within the five sampling lengths and then averaging these lengths. Five highest peaks and five lowest valleys are used in the calculation [113]. Equation 7 is used to calculate the Rz for the surface of the sample:

$$Rz = \frac{(Yp1+Yp2+Yp3+Yp4+Yp5)+(Yv1+Yv2+Yv3+Yv4+Yv5)}{5} \qquad (7)$$

Where $Yp(i)$: $Height\ of\ the\ top\ five\ peaks\ within\ sampling\ length.$

$Yp(i)$: $Height\ of\ the\ lowest\ five\ valleys\ within\ sampling\ length.$

Figure 2.23 shows an illustration of the calculation for Rz.

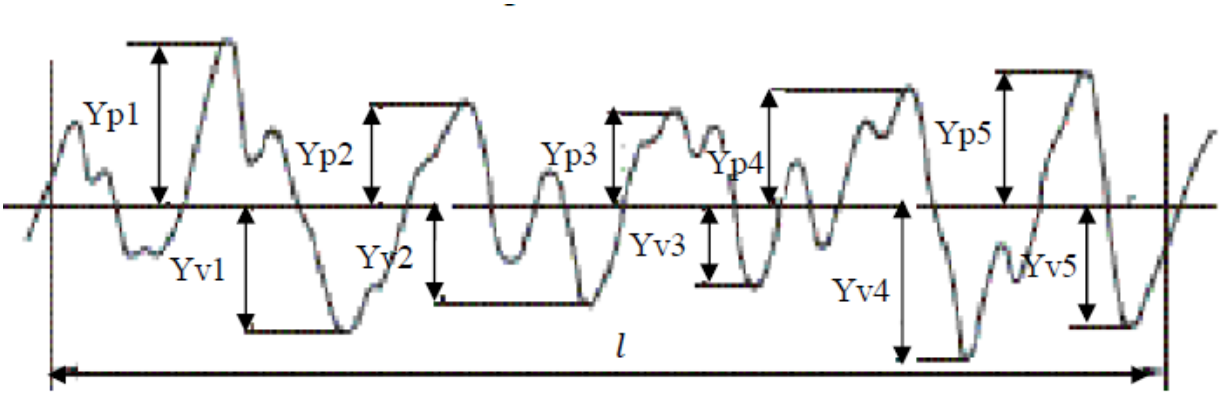

Figure 2-23. Illustration of the measurement of peaks and valleys for the estimation of Rz **[113].**

The peaks and valleys are averaged over the sampling length as shown in Figure 2.23. The resultant number signifies the estimated surface roughness of the measured material.

2.6.4. The Relationship between Shot Peening and Laser Shock Peening Treatment and Surface Roughness

Different surface treatment techniques result in varying surface roughness results. It has been reported that the LSP and the SP processing increased the roughness of treated material [79, 106, 114]. However, the LSP process was found to produce a desirable surface finish compared to SP processing. For example, the LSP produced improved surface finish in aluminium [79]. This reduced occurrences of surface folds, lapping, and other undesirable features found in SP-treated metallic material [115]. In SP, the surface roughness needed to be minimised by grinding or polishing treated surfaces for wear applications [116, 117]. However, this resulted in undesired partial stress relaxation of compressive RS on the metallic material.

Surface roughness, due to the SP or the LSP processes, has been found to cause fatigue in the metallic material [118]. Lu et al. [119] found that the fatigue strength of the metallic material decreased with the increased surface roughness of the metallic surface. In a different study, high

surface roughness was found to cause more crack initiation sites in the treated material [40]. These adversely affected fatigue life, corrosion, and wear resistance of the material.

Recently, laser power has also been found to have an effect on the resulting surface roughness of the material [99]. By varying laser energy of the LSP treatment, Kadhim et al. [99]found that the resultant surface roughness was affected. Results of LSP-treated AA2024 aluminium alloy using different laser pulse energies are shown in Figure 2.24.

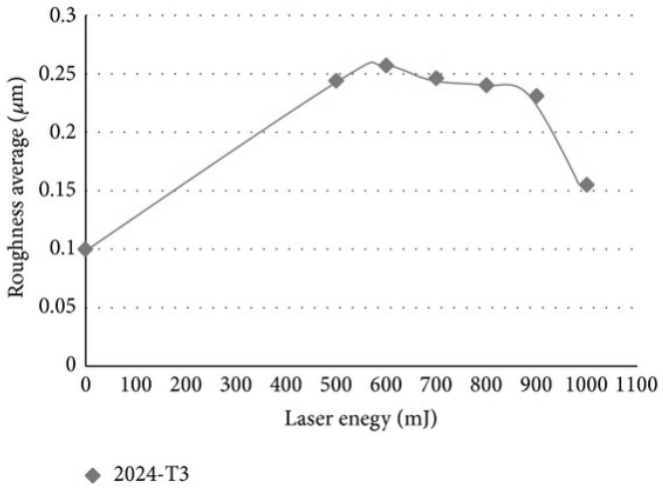

Figure 2-24. The surface roughness of AA2024-T3 treated region at different laser pulse energies **[99].**

Kadhim [99] found that further refinement of grains in the microstructure of the metallic material was achieved with the increase in LSP laser pulse energy.

However, the LSP and SP surface treatment resulted in the increased surface roughness of the material compared to baseline material [120]. To analyse the final surface roughness, the initial starting surface roughness must be measured. Surface roughness arithmetic mean Ra values for the baseline material, and the LSP and SP-treated materials are shown in Table 2.1.

Table 2.1 R_a values from different authors [120]

Material	Processing	R_a (μm)	R_z (μm)
AA7075 [79, 120]	As-milled	0.60	5.2
	SP*	5.7	42
	LSP**	1.3	11
A356			
	As-milled	0.70	6.2
	SP***	5.8	33
	LSP†	1.10	7.5

Note. R_a = Arithmetic mean. Adapted from "Laser shock processing of the metallic material. Application to high cycle fatigue behaviour", [79] P. Peyre, R. Fabbro, and P. Merrien, 1996, *Material Science Engineering,* A 210, 102–113. *SP Parameters: F20-23A (125%, 0.6 mm beads). The LSP parameters: 4 GW cm^{-2} (3 impacts). *** SP parameters: F38-50 N (0.3 mm beads). †The LSP parameters: 2 GW cm^{-2} (2 impacts).

Figure 2.25 shows typical surface roughness of the metallic material as a function of the confinement water layer of 1mm thickness.

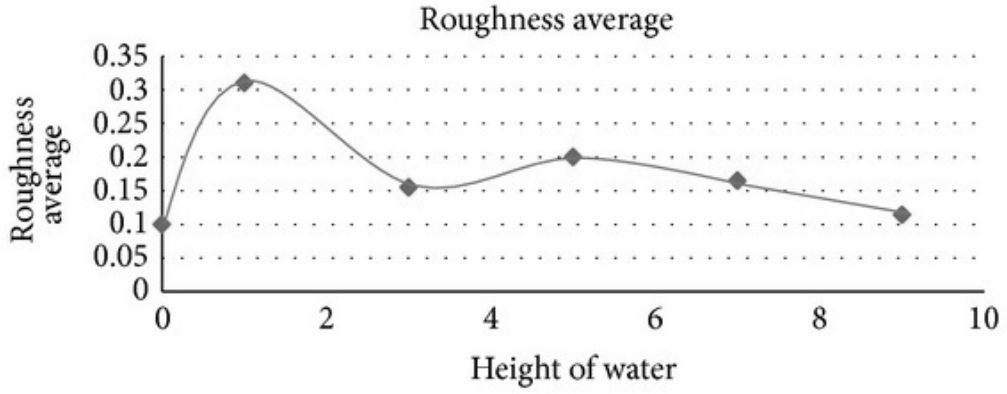

***Figure 2-25. The surface roughness of the treated region with the different thickness of water layer* [99].**

Kadhim [99] found that surface roughness decreased with increasing thickness of the confinement layer. The lowest average surface roughness measured was three times lesser than the peak surface roughness. This behaviour was attributed to the dependence of roughness on the ablation rate which decreased when the thickness of the confinement layer was increased [99].

2.7. Microstructural Analysis

Mechanical processing of the surface of the material, using the LSP or the SP, causes changes in the microstructure of the treated material. These microstructural changes result in improved hardness, changes to grain morphology, and in some material even phase transformation. It is these microstructural changes that are attributed to the beneficial results of treated material. Microstructural changes have been reported to result in improved strength. As fatigue toughness signifies material's resistance to damage, treated material will have improved resistance to the initiation of cracks of material.

2.7.1. Specimen Microstructure

Several types of microscopes are used to analyse the microstructure of the metallic material. The most common are the light microscope and scanning electron microscope (SEM). Each of these microscopes has distinct features and are suitable for different purposes. For example, the light microscope uses rays of light to form a magnified image of the structure of the material being examined; however, it produces less magnification and resolution compared to the SEM.

2.7.1.1. Scanning Electron Microscope

The scanning electron microscope (SEM) uses an electron beam from the electron gun to analyse the material sample. It also consists of a cathode of a filament made of tungsten wire, Lanthanum hexaboride (LaB_6) Cerium hexaboride or crystal, a Wehnelt cylinder that controls the flow rate of electrons, and a positively charged anode plate that accelerates the electrons to the sample [121] (Figure 2.26).

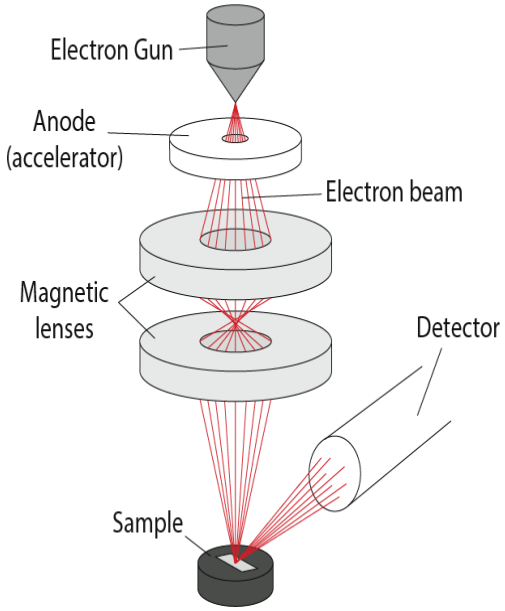

Figure 2-26. Scanning Electron Microscope **[121]**

When the electron beam hits the surface of the specimen, the electrons change direction into a new trajectory thereby forming different signals. This is referred to as scattering and is depicted in Figure 2.26. These signals are collected via a detector and used to characterise the elemental composition of the analysed volume. Unlike the light microscope, the SEM produces high resolution and magnification.

2.7.2. Microstructural changes due to Shot Peening and Laser Shock Peening

Metallic surface morphology influence fatigue behaviour [87]. The microstructure of the shot peened surface was found to have similar structure as the bulk material, except the irregular peened surface [122]. In Titanium alloy, the SP was found to be harmful to the mechanical integrity of the components that were subjected to high temperature exposure [123].

Several investigations have been conducted related to the morphology of LSP-treated material surface [124, 125]. Laser shock processing was found to cause severe surface melting and

vaporization of the aluminium when no protective laser-absorbent coating was used on the substrate.

In another study, the LSP-treated material underwent plastic deformation with high rates of strains of the order of 10^6 s^{-1} [63]. These strains induced microstructural changes closer to the metal surface [84]. The LSP microstructural changes resulted in refined grains of the metallic material. It is these refined grains that enhance material properties such as higher fatigue strength and strain hardness [126]. Other properties associated with refined grains are high tensile strength [124] and improved wear resistance [127, 128].

A subsequent study found that the grain sizes of LSP-treated material decreased with micrometres in a near-surface regime [99]. This was attributed to dislocation movement which led to a substantial hardening of treated materials. Clauer et al. [129] studied the effect of the LSP on microstructure in thin foil AA2024-T351. They used peak pressures of 6.5 GPa to process this metallic material. Clauer et al. [129] found that the dislocations were arranged in a uniform distribution of tangles like substructures after the LSP treatment. In a different study, comparable observations were cited using LSP-treated Al-Cu-Mg alloys at the same peak pressure [108].

In a further study, the AA2024-T852 was laser shocked at a lower peak pressure [129]. Clauer et al. [129] found that the microstructure of a treated metallic material also contained a relatively uniform distribution of dislocations. However, in a separate study incongruent results were produced for AA2024-T851 [67]. Differences were attributed to different shock hardening responses between T351 and T851 conditions and strain hardening behaviours of these materials. The T351 condition was found to strain harden much more than the T851 condition. In a different study, using 2024-T6 aluminium alloy, comparable microstructural changes were observed with apparently high dislocation density.

However, microstructural modifications were not evidenced in laser treated AA7449 [126, 130, 131]. The Fribourga [130] study found that the grain structure of the material was unchanged and no melting took place after the LSP treatment. Fribourga [130] evidenced substantial development of precipitate dissolution. Fribourga [130] concluded that since he did not detect melting nor changes in grain structure, the LSP processing could be referred to as a purely thermal process [130]. Fribourga [130] contended that the process involved changes in precipitate microstructure. A study of fatigue strength in aluminium alloy concluded that microstructural features were a factor of laser shock peening parameters used [84]. In a study of AZ31B Mg, Zhang [84] found that increased laser impacts caused plastic deformation thereby, and thus refinement of metallic grains (Figure 2.27).

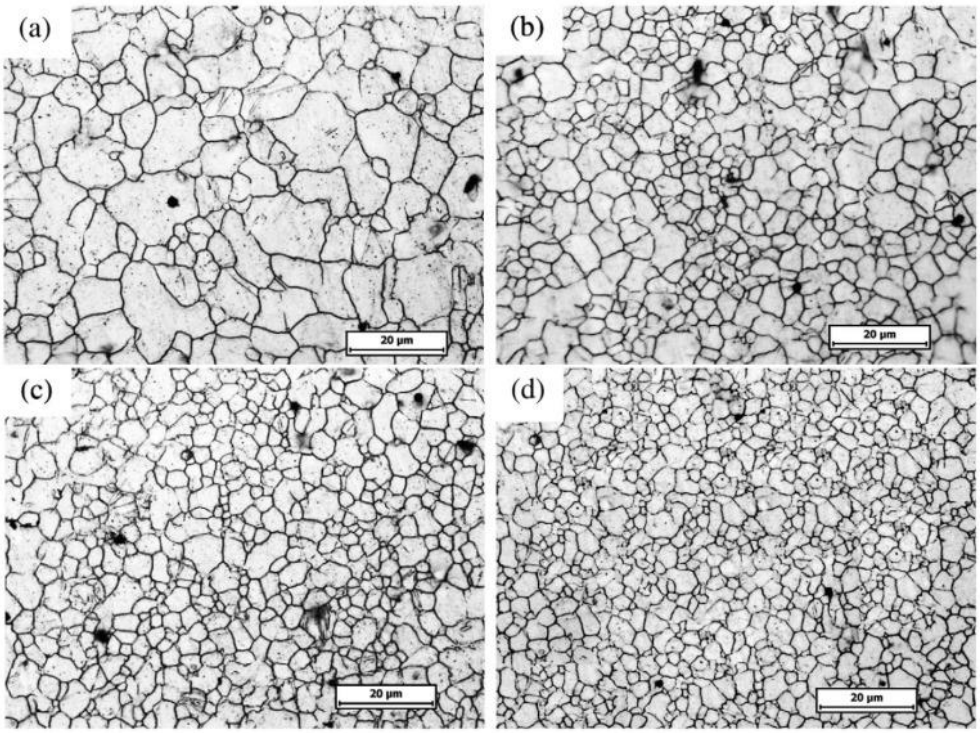

***Figure 2-27 Micrographs of AZ31B Mg alloy using the Optical Microscope (a) untreated with LSP; (b) 1-impact, 2-impacts; and 4-impacts* [84].**

The refined microstructure improved crack arrest and prevented stress corrosion cracking.

The Zhang [84] study confirmed that the LSP conditions and target material produced varying microstructural features. These features could either be detrimental or beneficial to material fatigue performance. Thus, based on the above, fundamental understanding of beneficial microstructural features caused by SP and LSP-treated materials are needed.

2.8. Microhardness Measurement

The microhardness is a characteristic of the material and it is not a physical property of the material. It is also referred to as a property of the material to resist indentation/ or penetration, and thus plastic deformation. This term could also refer to temper/ or resistance to abrasion, scratching or cutting of the material.

2.8.1. Measurement of Microhardness

Microhardness is determined by measuring the depth of an indentation produced by an indenter using a predetermined load. Different testing methods are used to measure the hardness of the metallic material:

- Brinell Hardness Test: 1kgf-3000 kgf
- Knoop hardness Test 10gf-1 kgf
- Rockwell Hardness Test 5kgf-150 kgf
- Vickers Microhardness Test 10gf-100 kgf

Where: gf = gram force, and kgf = kilogram force

2.8.2. Vickers Microhardness Test

The Vickers microhardness of the material is an indicator of the yield strength of a material [74]. It is determined by measuring the indentation of the diamond indenter produced with a given load. The indentations of Vickers microhardness (HV) are calculated by measuring the lengths of the

diagonal corners of an indent after applying a load to a material using a diamond indenter. The indenter is shaped like a pyramid with an angle of 136° (22° from the horizontal) between opposite faces of the diamond shown in Figure 2.28.

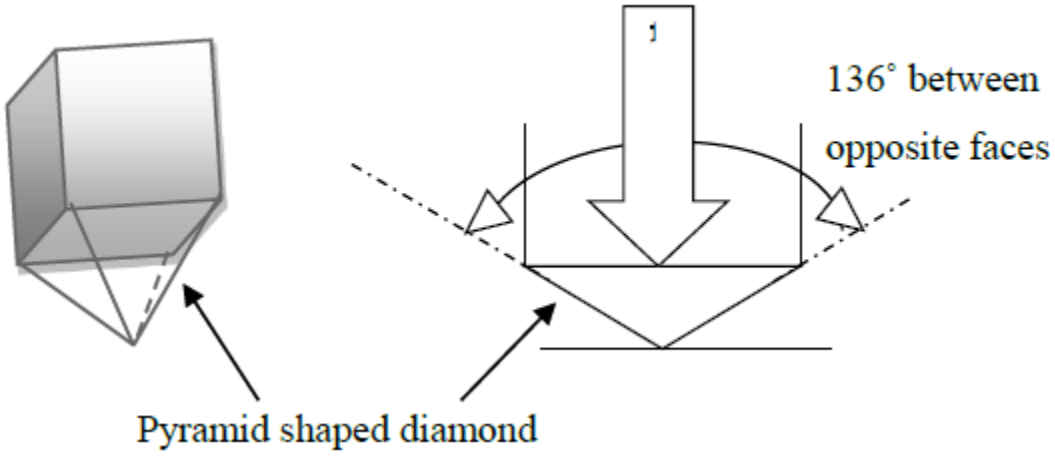

Figure 2-28. Microhardness Pyramid shaped diamond indenter **[132]**

The load was applied to the surface of the material for a dwell time of 10 to 15 seconds. Upon the release of the load, a diamond shape indentation was left on the surface of the material. The size of the indentation was then measured across the diagonals of the diamond shape and the sloping section of the indentation (Figure 2.29).

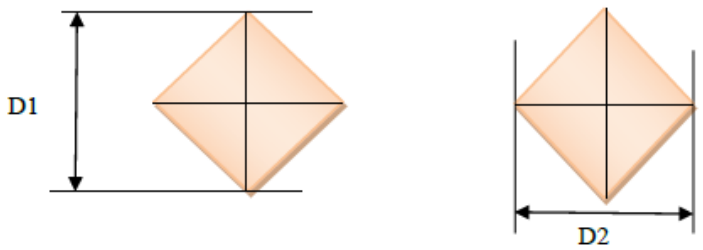

Figure 2-29 Vickers Hardness: Computation of the hardness indentation **[132].**

From the measurement of the D1 and D2, and the applied load, the microhardness value (HV) was computed using equation 8:

$$\boldsymbol{Vickers\ Hardness\ (HV)} = \frac{\boldsymbol{2.Force.Sin}(\frac{\boldsymbol{136^{\circ}}}{\boldsymbol{2}})}{(\frac{\boldsymbol{D1+D2}}{\boldsymbol{2}})} \quad (8)$$

where *HV* is measured in kgf.

Using Equation 8, the HV represents the amount of force used for a calculated value of 100kgf/mm^2 at a force of 300 grams and for a dwell time of 10 seconds depicted as HV 0.3. The Vickers microhardness value indicates the microhardness of the material [132].

Microhardness across LSP-treated surface was measured and reported in the literature [133-135]. Plastic deformation has been identified as the source of the increased hardness in LSP-treated material resulting in dislocation movement and multiplication [26, 120, 136]. However, microhardness measurement has limitations, particularly when measuring subsurface or in-depth microhardness of the material [40]. This is due to difficulties caused by the compressed layer of thickness resulting in difficulties in measurements.

2.9. Summary

Research shows that Shot Peening (SP) has been used extensively in the industry. It was considered the most effective technique of inducing compressive RS into metal surfaces to enhance their fatigue performance. SP was considered inexpensive and could be used on different sized areas depending on the application. However, the process had limitations; it relied on the use of an Almen gauge for measuring the SP intensity: a semi-quantitative method.

An alternative technique to the SP is the laser shock peening (LSP) method. This novel processing technique has been applied successfully to introduce residual compressive stresses in metals. The LSP has a wider range of applications compared to SP processing. Whilst the SP and the LSP create residual stresses, the LSP processing has been found to induce residual stresses with greater depth into the metallic material.

This research focussed on the assessment of the effect of using different LSP and SP parameters for improving the mechanical performance of AA7075-T651 aluminium alloy. This aluminium alloy has been used extensively in the aviation industry. Several studies have revealed benefits of the LSP or the SP processing on the mechanical properties of aerospace metallic materials. Moreover, past studies have revealed that the LSP is a better mechanical treatment method compared to the SP. The former has been found to produce finer microstructural grains, stain hardened alloy and improved surface.

2.10. Research Motivation

Research on thin metal sections using the SP and the LSP processing is limited [29]. There has also been a limited focus on the application of the SP and/ or the LSP techniques in aviation applications. Limited studies have been conducted on aircraft skin and airframe structures [59]. This is despite there being a strong interest by the aeronautical industry in the application of the SP and the LSP methods. However, available information indicates that processing the metallic material using the SP and/ or the LSP can improve its mechanical performance. These processing techniques can be useful in various phases of the life of the aircraft, i.e., during aircraft manufacturing, and for maintenance of in-service equipment. For example, ageing aircraft skin structures are prone to mechanical damages during aircraft service. The SP and LSP techniques can be used to prolong the life of these components.

2.11. Problem Statement

Aircraft passenger safety is considered of paramount importance [137]. However, due to budgetary constraints, some airlines are forced to operate older aircraft longer than their design life [59]. For example, Boeing 737s and Boeing 747s have been in use for several decades. These ageing aircraft

pose a risk for the safety of passengers and crew. Safety concerns on older aircraft relate to structural degradation due to fatigue and corrosion fatigue. Other safety concerns relate to fatigue cracks caused by stress concentrations, in aircraft parts, which compromise the structural integrity of the aircraft. Fatigue crack detection, repair, and control is a significant concern to the commercial aircraft and military industry. Military and commercial aircraft industry continually innovate to enable early crack detection and invent effective repair techniques to avoid aircraft accidents.

Several surface engineering repair techniques and processes have been proposed to improve the treated metallic material such as the SP and/ or the LSP [59]. The potential of using the SP and the LSP processing to increase fatigue resistance of the metallic material has long been documented in the aviation industry [138]. The beneficial effect of these techniques originates from the introduction of compressive RS profile closer to the surface region of the SP and/ or LSP-treated metallic materials. These processes result in strain hardening of treated surfaces which is beneficial to the mechanical properties of treated metallic materials. Compressive RS are key to producing high strength materials [2].

With softer metallic materials, which are treated with SP or LSP, strain hardening dominates [2, 139]. However, the presence of strain hardening can result in complete or partial relaxation of the compressive RS in these metallic materials. Strain hardening has the effect of decelerating microcrack growth, but accelerating propagation of long cracks due to low residual ductility [140, 141]. However, the benefits of compressive RS can be compromised due to the formation of cracks on the subsurface of high strength materials [2, 142]. This is particularly evident in sections where residual stresses balance the compressive residual stress field [2, 142].

SP processing suffers from the pronounced roughness of the metallic surfaces compared to the LSP [2]. Surface roughness results in premature commencement and proliferation of short fatigue cracks due to localised “intensification of the far-field stresses” [2, 143].

It is evident that the processes of the mechanical surface treatment are not straightforward. There are examples where such treatment has had a negative effect on treated metallic materials [2, 143]. Therefore, investigation must be undertaken to establish the circumstances under which the SP and the LSP technique can be used to produce beneficial results on aluminium alloys particularly those used in the aviation industry.

2.12. Purpose of the Study

The study explores the effect of varying processing parameters for the SP and the LSP processes and their effect on the induced compressive RS, surface roughness, microstructure and, microhardness in AA7075-T651 aluminium alloy. This alloy is currently used in various aerospace applications. This study further compares the SP and the LSP results. This is particularly important considering increasing interest in the use of the SP and LSP for aerospace applications.

2.13. Research Question

To evaluate the effect of using different sets of processing parameters for SP and LSP on the mechanical properties of AA7075-T651 aluminium alloy used in the aerospace industry.

2.14. Research Objectives

To evaluate the effect of the SP and the LSP processing parameters on AA7075-T651 metallic materials specifically, their consequences on:

- compressive RS state induced in the material;
- the surface roughness of the metallic material;

- microstructure;
- microhardness,
- varying laser parameters and its effect on compressive RS;
- varying shot peening intensity on compressive RS; and
- A comparative study between the SP and the LSP processing on AA7075-T651.

The experimental approach used, and results found will increase understanding of the effect of varying processing parameters. This will also lead to robust and quality-control of the SP and the LSP processes. Furthermore, positive results will potentially extend the SP and LSP applications in preventative maintenance environment and as repair solutions. This will also lead to a controlled design solution for an innovative airframe and aircraft skin structures.

2.15. Assumptions

The following assumptions have been made:

(a) The compressive RS introduced by the SP or LSP will not relax partially or completely as a result of thermal ageing [144];

(b) Residual RS are useful for improving mechanical properties of the metallic material [12];

(c) Surface roughening is expected to decrease the mechanical properties of metallic components by encouraging earlier commencement and proliferation of fatigue cracks [12, 144];

(d) The SP and LSP processing improve fatigue strength of the metallic material due to induced residual compressive stresses;

(e) During destructive RS measurement:

   i. stresses are relaxed elastically upon material removal or cutting, and

ii. during material removal or cutting, no further stresses are introduced to the sample being investigated, or these stresses are small enough to not cause any significant change in surface displacements [58].

CHAPTER THREE

3. EXPERIMENTAL METHOD

3.1. Material Selection

Aluminium alloys are widely used in industry, with a large amount being in the aviation/ or aerospace sector. They are lighter in comparison to steel and other metals and, have higher material strength. Aircraft manufacturers continually innovate to reduce weight and produce lighter aircraft that are fuel efficient. This is achieved by using, amongst others, lighter but high strength alloys such as aluminium alloys. Pure aluminium on its own is a very ductile material and has a low melting point of 660 ºC; however, introducing precipitates into pure aluminium enhances its material properties to suit its desired use.

3.1.1. Industrial Applications

The AA7075-T651 aluminium alloy is used in the manufacture of aircraft-wing and skin structure of fixed-wing aircraft (Figure 3.1).

Figure 3-1 Boeing Aircraft: use of the AA7075 alloy in skin structure and aircraft-wing

The alloy is preferred for its good mechanical properties, low density and corrosion resistance [145].

The AA7075-T651 aluminium alloy is used in this study. It is a 7xxx series aluminium alloy and is also known to have high strength, good formability, and good weldability. The T651 in the aluminium alloy description shows that the alloy has been solution heat-treated, quenched, and naturally aged at room temperature. Table 3.1. shows the properties of the material.

Table 3.1 Chemical composition of AA7075-T651 (Weight percentage) [146].

Composition	Si	Mg	Cu	Mn	Fe	Zn	Ti	Al	Cr
Wt.%	Max 0.4	2.1-2.9	1.2-2	Max 0.3	<0.5	5.1-6.1	Max 0.2	87.1-91.4	0.18-0.28

Note. Si = Silicon; Mg =Magnesium; Cu = Copper; Fe = Iron; Zn = Zinc; Zr = Zirconium. Adapted from "Chemical Composition of AA7075-T651," by Dif, R., Bès, B, Ehrström, J.C, Sigli, C, Warner, T, Lassince, P, Ribès, H (2000). Journal of Material. Science Forum, 331, 1613–1618.

High magnesium in the alloy allows for control, recovery, recrystallisation, and grain growth of the strengthened precipitate [146]. The silicon in the alloy helps to increase its strength. Table 3.2 shows a summary of the material properties of the 7075 aluminium alloy. The inspection certificate for the 7075 aluminium alloy with similar material properties used in this research can be found in Appendix C.

Table 3.2 Material properties for AA7075 -T651 [147], [148].

Material Property	**Value**	**Unit**
Hardness (Vickers)	175	
Ultimate Tensile Strength	405	MPa
Mass Density	2800	Kg/m^3
0.2% Proof Stress	480	MPa

Material Property	Value	Unit
Modulus of Elasticity	72	GPa
Shear Strength	331	MPa
Melting Range	475-630	°C
Yield strength	230	MPa
$K_{IC,}$ MPa$\sqrt{m}$	30.3[a]	MPa
Fatigue Strength	159[b]	MPa
Bulk Poisson's Ratio	0.33	
{311} Lattice Plane Modulus of Elasticity	69.0	GPa
{311} Lattice Poisson's Ratio	0.35	

Note. (a) by [147]. (b) at 500 million cycles K_t = 1, R = -1 [148].

This alloy material has ultimate and yield strength of 405 MPa and 230 MPa respectively.

3.2. Sample Preparation

Test samples were prepared from a rolled plate of 15mm thick AA7075-T651 purchased from NK Cuttings CC. The rolling direction was indicated with an arrow on the surface of the material. One millimetre was machined from one side of the plate to be used as the SP and LSP surface. This was done to ensure that the peening surface had consistent machining conditions. It was this face that was then used for the SP and LSP processing. To prepare samples for the SP and LSP processing, further machining was carried out on the opposite side of the peening surface (Figure 3.2).

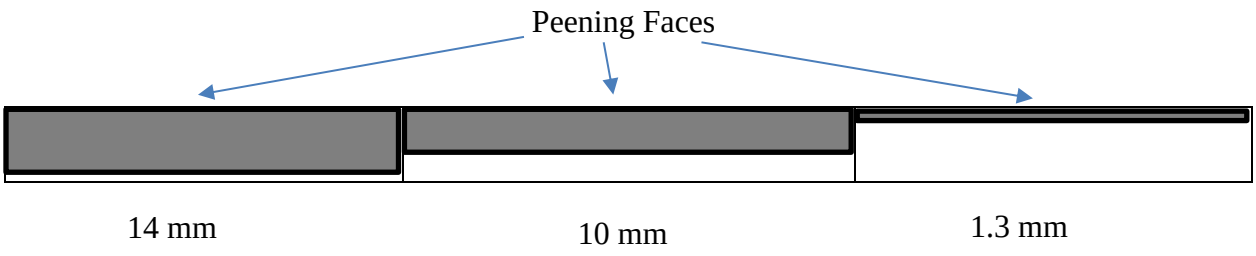

Figure 3-2. Preparation of samples for SP and LSP.

Final machining resulted in samples of 10 mm thickness. To prepare Almen strips, from the AA7075-T651, the thickness of the plate was further reduced to 1.3 mm thickness. These samples were to be used for SP intensity testing (Figure 3.2).

Figure 3.3 shows sample geometry for the SP and LSP processing as well as the Almen strip geometry.

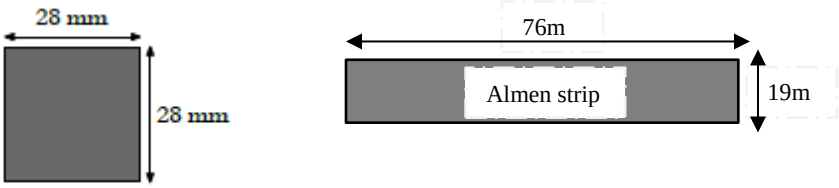

Figure 3-3. Geometries of samples for SP and LSP.

The first batch of the test samples of 28 mm x 28 mm x 14 mm of the AA7075 aluminium alloy specimens were then prepared (Figure 3.3). The second batch of the test samples, used as Almen samples of dimensions of 76 mm length with dimensions, 19 mm width, and 1.30 mm thickness, were also prepared [149].

3.3. Shot Peening and Laser Shock Peening Processing

The first batch of samples was split into two, the first pair was SP processed. The other pair was LSP processed. The SP and the LSP were performed at different facilities.

3.3.1. Shot Peening Processing

The South African Airways Technical (SAAT) robotically operated Shot Peening (SP) blasting chamber was used for the Shot Peening of AA7075-T651 samples. The equipment used is shown in Figure 3.4.

Figure 3-4. Robotically Operated SP Machine.

It has an area of 10 feet (approx. 2.048 m) wide by 12 feet (approx. 3.657 m) long and 14 feet (approx. 4.267 m) high. The machine consists of blast generators that deliver shots at a controlled feed rate through a blast nozzle, thereby shot peening the specimens. The SP machine was robotically operated under the supervision of a SAAT technician. SP parameters used in this study are shown in Table 3.3.

Table 3.3 Experimental Parameters for Shot Peening Processing of the AA7075-T651

Parameter	Value
Intensity (Almen)	12
Coverage (%)	100
Media Hardness (HRC)	45-50
Media Size (Cut Wire - Steel)	S230
Number of Nozzles	1
Cycles	6
Shot Peening Time (Minutes)	1.49
Flow Rate (per nozzle) kg/min	3.5
Pressure (kPa)	2000

Shot peening intensities were produced in accordance with SAEJ442 [150] and J443 [151] specifications by A-type strips. Table 3.4 gives SP conditions used to obtain different peening intensities.

Table 3.4 Shot Peening Parameters

Almen intensity (deflection of the Almen strip)	Pressure (psi)	Shot size (mm)
6.4A	6	CW-230
10A	12	CW-230
14.3A	24	CW-230

Note: Largest diameter shot sizes available on this type of machine.

In Table 3.4, peening intensities were selected are used at SAAT for maintenance of aircraft components such as the landing gear struts and wheel hubs. To validate the repeatability of results, three samples of each peening intensity were prepared. These samples minimized any errors

between and within sample collection. Statistically, a larger sample would have increased the validity of the results. However, due to timing and limited equipment accessibility, three samples were the balance. In the analysis, results were compared if data was spurious of outliers. A robotically controlled SP machine reduced SP process variability.

Almen strips are used in industry to measure SP intensity of the material. When the Almen strip is SP-treated, induced compressive RS causes the strip to bend or "arc" towards the peened side thereby producing an "arc height" (Figure 3.5).

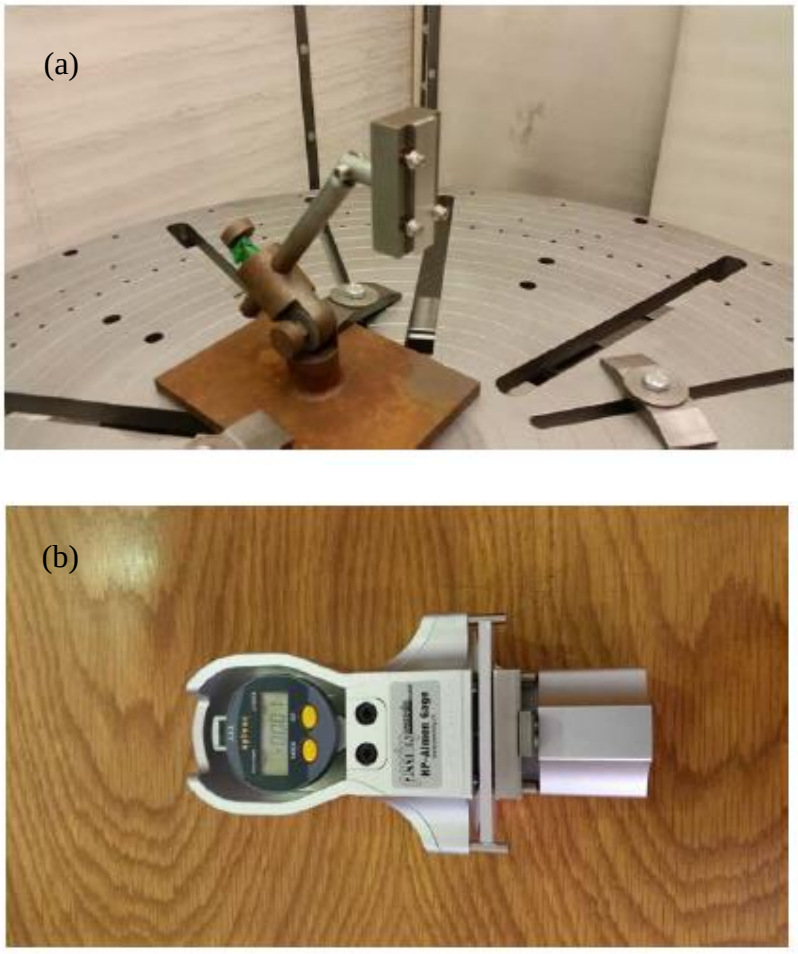

***Figure 3-5. Shot Peening of the Almen strip (a) Test Block used to hold Almen strip, and (b) Almen Gage* [18].**

Figure 3.5(a) shows peened material in the Peening chamber. To measure the "arc height" an Almen gauge is used across the length of the Almen strip (Figure 3.5(b)). The highest compressive RS are signified by the highest deflection point of the SP-treated samples. This position usually occurs in the middle of the SP-treated sample.

To ensure that the Almen strip test provides reliable and repeatable intensity verification, it is important that tests are conducted with samples of similar thickness, flatness, and hardness. In this study, "A" type Almen strips of SAE 1070 steel were used as reference measurement of coverage and exposure time due to SP processing. After 100% coverage had been reached using the "A" type Almen strip, the aluminium alloy 7075-T651 Almen strip (76 mm long, 3.98 mm thick and 19 mm wide) were SP-treated at the same intensity as used on the "A" -Almen strip. This procedure was followed to validate the transferability of the "A" type Almen Strip results to aluminium alloy 7075-T651 (Figure 3.5(a)).

3.3.2. Laser Shock Peening Processing

The LSP processing of test samples was conducted at the South African CSIR National Laser Centre (NLC). This is a state-of-the-art facility equipped with a laser facility shown in Figure 3.6 (a) and (b).

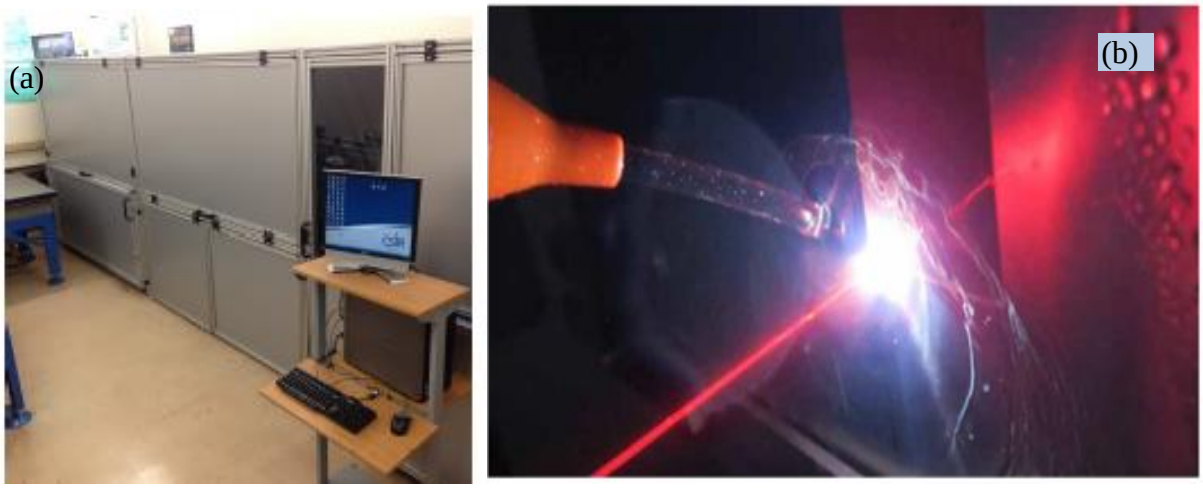

Figure 3-6. (a) National Laser Centre; (b) Laser Shock Peening processing **[152].**

The laser used by the NLC is the Spectra Quanta Ray PRO270 Q Switch Nd: YAG pulsed. The LSP testing was carried out at a laser wavelength of 1064 nm, and a frequency of 20 Hz [152]. As this equipment was available on a limited basis; it limited the number of test samples that could be used in this research.

3.3.2.1. Spectra Quanta Ray PRO270

The beam of the Spectra Quanta Ray PRO270 machine was focused to a pre-set spot size and targeted to the middle of the sample. The power output of the laser was kept constant (at Ep =450 mJ before the lens) to eliminate variations due to thermal lensing beam properties [152]. A thin layer of water of approximately 0.8 mm – 1 mm [152], flowing on the specimen surface, was applied through a spray nozzle. This was done to contain the laser thus generating a pressure-wave towards the depth of the specimen.

To study the effect of the LSP processing on compressive RS induced, surface roughness, microstructural changes, and microhardness, the following parameters were used:

- Effect of the Spot Size (SS) at a constant Pulse Density (Np).

- Effect of the SS at constant overlap/ or percentage Coverage, and
- Effect of percentage coverage and Pulse Density (Np) at constant SS.

To achieve these results the following laser parameters were used in Table 3.5.

Table 3.5 Laser Parameters used on AA7075-T651 samples

Sample Type	Pulse energy	SS (mm)	Np (pulse/mm^2)	C (%)
Sample 1	450	1.5	1.23	40
Sample 2	50.7	0.5	4.5	70
Sample 3	450	1.0	4.5	70
Sample 4	455.9	1.5	5	70
Sample 5	455.9	1.5	11.25	80
Sample 6	202.6	1	11.25	70
Sample 7	50.7	0.5	11.25	40

Note: Power intensity will remain constant at 3 GW/cm^2. Np = Pulse Density; SS = Laser spot diameter; C = Percentage Coverage.

To vary the Pulse Density Np, the raster speed and pitch of the LSP machine was changed in the X and Y axis directions respectively [152]. Percentage overlap or coverage was varied by increasing or decreasing the Spot Sizes.

To investigate the effect of coverage at constant pulse density (Np), three coverage or percentage overlap ranges were produced at three intervals of 40%, 70% and 80% whilst maintaining constant Pulse Density (Np), and Spot Size. These ranges have sufficient variability and can be compared with previous literature results [72].

Thirdly, to study the effect of the spot size, at constant Np, three Spot Size measurements were used of 0.5 mm, 1 mm, and 1.5 mm diameters. These diameters can be compared to previous studies [72]. Lastly, the effect of percentage (%) coverage and pulse density (Np) at constant spot size was studied by varying the above parameters, i.e., percentage (%) coverage and pulse density.

3.4. Residual Stress Measurements

RS measurements were performed using two types of techniques: increment hole drilling tests and the X-Ray Diffraction tests. Both techniques are discussed in this section.

3.4.1. Incremental Hole Drilling Testing

Residual stress measurement were performed using the SINT MTS3000 incremental hole drilling instrument [69]. The machine uses a high-speed end mill with a drill bit at the end. The experimental test setup is shown in Figure 3.7.

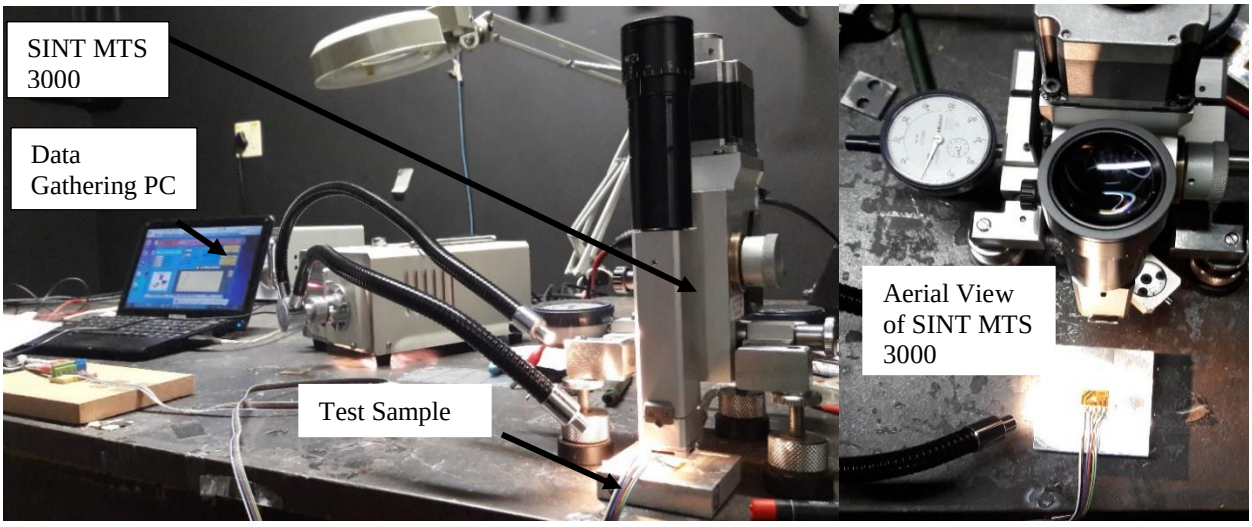

Figure 3-7. SINT MTS 3000 incremental hole drilling instrument, (a) hole drill and data laptop for data capture, (b) Aerial view of the hole drilling machine with the drill.

A diameter hole of 5.13 mm was drilled through the target point of the strain gauge rosette. Incremental readings were taken of the relaxed strains within the SP and LSP-treated samples for each test cycle. As the direction of the principal stresses on the test sample are usually unknown, the CEA-12-062UL-120 strain gauges were used (Figure 3.8).

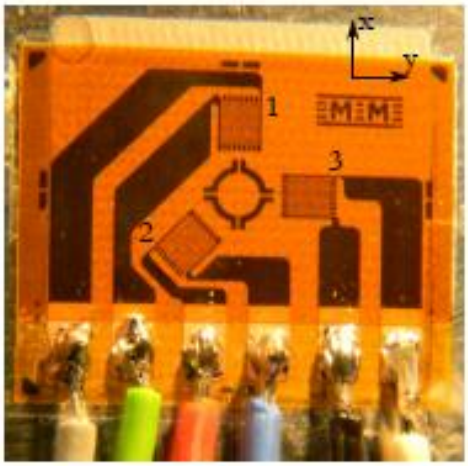

Figure 3-8. CEA-12-062UL-120 Strain gauge rosette.

These strain gauges consist of three independent strain gauge rosettes oriented at 60° and 120° away from each other from the first grid. These measure strains in different directions [73]. The orientation of the strain gauges allowed for the computation of compressive RS up to 1 mm depth in the sample material [67, 100]. Several factors were considered when selecting the strain gauge rosette for each application [73]. These included, amongst others, self-temperature-compensation number, backing material, gauge-length, and strain-sensitive alloy. Two other important factors were the rosette type and the rosette construction [73].

Drilling was conducted at 60 increments of 0.02 mm each and the reported stresses were as per the ASTM E837-13 EX [71] formulation for non-uniform residual stresses. The computation of compressive RS were performed using the RESTAN Eval Software. The following material properties were assumed for the AA7075 aluminium alloy, Modulus of Elasticity = 71.7 GPa, Yield stress = 405 MPa, and Poisson's ratio of = 0.33 [145, 153]. From these compressive RS, principal stresses were determined at each depth. Appendix E shows the Hole Drilling Machine specifications.

3.4.2. Laboratory X-Ray Diffraction Testing

Residual stresses measurements were carried out at NECSA using the Bruker D8 Discover Diffractomer shown in Figure 3.9.

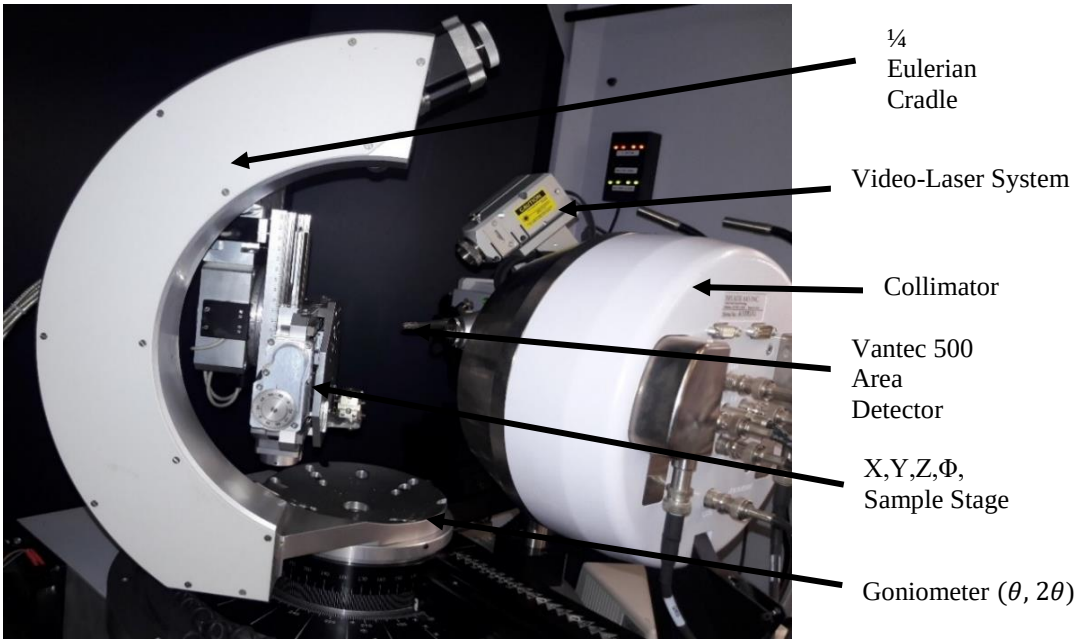

Figure 3-9. The Bruker D8 Discover instrument used for RS analysis on the Aluminium alloy.

The XRD machine is equipped with a Vantec 500 area detector. It also has X-ray 2 theta goniometer in a side inclined mode. This type of detector is usually used to perform analysis of residual stresses [154]. The machine consists of ¼ Eulerian Cradle: larger sections of diffraction cones can be collected with ease. Residual stress measurements are analysed in two orthogonal directions using the conventional $Sin^2\psi$ technique (where spacing at $\psi = 0°$ depicts the stress-free spacing (Figure 3.10).

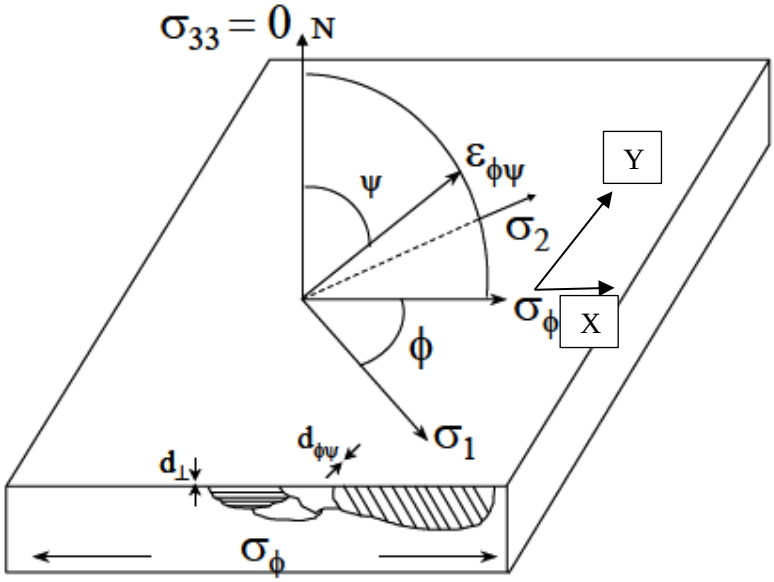

Figure 3-10 Diagram showing planes parallel to the surface, and at an angle $\phi\psi$. Note σ_1 and σ_2 both lie in the plane of the specimen **[155].**

In Figure 3.10, to change the ψ angle, the specimen is rotated about its ω-axis [156]. The ψ signify the angle of tilt of the sample being analysed from the surface normal. Measurements were taken in the middle of the section of the SP and LSP-treated surfaces. Several measurements were recorded at different ϕ orientations, at 0°, 45°, 90°,180° 225°, and 270°, where the ϕ angle is measured with reference from the x-direction. In computing residual stresses, elastic constants of $-S_1 = 2.83\text{x}10^{-6}$ MPa and $1/2S_2 = 11.89\text{x}10^{-6}$ MPa^{-1}, in accordance with ASTM E1426-94 [157], were assumed. At each ϕ orientation, lattice spacing measurement was taken at ψ angles and the 36 $d_{\phi\psi}$ was produced for each specimen. To validate the reliability of the results, measurements were taken at different surface locations and averaged [72].

The principal stresses were calculated for each test sample using the Equation 9.

$$\sigma_{\phi} = \sigma_{11} \cos^2\phi + \sigma_{22} \sin^2\phi + \sigma_{12} \sin 2\phi \quad (9)$$

Equation 9 calculates principal stresses at any given point of interest on the specimen. At this point, the component of the shear stress is zero, i.e., maximum stress and minimum in-plane stresses at a point. These principal stresses were used to complement principal stress values obtained at the surface of the material using IHD test results. The machine was calibrated in accordance with the ASTM E915-10 [158]. The parameters used in this research are provided in Table 3.6.

Table 3.6 Parameters for XRD compressive RS measurement

Perimeter	Description
$\kappa - \beta$ filter	Nickle
Anode Settings (kV)	40
(mA)	40
(2 - Θ)	137.5°
Goniometer	Θ -2Θ
Target Tube	Cu
Radiation	Cu-Kα1
Psi Tilt (ψ)	0.10 -60.10*
Azimuthal Orientation (ϕ)	0°, 45° and 90°
Aperture diameter (mm)	8
Counting Time. Frame (s)	200
Planes analysed (*hkl*)	(422)

*Note. *Degrees in steps of 10, giving 7 sample tilt angles. Adapted from "Determination of Residual Stresses by X-Ray Diffraction" by M.E. Fitzpatrick, A.T. Fry, P. Holdway, F.A. Kandil, J. Shackleton, and L. Suominen, 2005; 2; Middlesex, UK: National Physics Laboratory.*

Measurements of compressive stresses were limited to the near-surface regions of the material. The accuracy of residual stress measurement of the XRD technique is +/- 20 MPa [74]. The XRD depth penetration for aluminium is < 50 µm [154, 159], however, this penetration depth had to be verified as it is known to be prone to experimental errors. For example, maximum penetration of Cu source X-rays on Aluminium alloys has been reported as ~ 50 µm in the literature [154].

3.4.2.1. XRD Intensity for Residual Stress Measurement

Figure 3.11 shows typical XRD intensity vs Energy obtained from the LSP-treated material. The lattice plane for each peak is also shown.

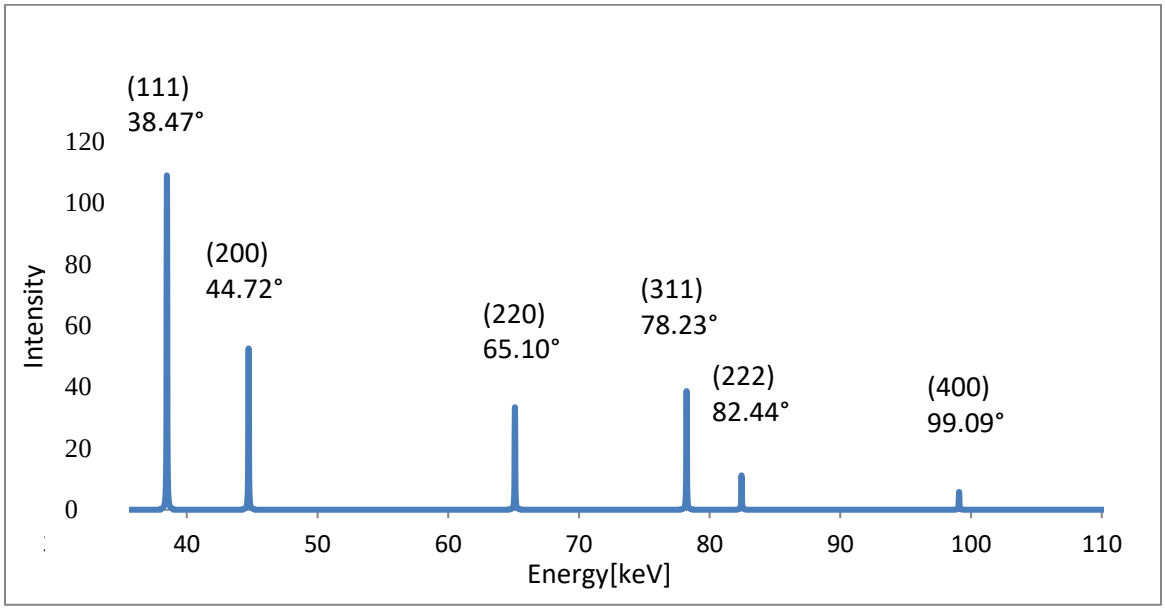

Figure 3-11. Data of the XRD-ED for LSP treated samples

In Figure 3.11, heights changed with the position and orientation of the sample signifying texture changes.

3.5. Surface Roughness Testing

Surface roughness measurement was conducted in accordance with the British Standard BS 1134:1988 [160]. In this research, the length of each specimen was divided into five equidistant segments. These segments were used to calculate the mean average of five surface roughness. To measure the surface roughness, each test sample was analysed using the Surface Roughness Tester TR220 shown in Figure 3.12 (a) and (b).

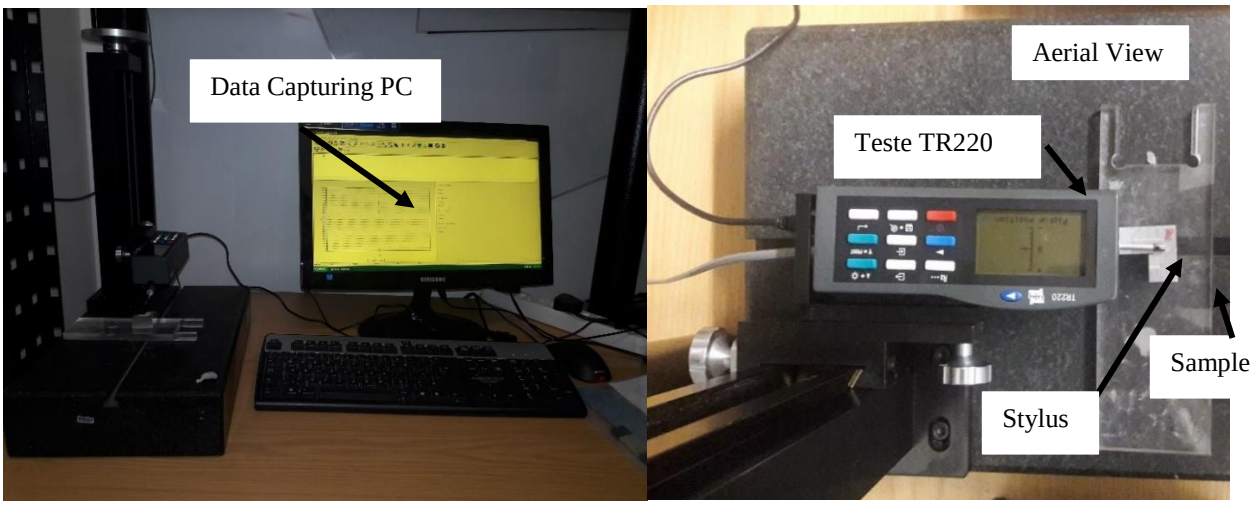

Figure 3-12. (a) Surface Roughness Tester TR220 and PC, (b) Aerial view Tester TR220 Surface Roughness Tester

Before performing actual tests, the machine was first calibrated. This was performed by dragging the stylus of the machine across the surface of the test block. A close approximation of the roughness height could then be calculated from the profile of the output chart of the software. Once calibration of the equipment had been verified, two tests were conducted for each specimen type. Table 3.7 displays calibration specifications for the Time TR220 machine.

Table 3.7 Specifications for the TR220

Parameter	**Values**
R_a Measuring Range (μm)	0.025-12.5
Resolution (μm)	0.01
Pick-up Measuring Range (μm)	80
Measuring Length	3L-7L
Evaluation length	1L – 5L
Cut-off Lengths (mm)	0.25, 0.8, 2.5, Auto

Parameter	Values
Minimum Driving Length (mm)	1.3
Radius of Stylus Tip (μm)	5

In this research, the evaluation length was set to 6L and the cut-off was set to 0.8 mm. Thus, the riving length was 4.8 mm. The first measurement was conducted on the unpeened surface. Readings of mean roughness, Ra and Rz, and peak height were recorded. These were measurements of the baseline surface roughness. The second test was conducted on the SP and LSP surfaces of the samples. The Ra and Rz and peak height values were also recorded. From both sets of readings, the characterisation of various surface attributes could be analysed.

3.6. Metallographic Testing

To conduct a metallographic analysis of the base material, SP and LSP, samples had to be prepared. Samples had to be sectioned, mounted to a resin and then polished to achieve a mirror finish. In this is research, hot-mounting was preferred as this enabled the use of SEM for microstructural analysis.

3.6.1. Sectioning of Sample

The samples were cut using the Buehler IsoMet cutting machine shown in Figure 3.13, at the School of Physics at the University of Witwatersrand. The Buehler IsoMet machine is fitted with a diamond-tipped blade.

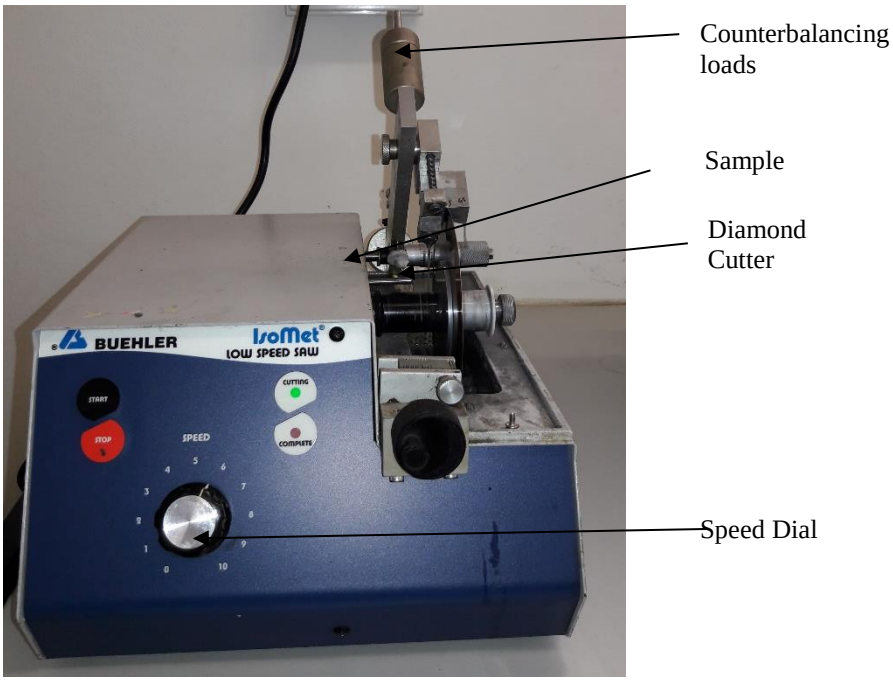

Figure 3-13. Cutting machine Buehler IsoMet.

This machine has a speed dial which can be adjusted to vary the speed of the cutting blade. The machine was set at a low speed of 3 rpm to avoid modifications of the specimen's microstructure due to the heat of the sectioning process. To further minimise the generated heat, the cutting blade was continuously lubricated during the sectioning using cutting oil solution. The machine's counterbalancing loads were used to control applied pressure to the sample. This further minimised damage to the surface of the test sample.

Figure 3.14 shows the sample marked in preparation for sectioning. The samples were first cut in the vertical direction through the middle. The right side of the sample was further cut in half to produce two-quarter samples.

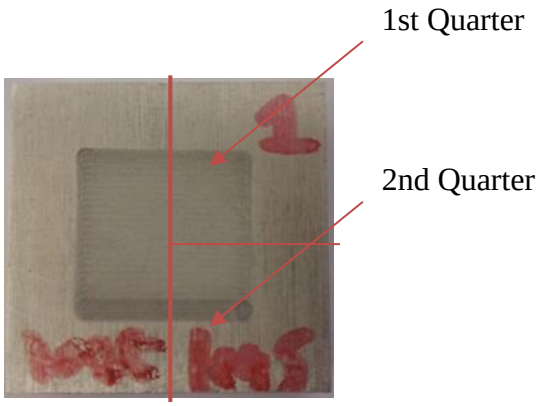

Figure 3-14. Sectioning of the Sample.

Two quarters to be analysed were marked "1st" and "2nd" as shown in Figure 3.14. The first quarter of the sample, from the SP and LSP, was used to analyse the surface roughness treated material. The second quarter of the sample was hot-mounted such that the cross-sectional area of the sample was exposed for microstructural analysis and microhardness tests.

3.6.2. Sample Mounting

Mounting enables better sample handling and minimises potential damages during polishing procedures. To examine microstructural changes and microhardness of treated materials, samples were then sectioned. Sectioned samples were then hot-mounted using the ALS OPAL 410 machine and PolyFast resin/ or compound. Hot-mounting the sample enabled the use of the scanning electron microscope (SEM) to conduct the microstructural analysis of the sample. The apparatus used for the hot-mounting process is shown in Figure 3.15.

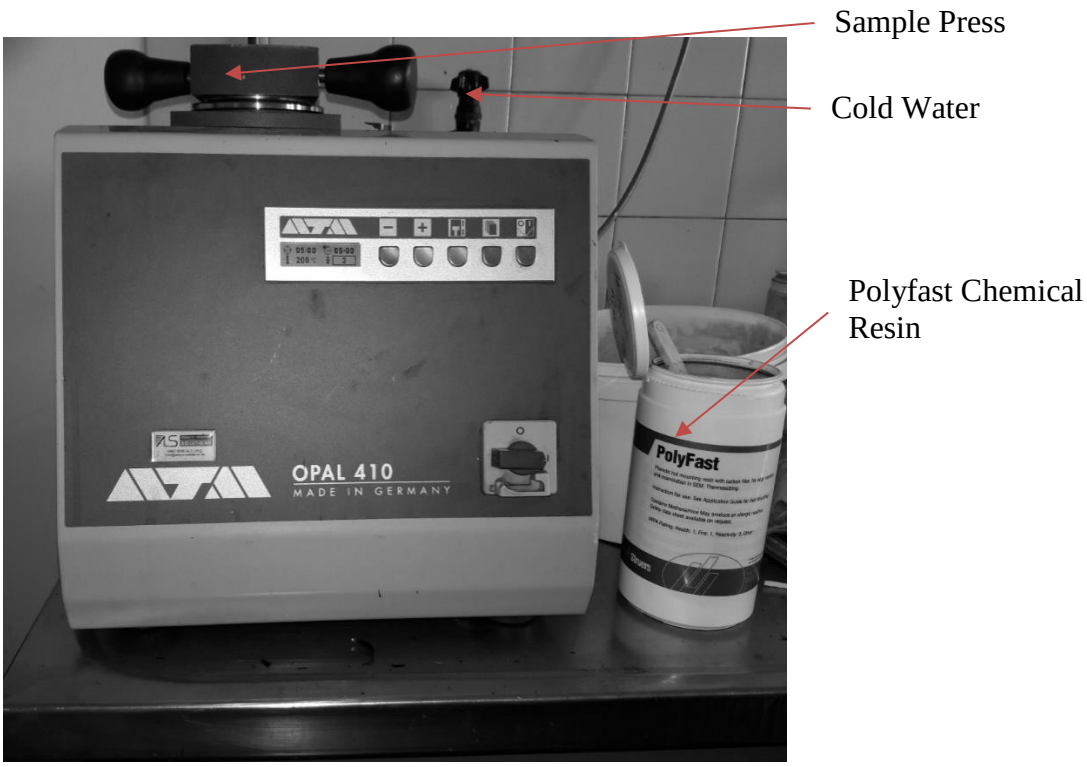

Figure 3-15. Hot-Mounting of samples using OPAL 410 Machine and PolyFast chemical resin mixture.

The surface to be analysed was placed faced downwards in the pot of the machine. The resin mixture was then poured over the sample. The mounting process was conducted at 200° Celsius and for 10 minutes per sample. Water was used to control the sample temperature during the mounting process to prevent microstructural changes. Figure 3.16 shows mounted samples of the SP and LSP-treated material.

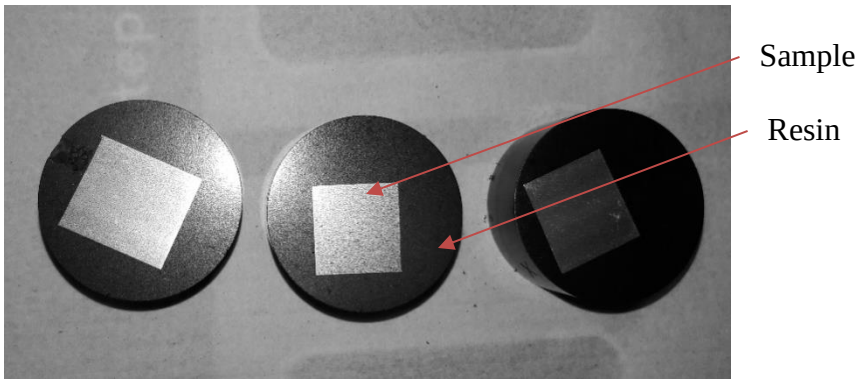

Figure 3-16. Resin mounted samples.

In this study, specimens were mounted for ease of handling during grinding, polishing, and etching steps. Mounting further provides proper specimen orientation and support for the mechanical test, e.g., microhardness testing.

3.6.3. Sample Grinding and Polishing

Test specimens were subjected to successive grinding and polishing steps to obtain a mirror finish with SiC paper of grit size 800 and 1200. Figure 3.17 shows the machine used to prepare the surface of the cross-sectioned sample.

Figure 3-17. Grinding and Polishing Machine.

Water was used during the grinding process to lubricate the ground surface and to remove debris. For each grinding process, a different polishing disc, and different suspension lubricant were utilised. This process was repeated to ensure uniform and smooth surfaces. Once the surface had been ground sufficiently, the samples were then polished using the polishing machine. Table 3.8 further outlines the procedure, and parameters used for grinding and polishing of samples.

Table 3.8 Grinding and Polishing of the specimens.

Phase	Procedure	Lubricant	Material type	Duration (min)	Force (N)	Speed (RPM)
1	Grinding	Water	800	3	10	130
2	Grinding	Water	1200	3	10	130
3	Diamond Polishing	DialDuo 9 µm	MD-Mol	6	10	150
4	Diamond Polishing	DialDuo 6 µm	MD-Mol	6	10	150
6	Polishing -Alumina Powder Solution	Water	LECO-Cloth pad	5	10	150

Note. N = Newtons; RPM = revolutions per minute; min = minutes.

The surfaces were then further polished using a LECO Alpha Alumina powder solution and pad to obtain a mirror finish. Soapy water was used to remove contaminants and thereby avoiding later cross-contamination from earlier polishing steps.

After the samples had been rinsed, they were cleaned with the ethanol solution, then dried up with a hair dryer, and examined for scratches and contaminants. The process was repeated if scratches and/ or contaminants were observed on the surface of the sample.

3.6.4. Etching of Samples

Etching is a controlled corrosion process used to reveal the microstructure of the metallic material. It is produced by the electrolytic action between surfaces of different potential. Potential differences are present between phases of different composition in multi-phase alloys [161]. Potential differences, due to etching, produce a controlled dissolution of the sample surface to reveal the sample grain structure of the metallic material [162].

Various chemical etching methods are used to reveal the microstructure of the aluminium alloys [64]; however, some of these methods do not always yield high grain boundary contrast [162]. The

Keller's reagent solution has been used successfully in exposing aluminium alloys microstructure [163]. Table 3.8 shows the chemical composition of Keller's reagent solution.

Table 3.9 Keller's Reagent and chemical quantities [163]

Chemical Constituent	Quantity (ml)
Hydrofluoric Acid	1.0
Hydrofluoric Acid	1.5
Nitric Acid	2.5
Distilled Water	95

Note. ml = millilitres. Adapted from "Development of Metallographic Etchants for the Microstructure Evolution of A6082-T6 BFSW Welds," by A. Tamadon, D.J. Pons, K. Sued, and D. Clucas (2017), Retrieved from https://www.metallographic.com/Etchants/Aluminum%20etchants.htm

In this research, specimens were etched by gently agitating them in the Keller's reagent solution for the 20s. Figure 3.18 shows a sample being etched in the Keller's reagent.

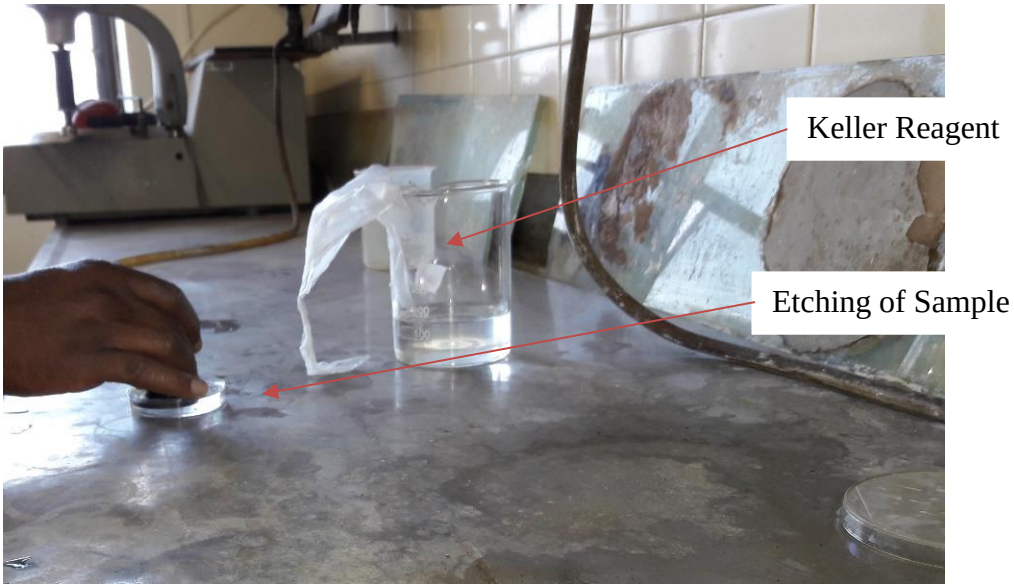

Figure 3-18. Etching of the AA7075 samples.

After the samples have been etched, they were then removed and rinsed with warm water and cleaned with ethanol solution. This process was repeated until grain boundaries were evidenced

under the microscope. Where over-etching had occurred in a sample, it would be re-polished and re-etched with the Keller's reagent solution and again examined under the microscope.

3.7. Microstructure Analysis

Analysis of the microstructural changes of the SP and LSP specimens was conducted at the University of Witwatersrand Microscopy Unit using a Zeiss Sigma SEM. The microstructure of treated and untreated material was assessed (Figure 3.19).

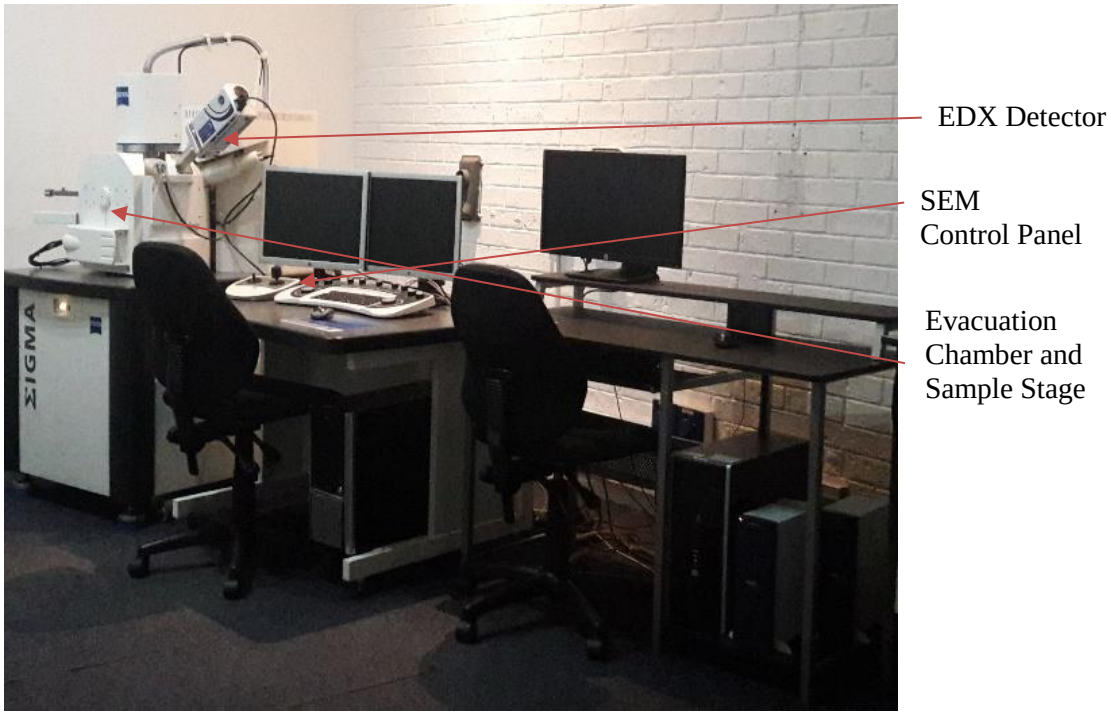

Figure 3-19. Scanning Electronic Microstructure (SEM)

Four points were scanned at various positions on the surface of the aluminium alloy sample. Effects of the SP and LSP techniques on the microstructure of treated specimens were then compared with untreated specimens to better understand the two processes. The SEM/ EDS chemical microstructural analysis technique was used to understand the elemental composition of untreated and treated sample material.

3.7.1. Microstructural Processing

Microstructural images were taken at different microscopic resolutions (by taking SE2 and BSD images at 100x and 5000x) to verify any macroscopic changes in the grains of the material. To ensure that accurate inferences could be drawn about the effects of the LSP and SP processing, in the treated materials, both samples were analysed at the same microscopic resolution. SEM images were taken at the following locations:

- Base material (without SP/ LSP)
- The SP or/ LSP area, and
- The border of the SP/ LSP and the base material

Cross-sectional area images were taken at different magnifications (200x, 500x and 2000x) on the border of the SP/ or LSP-treated material. The results of both tests were analysed.

3.8. Microhardness Testing

Microhardness tests were conducted on the surface of the test specimens using the Innovatest Falcon 500 Vickers Microhardness testing machine. The Vickers microhardness testing machine from the University of Witwatersrand Metallurgical Engineering Department was used and is shown in Figure 3.20.

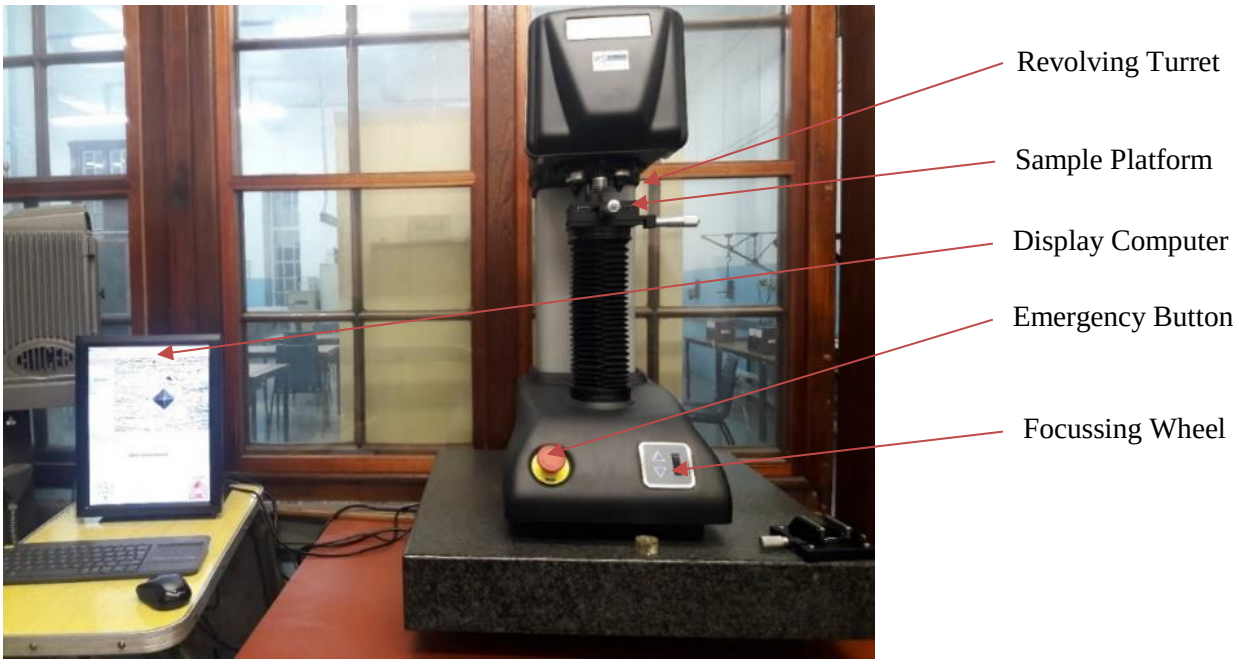

Figure 3-20. Innovatest Falcon 500 Vickers Hardness Tester [74]

In this research, microhardness testing was conducted as per the ASTM Standard E92-82 [164]. A load of 100gf was applied to the surface of the material using the hardness test machine with a diamond indenter and at a dwell time of 10 seconds. Upon the release of the load, a diamond shape indentation was left on the surface of the material (Figure 3.21).

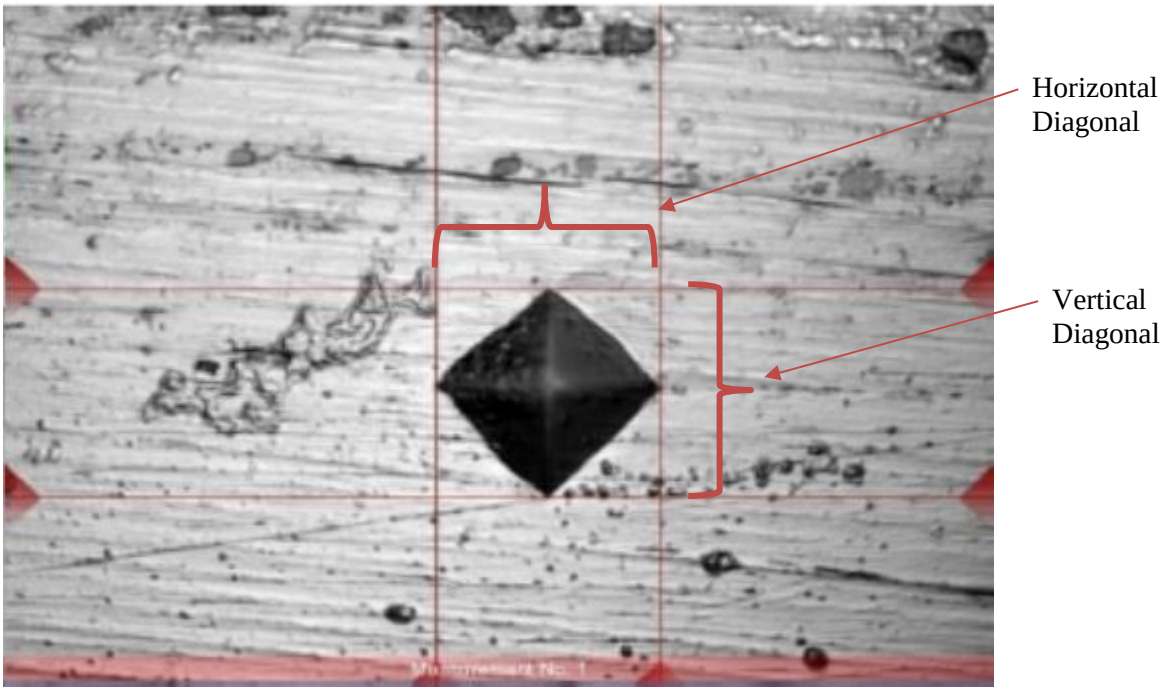

Figure 3-21. Typical Microhardness Results.

In Figure 3.21, the diamond shape was measured across the diagonals of the indentation. Eight measurements were taken from the surface of the cross-sectional area of the material and, gradually moving into the sub-surface of the material at increments of 0.1 mm. Points of microhardness measurements were then plotted and analysed. Appendix F shows the results of the SP-treated material microhardness raw data.

CHAPTER FOUR

4. Experimental Results and Observations

This chapter presents the experimental results undertaken as part of this research. Section 4.1. of the chapter presents the results of the compressive RS measurements using the IHD and the XRD diffraction techniques on the SP and LSP-treated AA7075 alloy material.

This is followed by a presentation of results of the surface roughness. The results obtained from the microstructural analysis of the LSP and SP-treated samples are thereafter presented. Lastly, the Vickers microhardness results of the AA7075 specimen are presented at the end of the section.

4.1. Residual Stress Results

In this section, test results of the SP and LSP-treated samples are reported. General observations are made on the SP and LSP-treated surfaces compared to the untreated material. This is followed by an analysis of the effects of changing SP intensities and its effect on the induced compressive RS. The results of the LSP residual stress measured are then plotted on various graphs.

4.1.1. Shot Peening on Residual Stress Results

It was observed that the intensity of the SP-treated samples influenced the texture of the surface. Results of peened Almen strip treated at machine pressure of 6 psi are shown in (Figure 4.1).

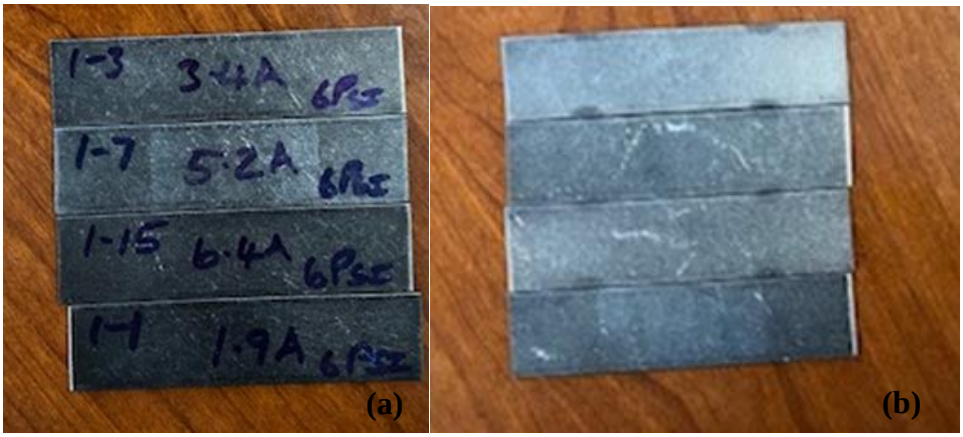

Figure 4-1. Almen strip peened at 6.4A (a) Unpeened Surface of the Almen Strip (b) Peened Surface of the Almen strip.

The Almen strip was shot peened on one side as shown in Figure 4.1 (b). Different peening intensity was achieved at different machine pressures. Figure 4.2, SP saturation curves were used to measure the saturation point for each peening process intensity. Varying peening intensities were produced at different peening pressures. In Figure 4.2, it is observed that the "arc height" increases with the magnitude of the SP intensity. The "arc height" correlates with the compressive residual stressing infused in material.

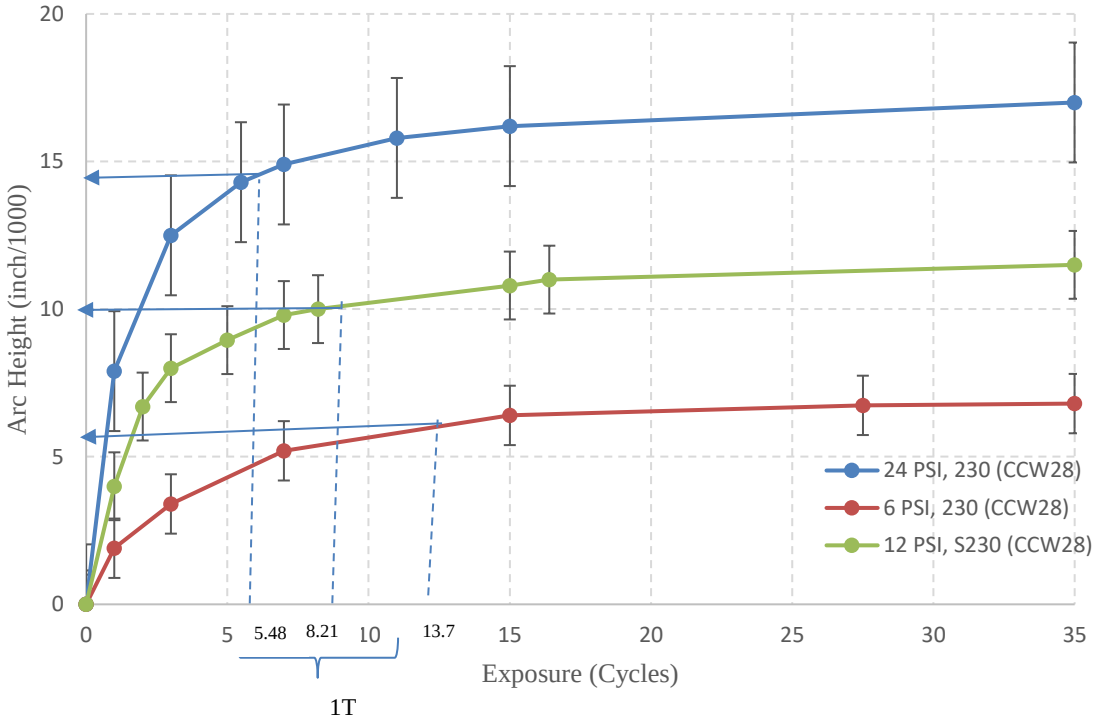

Figure 4-2. Shot Peening results using S230 (CCW28 Shots). The error bars represent the standard deviation of the arc height data. Each circle marker is obtained from the statistical average of three tests at each peening intensity.

Figure 4.2 shows that the 100% coverage is reached at various points of saturation for the respective SP parameters. The SP pressure of 6 psi produces the lowest "arc height". At the SP machine pressure of 6 psi, saturation intensity was recorded at 6.4A, whilst at 12 psi, saturation reached was 10A and at 24 psi the corresponding saturation reached was at 14.3A. These peening intensities occurred at 100% coverage in the AA7075-T651 samples.

Figure 4.3 shows the results of different SP intensities produced at various peening pressures. The graphs display similar shaped slopes and reached their respective maximum values at different depths, i.e., 6.4A (at machine pressure of 6 psi), 10A (at machine pressure of 12 psi), and 14.3A (at machine pressure of 24 psi) at 0.075 mm, 0.125 mm and 0.125 mm respectively.

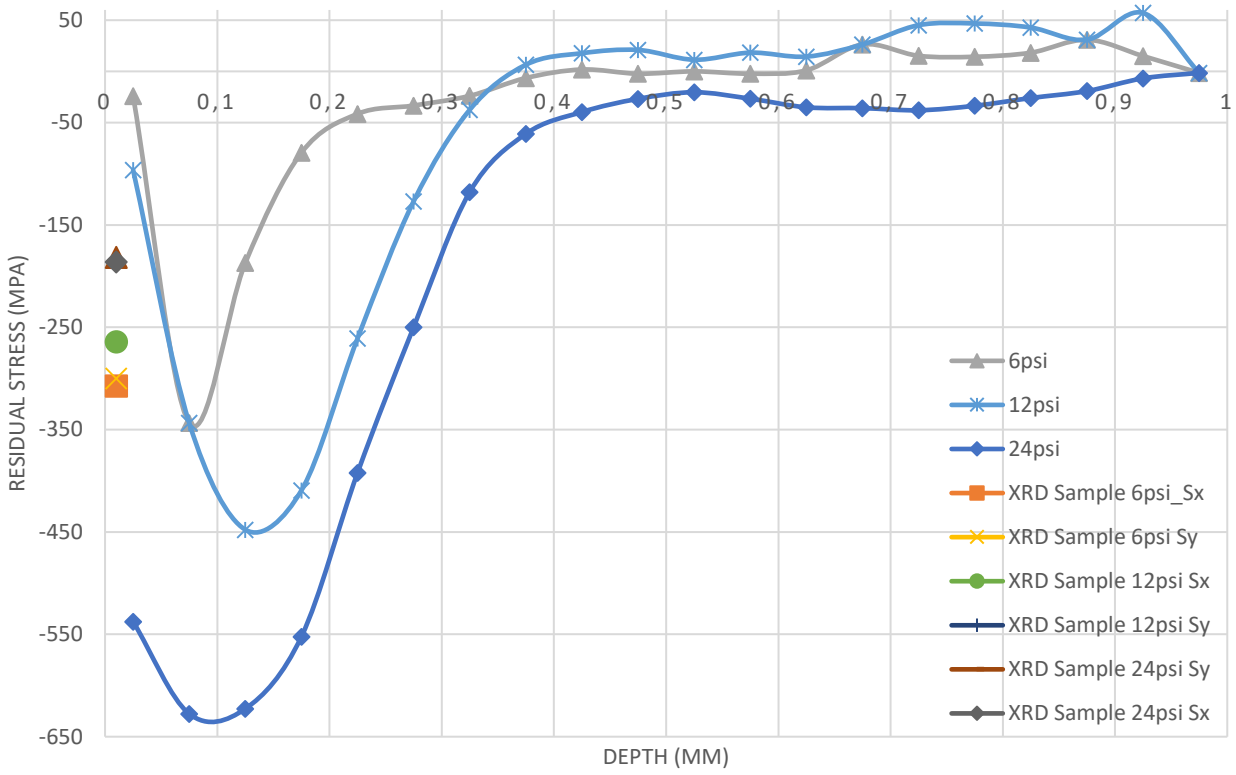

Figure 4-3. IHD Residual principal Stress Induced into the AA7075 by Shot Peening Process at different intensities compared with XRD results

It was also seen that samples had different hardening depths and different values of compressive RS. The maximum compressive stress level was generated below the material surface of the material. The highest maximum compressive stresses were obtained at an intensity of 14.3A and the corresponding depth of 75 µm, at an intensity of 10A and power pressure of 12 psi at -448 MPa and the corresponding depth of 75µm. The intensity of 6.4A and power pressure of 6 psi produced compressive RS of -329 MPa with a corresponding depth of 75 µm. The magnitude of the RS decreased as the depth of the compression layer increased. The compressive RS level was deeper at higher intensities. It could be seen that the surface stress produced by SP depended on the degree of the SP, i.e., peening parameters and the material properties of the treated sample. It was also seen

that the degree of the SP at 14.3A (at peening pressure of 24 psi) produced the highest surface stress level at -628 MPa at a depth of 75 µm and lowest at 6.4A (at peening pressure of 6 psi) at -329 MPa at a depth of 75 µm.

Results of residual stress values near the surface were estimated using the XRD technique. Using this technique, the residual stress values ranged between -185 MPa to -300 MPa. These values were within the band of the near-surface residual stress values obtained using the IHD technique.

4.1.2. Laser Shock Peening Effects on Residual Stress

In Figure 4.4 (a) and (b), the LSP-treated samples at different LSP peening parameters are shown.

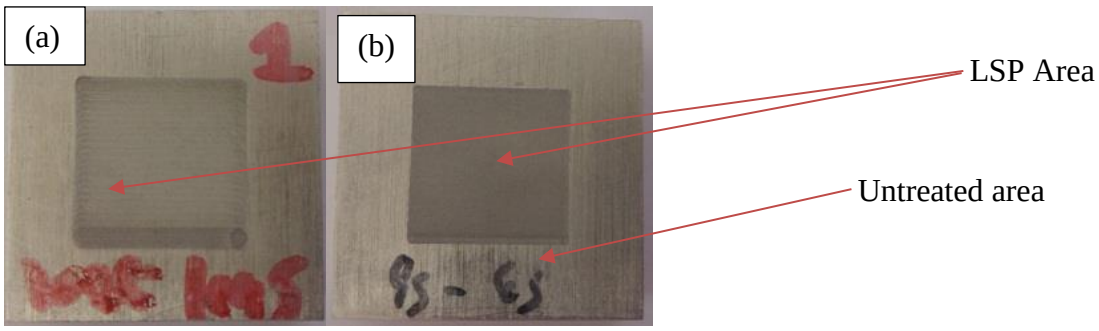

Figure 4-4. LSP of thick AA7075 Aluminium Alloy (a) LSP parameters for sample: SS= 1.5 mm (b) LSP parameters SS=0.5 mm.

There was no observable deformation of the sample surfaces after the LSP treatment. This could be due to the thickness of the material being treated. It was seen that the surface of the LSP-treated material at SS=0.5 mm was smoother than that produced by SS = 1.5 mm. Thus, the surface finish improved with smaller LSP spot sizes.

4.1.2.1. Effect of Coverage and Spot Size on Residual Stress

The results of the IHD test with changing LSP parameters, i.e., percentage coverage, Np, in spots/mm^2, spots size (SS) in mm, Power intensity in GW/cm^2, were plotted. The effect of the LSP on RS distribution and depth using IHD technique was analysed. The RS of samples No. 9 (Coverage of 40%; SS = 1.5 mm) and No. 13 (Coverage of 40%; SS = 0.5 mm), which were peened using LSP with spot sizes of 1.5 mm and 0.5 mm respectively at constant coverage, are compared (Figure 4.5).

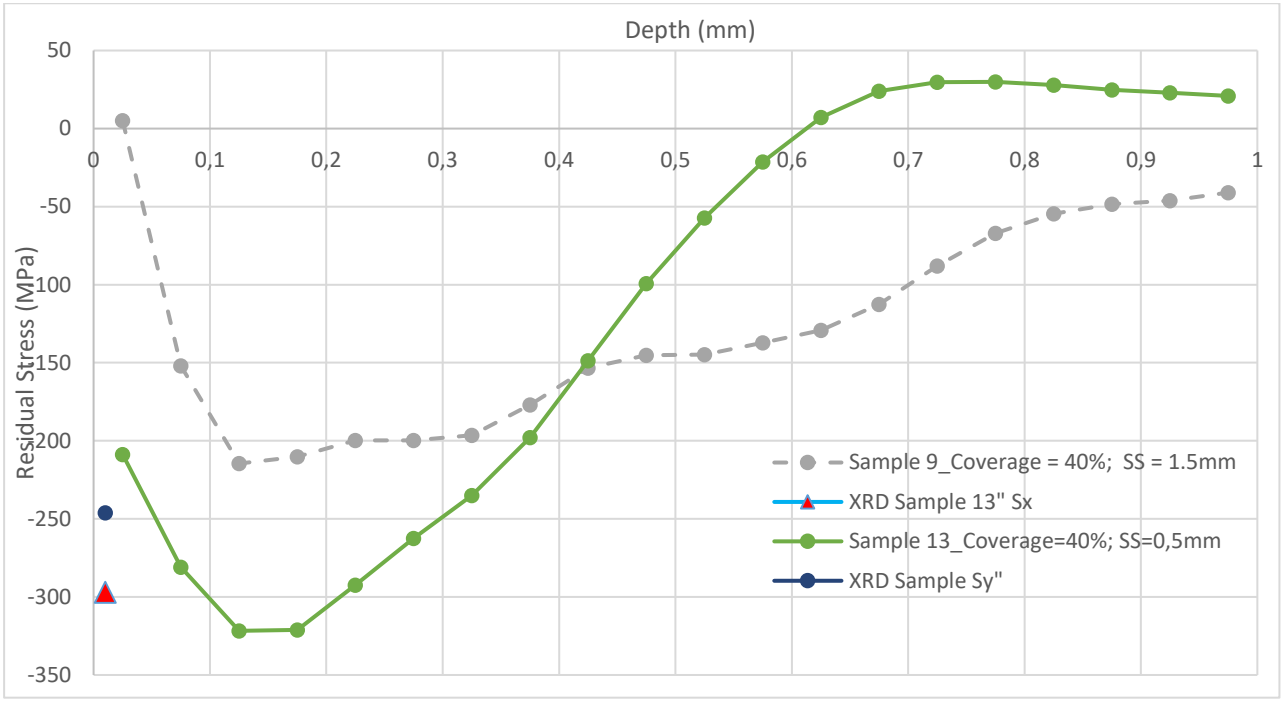

Figure 4-5. Effect of the Spot Size at constant Coverage using IHD Technique

It was observed that the curve of sample No. 9 (Coverage of 40%; SS = 1.5 mm) is flatter at the peak compared to the sample No. 13 (Coverage of 40%; SS = 0.5 mm). It can further be noted that decreasing the spot size does result in higher compressive RS. The spot size of 0.5 mm produced the highest compressive RS level of -321 MPa at a depth of 0.125 mm. At a spot size of 1.5 mm, the corresponding peak compressive RS achieved was -214 MPa and at a depth of 0.125 mm. The zero-depth, i.e., the depth at which the compressive RS turns to tensile, is reached at a depth of 0.625 mm in sample No. 13 (Coverage of 40%; SS = 0.5 mm) and deeper than in sample No. 9 (Coverage of 40%; SS = 1.5 mm). However, the depth at which sample No. 9 (Coverage of 40%; SS = 1.5 mm) turned tensile could not be determined due to drilling depth limitation.

The results of the surface XRD (conducted at NERSA) for sample 13 are also shown (Figure 4.5). These results show a good correlation with the results of the IHD at the near-surface depth of 0.01 mm. The principal stress levels using XRD were estimated at S_x = -297.2 MPa and S_y = -246.6 MPa at angle planes of -2.50° and 87.50° degrees respectively and at an estimated penetration depth of 0.01 mm.

The increase in spot size seems to result in widening of the peak compressive RS. This observation was confirmed amongst the samples with 70% coverage and different spot sizes, shown in Figure 4.6.

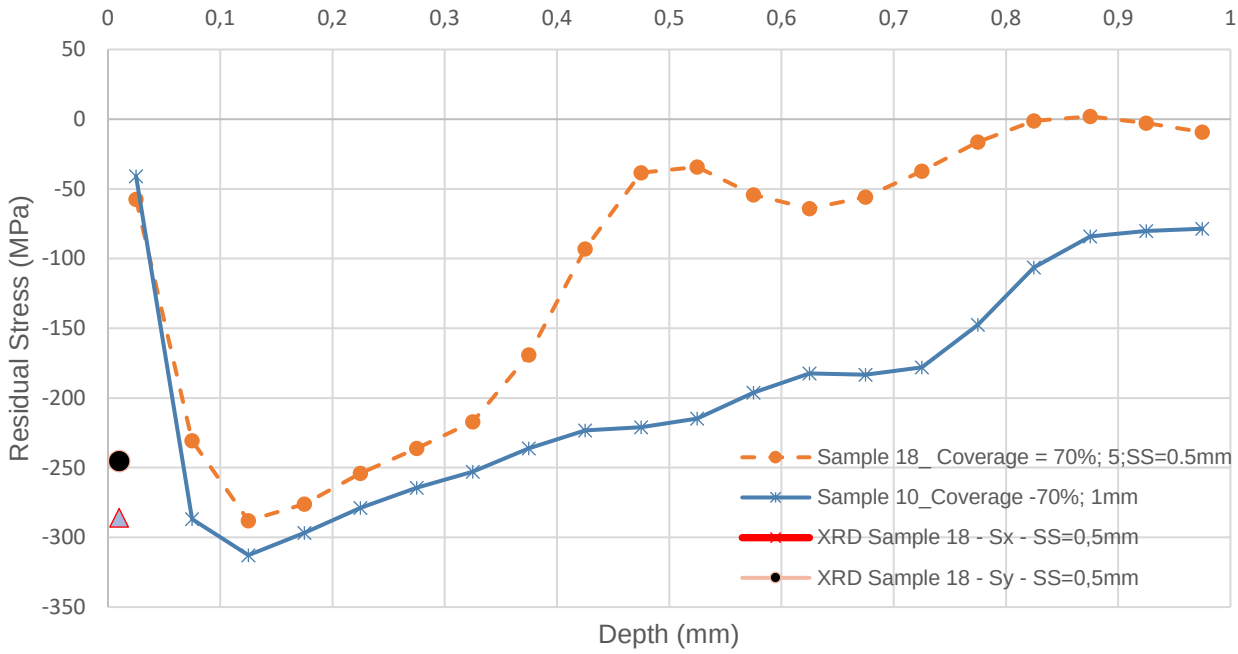

Figure 4-6. Effect of the Spot size at constant Coverage using IHD Technique

A peak was observed at approximately -312 MPa for sample No.18 (Coverage 70%; SS = 0.5 mm) and for sample No.10 (Coverage 70%; SS = 1.0 mm) at -288 MPa at a depth of 0.125 mm. However, the tension reaction of sample No.10 (Coverage 70%; SS = 1.0 mm) could not be determined due to drilling depth limit. If the graph of the sample No. 10 (Coverage 70%; SS = 1.0 mm) were to be extrapolated beyond the depth limit, the tension reaction could have been estimated at a value higher than 1 mm depth. Thus, zero depth seems to increase with the increase in spot size.

4.1.2.2. Effect of Changing Pulse Density on Residual Stress

The effect of changing Np at a constant spot size and constant power intensity is shown (Figure 4.7). The compressive peak RS value significantly increased (19%). This also resulted in an increased tensile reaction; i.e., the zero depth increased by (17%) when compared to increase in SS.

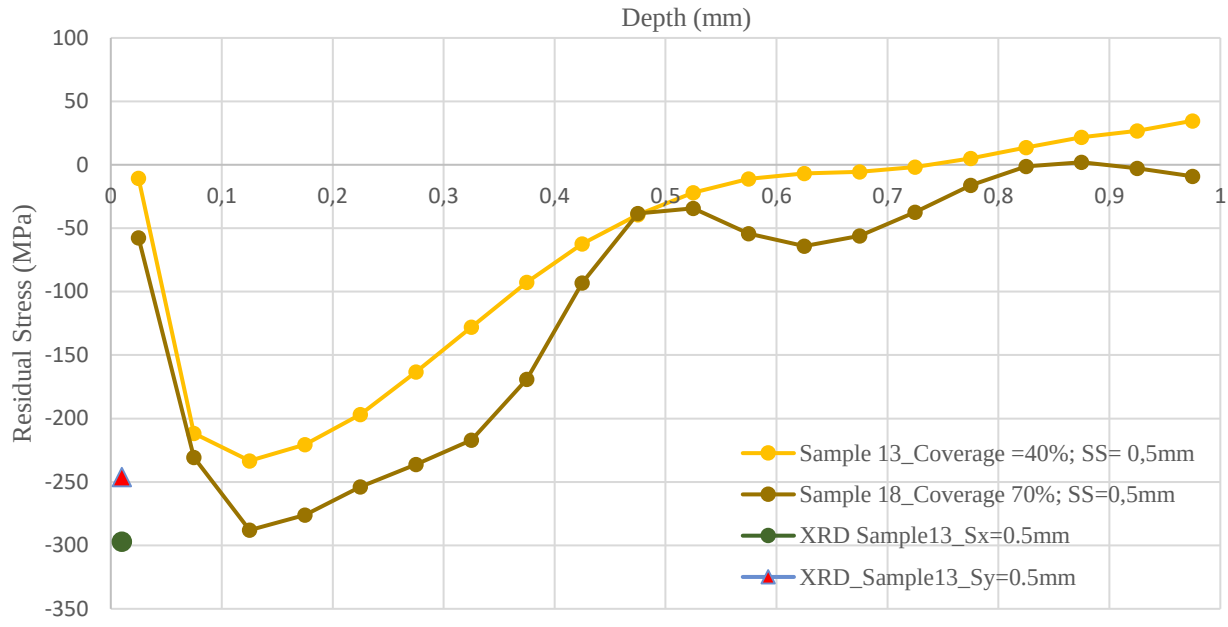

Figure 4-7. HD results of two samples using Spot size of 0.5 mm at different Coverages

There is an observed correlation between the change in coverage and resultant compressive RS induced in the AA7075-T651. It was further observed that an increase in coverage resulted in deeper compressive RS induced in the material. The RS distribution of the sample with 40% coverage is lower compared to the RS distribution of a sample with 70% coverage. Figure 4.8 further illustrates the effect of increasing the coverage for samples with a spot size of 1.5 mm.

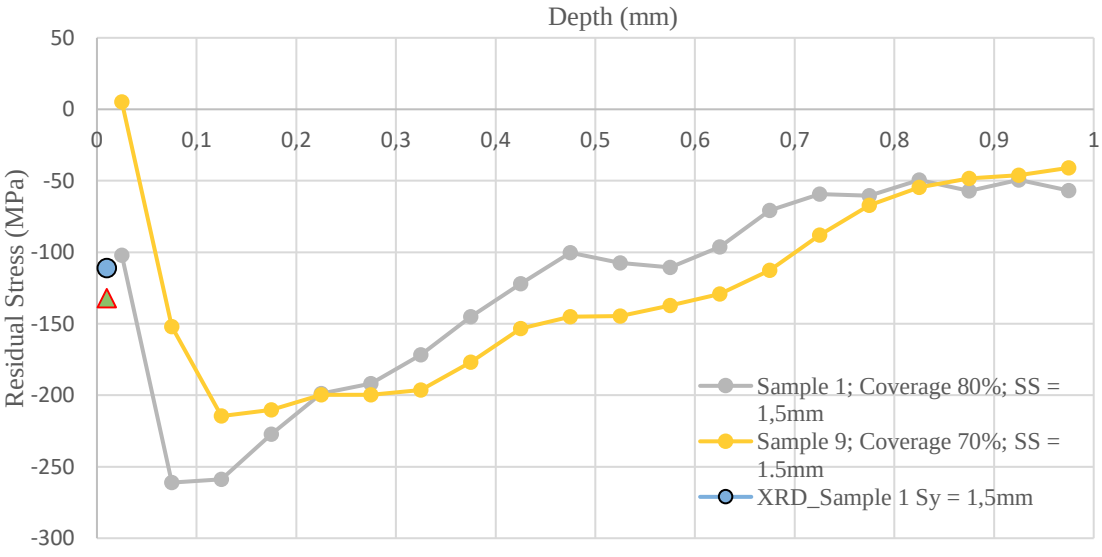

Figure 4-8. HD results for two samples using Spot size of 1.5 mm at different Coverages

In 1.5 mm diameter, an increase in the coverage results in increased peak compressive stress of (18%). This is due to the amplification effect due to the overlapping of laser spots. Where coverage is increased; the area of overlap increases, thereby resulting in higher magnitudes of residual compressive stresses. Figure 4.9 shows IHD results were spot size is constant and at different pulse densities (Np).

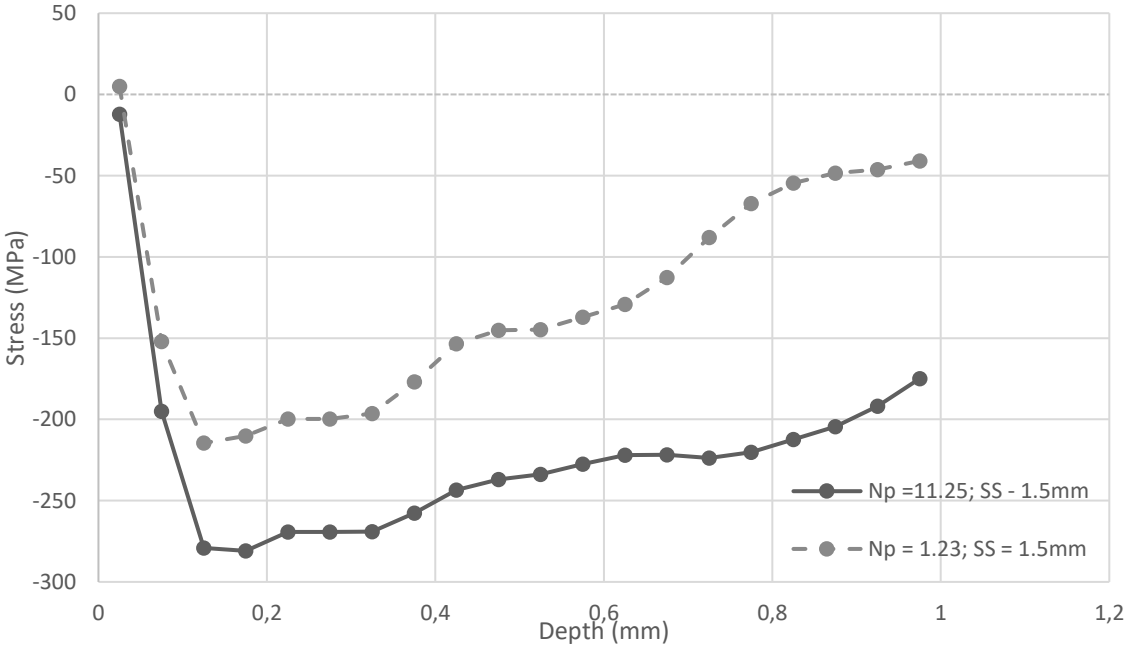

Figure 4-9. LSP changing pulse density at a constant spot size (SS) and power intensity

The compressive stress achieved at Np of 11.25 is approximately -279 MPa compared to -214 MPa at Np of 1,23. This translates to an increased compressive residual stress of approximately 23%. The compressive stress seems to increase with increasing Np. The effect of changing both coverage and spot size is shown below (Figure 4.10).

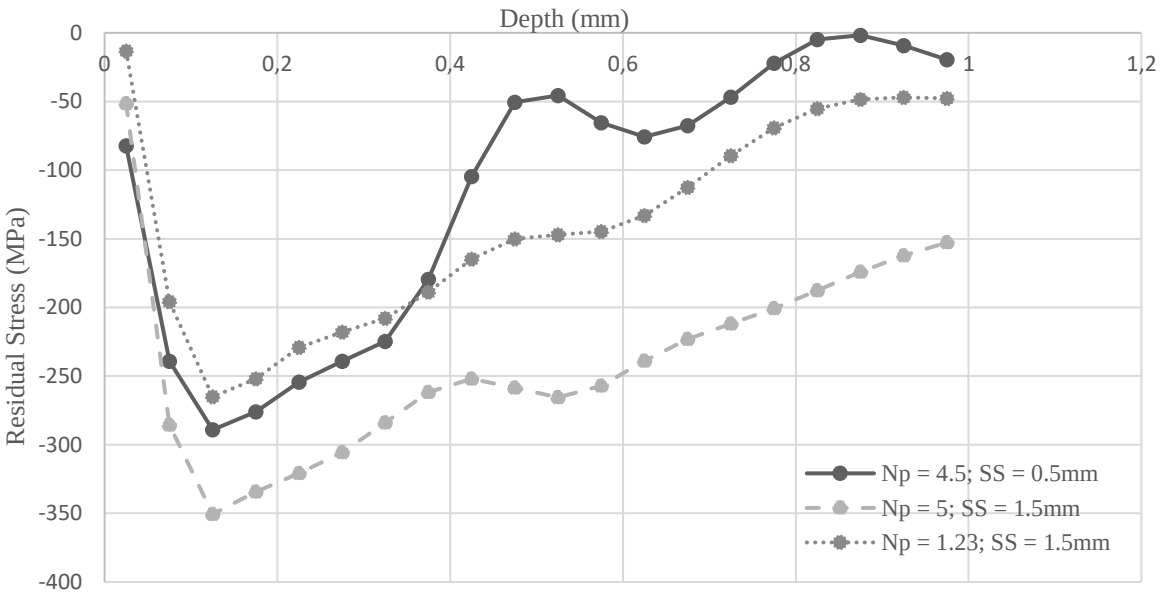

Figure 4-10. Change in Np and Spot Size at constant Power intensity

It can be observed that the highest compressive residual stress value is achieved at higher coverage and spot size, i.e., at a pulse density of 5 and spot size of 1.5 mm. The compressive residual stress value is estimated at -350 MPa. This further confirms the correlation between Np and corresponding compressive residual stress values achieved.

4.2. Surface Roughness Results

Test results of the SP-treated samples followed by the LSP-treated samples are reported in this section. Results of untreated samples and that of the SP-treated sample results for varying SP intensities are also reported. The results are tabulated in this section.

4.2.1. Shot Peening Effect on Surface Roughness

Results of the surface roughness obtained for the material using untreated and SP-treated samples are shown in Figure 4.11.

Figure 4-11. Surface Roughness of the SP at varies intensities

It is observed that the surface roughness increases with SP intensity. The SP surface roughness is highest in the SP-treated material at 24 psi compared to SP treatment at 6 psi and 12 psi. These results are confirmed by surface roughness measurements tabulated in Table 4.1.

Table 4.1 Surface Roughness obtained for different SP processing treatments using SP on AA7075

Sample	**Processing parameters**			**Surface (μm)**	**Roughness**
	Pressure (psi)	**Intensity (A)**	**Coverage (%)**	**Ra**	**Rz**
Untreated	-	-		0.066	3.046
Sample 1 Parameters	6	6.4	100	3.09	4.65
Sample 2 Parameters	12	10	100	3.94	4.02
Sample 3 Parameters	24	14.3	100	1.50	1.01

Notes. *Peening shot size used is S230 (CCW28).

The surface roughness of the LSP-treated specimens exhibit higher surface roughness (roughness arithmetic, Ra) compared to the untreated samples. The average roughness of the SP-treated sample at peening intensity of 6.4A (at machine pressure of 6 psi), 10A (at machine pressure of 12 psi), 14.3A (at machine pressure of 24 psi), was estimated at 3.51, 3.94 and 1.50 μm respectively. From the results, it can be seen that the Ra of the SP-treated samples increased with decreasing power intensity.

4.2.2. Laser Shock Peening Effect on Surface Roughness

The results of the surface roughness obtained for the material using untreated and the SP and LSP-treated samples are tabulated in Table 4.2. The surface roughness of LSP-treated specimen shows slightly higher surface roughness (roughness arithmetic, Ra) compared to the untreated samples.

Table 4.2 Surface Roughness obtained for different laser shock peening treatments using LSP on AA7075

Sample	**Processing parameters**			**Surface (μm)**	**Roughness**
	Np	**Spot Size (mm)**	**Coverage (%)**	**Ra**	**Rz**
Untreated	-	-		0.066	3.046
Sample 1 Parameters	11.25	1.5	80	2.01	5.5
Sample 2 Parameters	1.23	1.5	40	1.78	6.32
Sample 3 Parameters	11.25	1.0	70	1.59	5.54
Sample 4 Parameters	5	1.5	70	1.72	5.89
Sample 5 Parameters	4.5	0.5	70	1.46	6.25

Notes: Power was maintained at 3GW.

The average roughness in the untreated sample were estimated at 0.066 μm whilst the average Ra roughness after LSP using 0.5 mm, 1.0 mm, and 1.5 mm beam spot sizes at 70% coverage, increased to values of 1.46, 1.59, 1.72 μm respectively. The surface roughness increased with pulse density (Np) at a constant spot size (SS). It was further observed that the coverage increased the surface roughness of the sample at a constant spot size. The surface roughness of LSP-treated samples were lower than those of the SP-treated samples.

4.3. Surface Analysis and Microstructure

The composition of the AA7075-T651 was determined using the SEM Energy Dispersive X-Ray Spectroscopy (EDS). The results of the EDS spectrum for the AA7075 alloy composition are shown below (Figure 4.12).

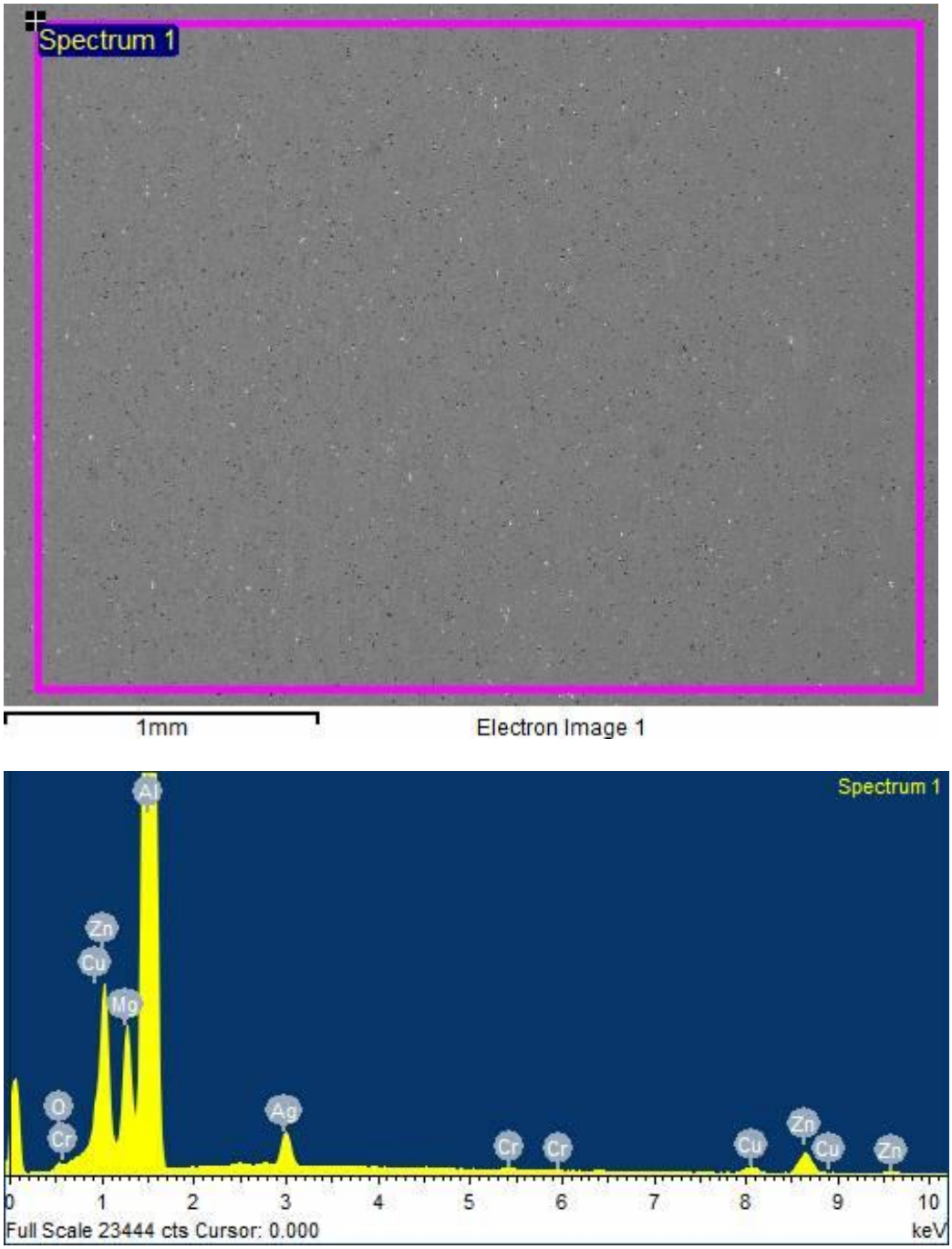

Figure 4-12. EDS Spectrum 1 for Alloy AA7075 specimens

In Figure 4.12, widespread Al(ZnCuMg) precipitates were observed throughout the cross-sectional area of the aluminium alloy. These precipitates were evenly distributed throughout the alloy. The mean average weight percentages of all the elements in the specimens were within the guidelines given by the Aluminium Association [165]. (Table 4.3).

Table 4.3 EDS mean average weight percentages of elements in AA7075-T651.

Element	C	O	Mg	Al	Cr	Cu	Zn	Ag
Weight percentage (%)	2.52	0.62	2.46	83.93	0.17	1.19	5.57	3.53

Figure 4.13 shows the microstructure of laser unpeened AA7075-T651 material. There are small, uniformly dispersed particles of the second phase precipitates shown by dark spots throughout the sectioned area.

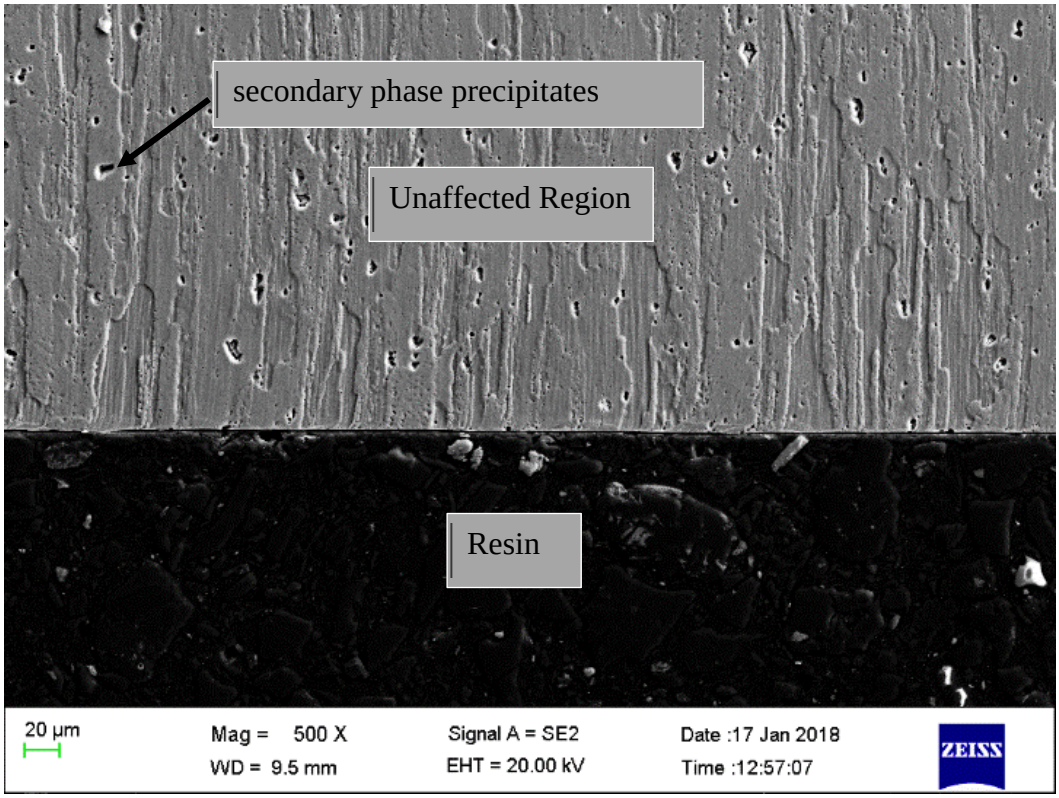

Figure 4-13. SEM cross-sectional micrographs of laser peened AA7075 surface before LSP at a magnification of 500X.

From the results shown, it is observed that the grains of the microstructure of untreated samples have a distinct pattern. This pattern extends to the surface of the material. Grains of the specimens are

visibly elongated in the same direction. This could be attributed to the mechanical rolling action used during processing of the plate.

To investigate the mechanical properties of the precipitates after LSP and SP, microstructural analysis of the cross-sectional area of the specimens was carried out just after polishing the sample. This allowed us to analyse the same areas with SEM technique. Figure 4.14 (a), (b), (c) shows manifests of periodic undulations corresponding to impact overlaps.

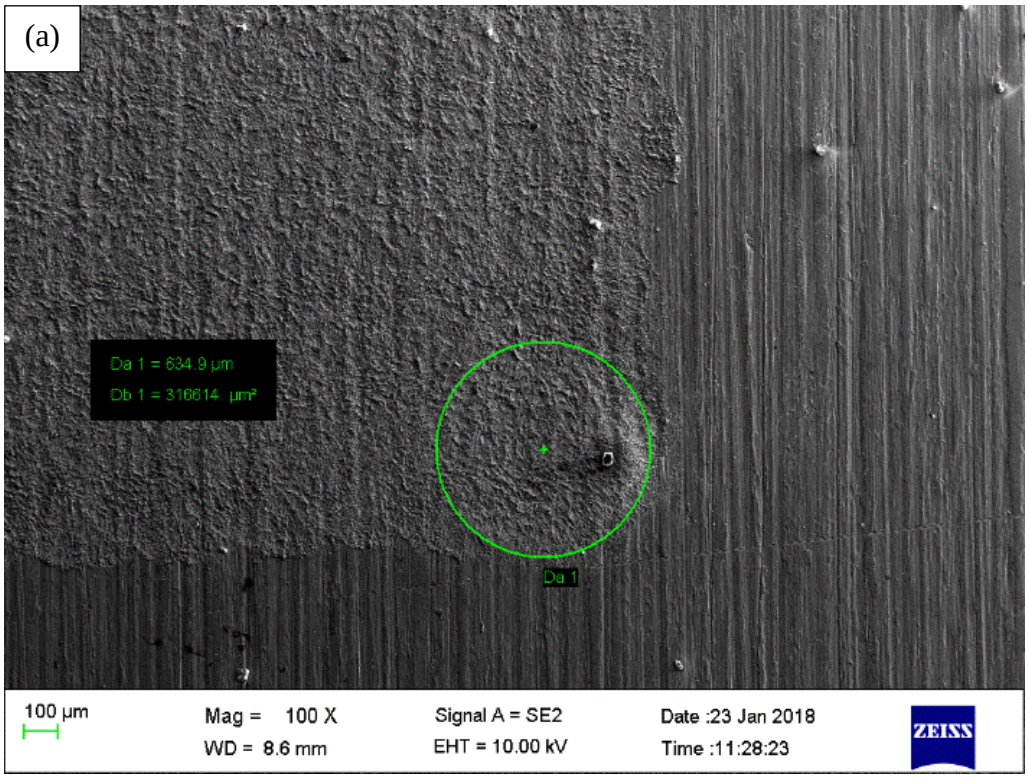

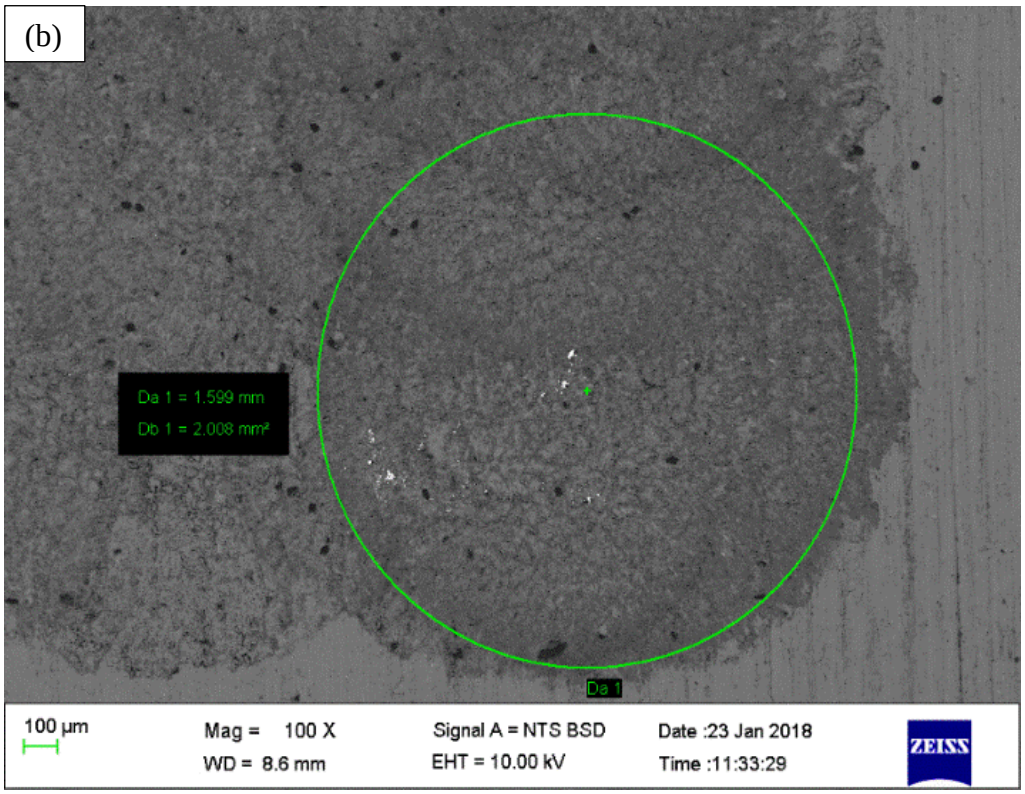

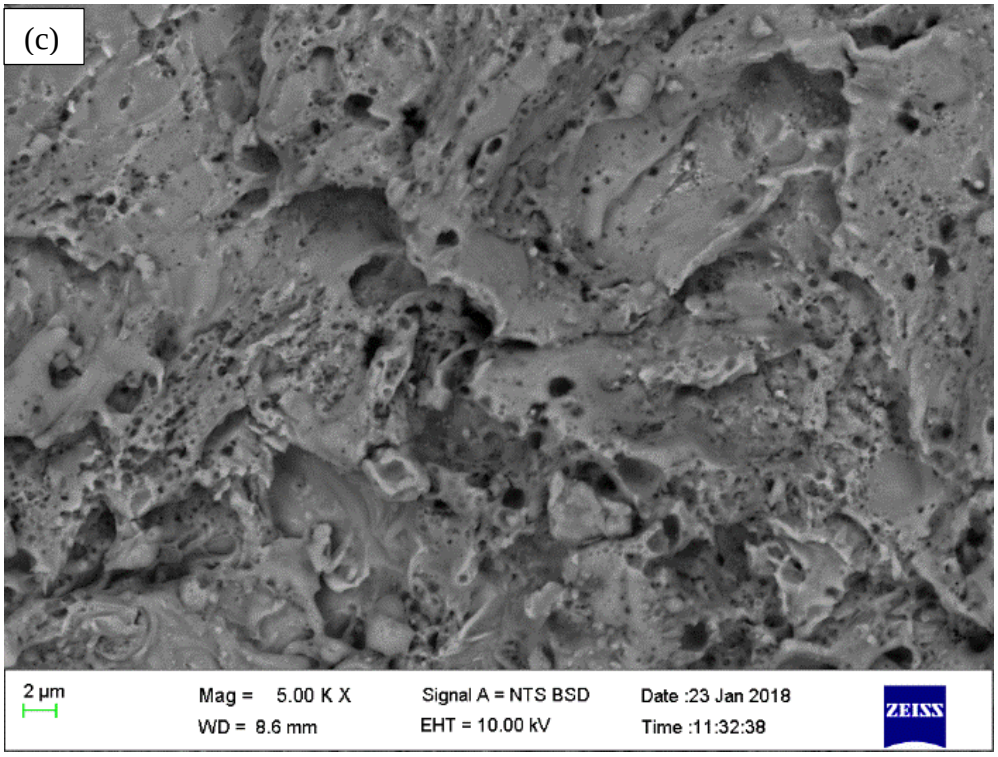

Figure 4-14. SEM micrographs of the LSP-treated surface (a), a spot size of the LSP at 100 magnification (b) spot size of the LSP showing overlap of the spots at 100 magnification, (c) feathery-like structure in the treated layer at a magnification of 5000 times.

These periodic undulations resulted in increased roughened surfaces of the treated material. However, no apparent microstructural modification by the LSP and SP were observed in treated specimens.

The melting effect in the LSP-treated material was also seen in the cross-section of the material. It was found at the near-surface of the laser treated surface and stopped at a certain depth within the cross-section of the material.

The cross-section area of the SP-treated sample is shown in (Figure 4.15).

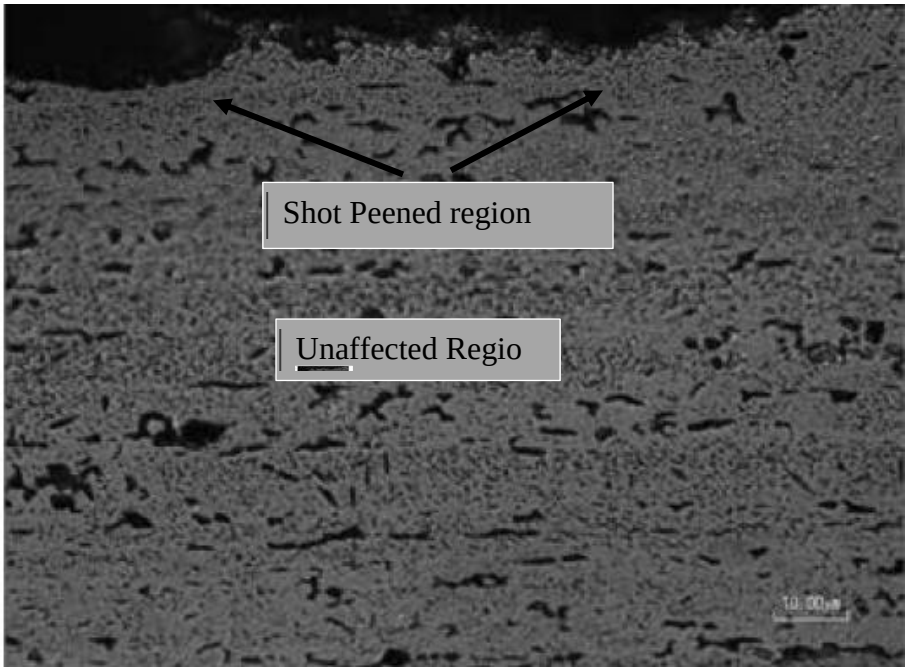

Figure 4-15. Cross-Sectional view of microstructure Shot Peened A7075-T651 at 500X.

These melted areas can be distinctly identified on the surface of the material. Figure 4.15 shows the effect of the SP on the surface of the material. Treated surface has undergone visible changes characterised by an uneven top surface. Figure 4.16 shows the LSP cross-sectional area at magnification of 500 times.

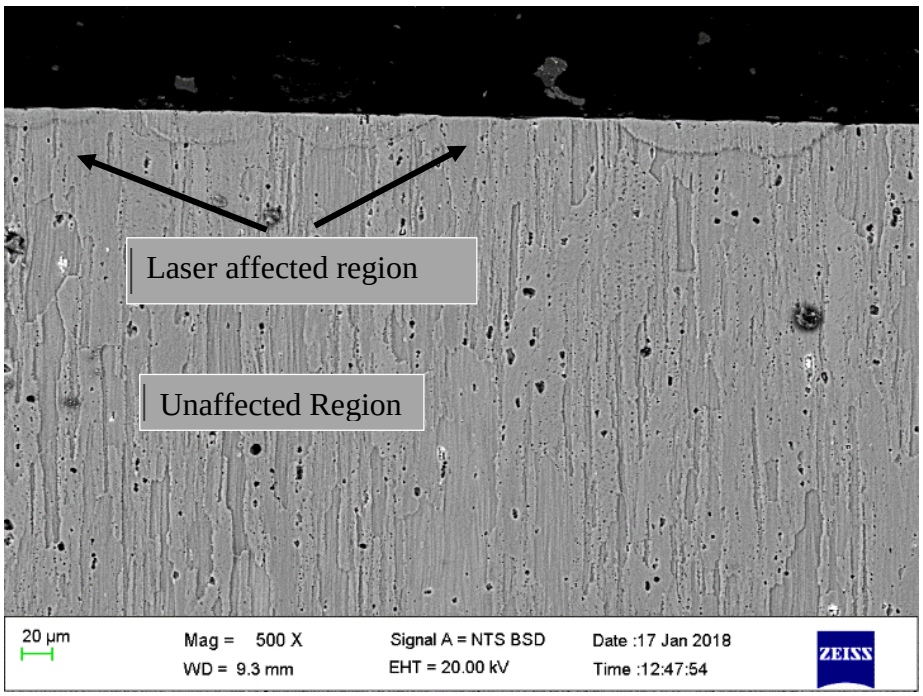

Figure 4-16. Cross-Sectional view of microstructure: (a) laser Shock peened AA7075-T651 at 500 Mag 500X.

It is observed that the LSP surface of the material has melted in areas that were exposed to the laser treatment (Figure 4.16).

The strengthening precipitates were observed by the SEM at a magnification of 200X are shown in (Figure 4.17).

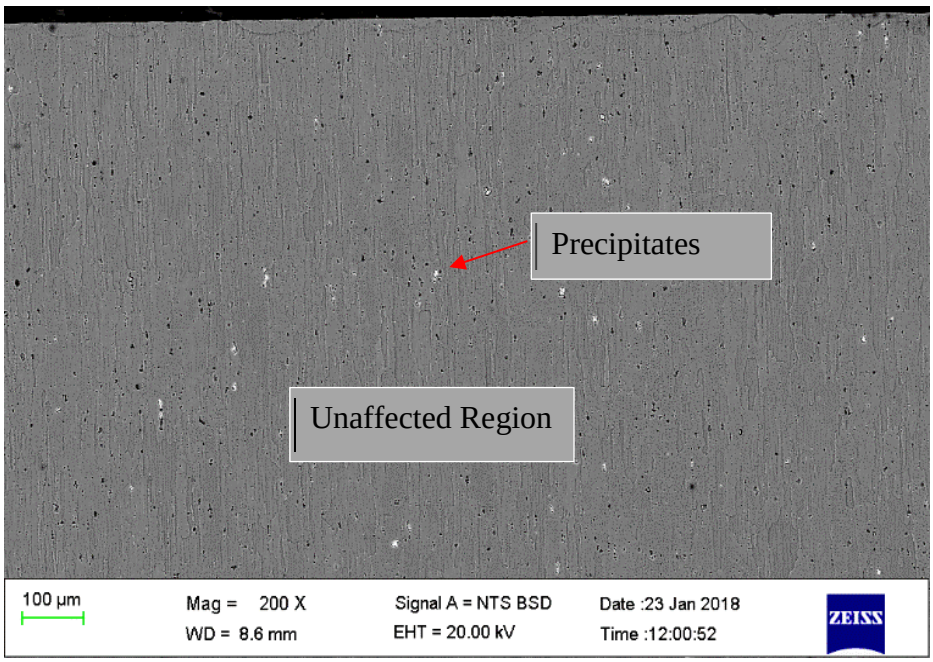

Figure 4-17. SEM cross micrographs of the AA7075 surface after LSP at a magnification of 200x times

The scan also showed precipitates throughout the material of the cross-section. At higher magnification (2000x), strengthening precipitates were more apparent. Secondary phase precipitates could also be seen in the microstructure of the sample. These are shown as darker spots in the cross-section of the material (Figure 4.18).

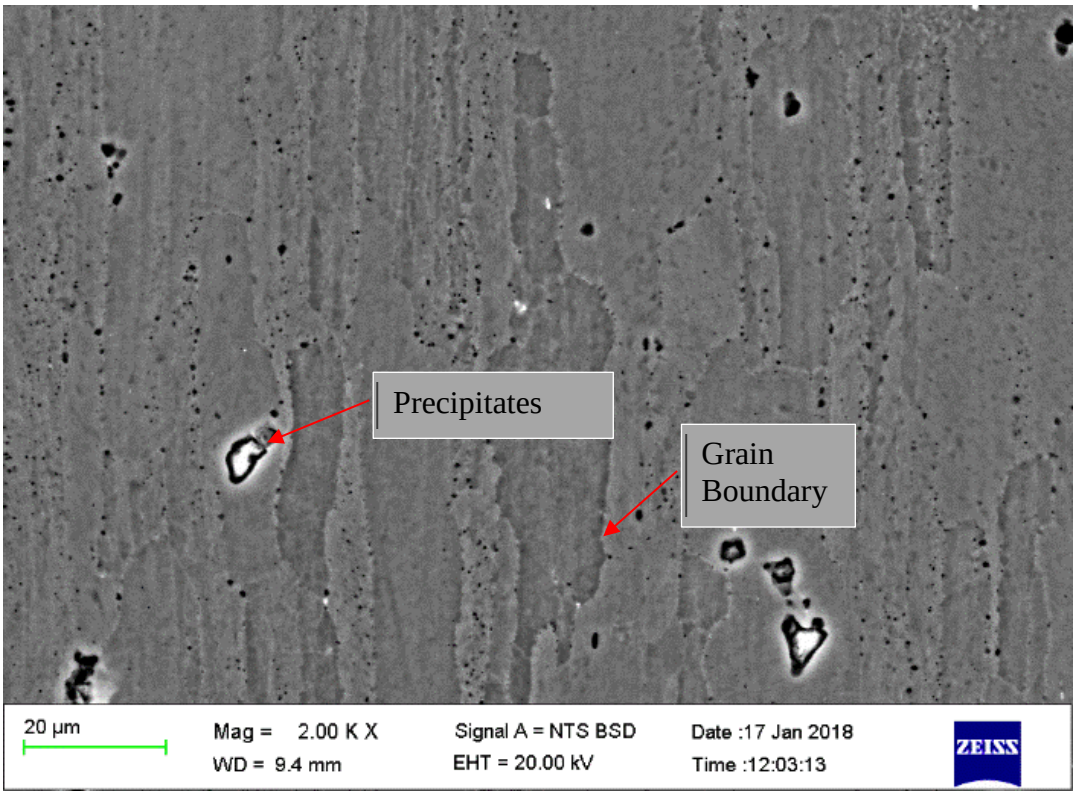

Figure 4-18. SEM cross-sectional micrographs of the AA7075 surface (b) after LSP at a magnification of 2000 times showing strengthening precipitates.

Figure 4.18 shows several populations of precipitates. These are shown with a distinct white colour throughout the cross-sectional area of the material. The precipitates are oriented in the rolling direction of the plate. The LSP changes the topography of the treated surface; microstructural grain boundaries in treated areas are not distinguishable unlike in untreated areas. The depth of the affected areas can be measured at higher magnifications (Figure 4.19).

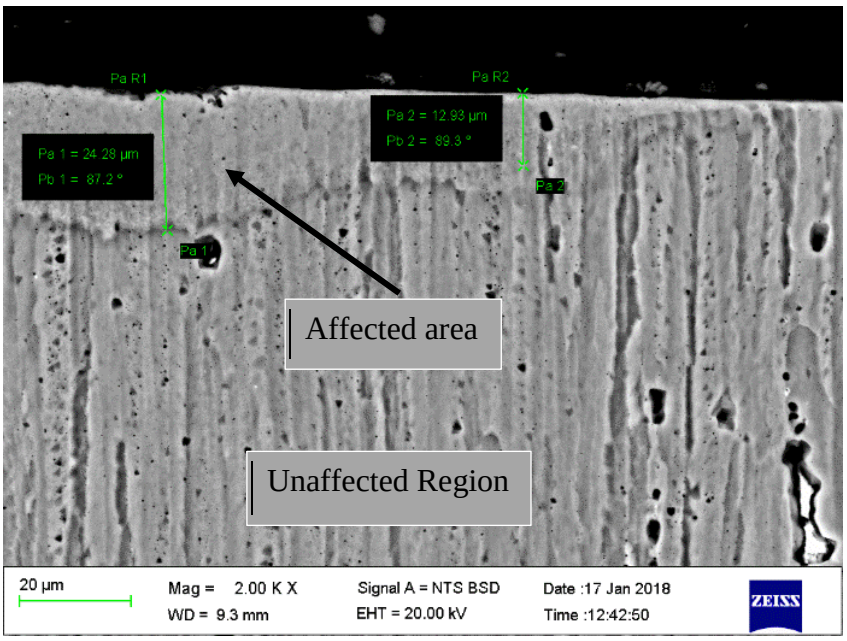

Figure 4-19. SEM cross-sectional microstructure of the AA7075 after LSP at a magnification 2000 times cross-section treated and unaffected region at SS=1.0 mm.

It is observed that microstructural boundaries have disappeared on the surface of the cross-sectional area. The maximum depth of the affected area is between a maximum depth of 24.28 µm and a minimum of 12.93 µm. The melting effect seems to increase with spot coverage. Figure 4.20 shows the results of the effect of the LSP SS=0.5 mm.

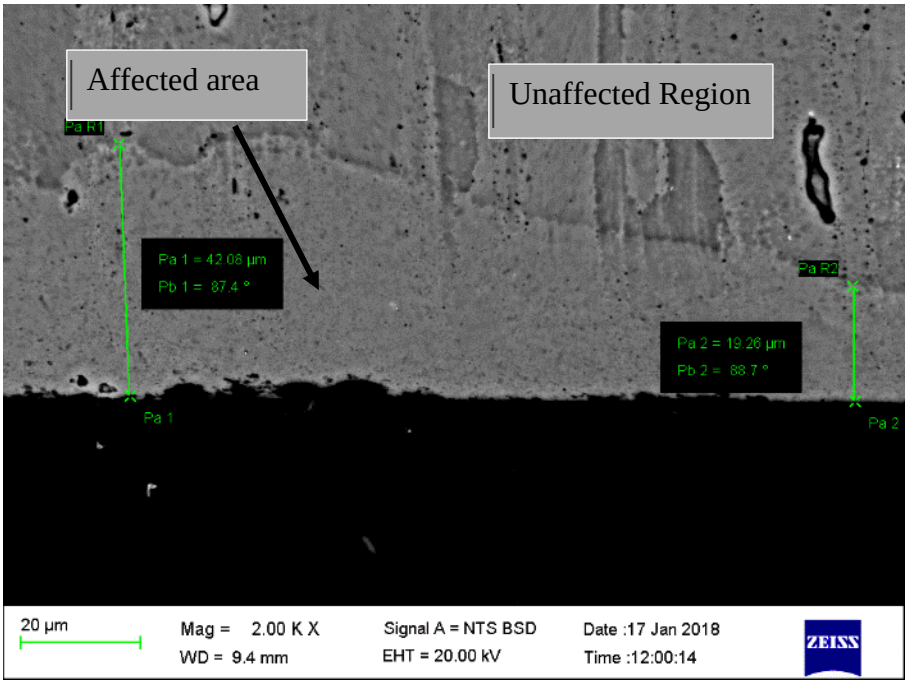

Figure 4-20. SEM cross-sectional microstructure of the AA7075after LSP (coverage 70; SS=0.5 mm) at a magnification 2000 times, cross-section treated section

Measured peaks of modified grain structure were estimated at 24.28 µm and 42.68 µm for LSP-treated material (coverage 70 and SS = 0.5 mm) in Figure 4.19 and Figure 4.20 respectively. The maximum depth seems to be at the centre of the laser spot.

4.4. Microhardness Results

The hardening effect of the SP and LSP was studied through microhardness tests. The microhardness results of the SP-treated samples are discussed first, followed by a discussion of microhardness results of the LSP-treated samples.

4.4.1. Shot Peening Effect on Microhardness

Figure 4.21 shows the test results of the Vickers microhardness test for SP processing at saturation, i.e., at 100% coverage. Microhardness measurements were taken from the top of the peened surface area to a depth of 500 µm of the test sample.

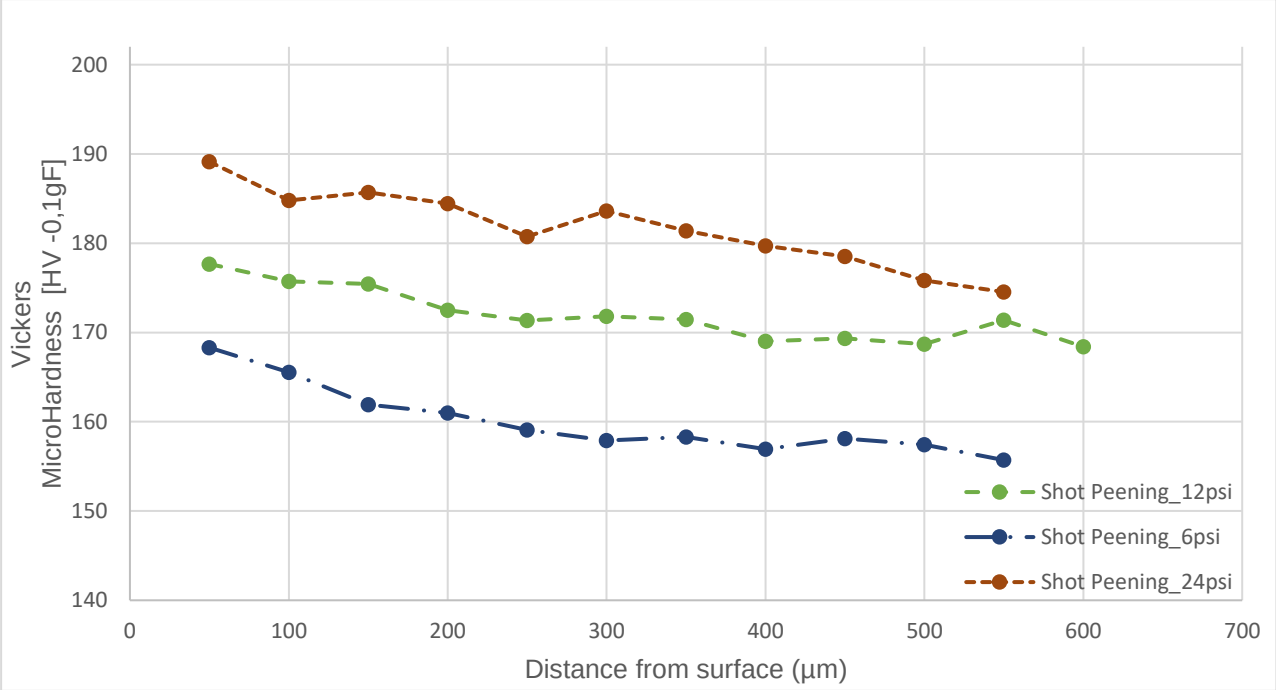

Figure 4-21. Microhardness depth profile for various shot peening parameters

Measurements taken on SP-treated samples suggests that SP may have changed near-surface mechanical properties of the treated metallic material. Like the LSP-treated samples, the microhardness for SP-treated material decreased with increasing distance from the surface of the

material. It was further observed that the microhardness value increases with increasing laser power. It was further observed that shot peened samples of 14.3A intensity (at peening pressure of 24 psi) had higher Vickers microhardness values compared to a peened material at 6.4A (at a pressure of 6 psi). The SP specimen's near-surface hardness varied between 189-169 HV compared to the baseline of 150 HV on untreated surfaces. The SP specimens near-surface hardness improved to 189 HV (12 psi), 198 HV (12psi) and 168 HV (6 psi). The induced microhardness propagated through the thickness of the material up to a depth of 500 µm. However, the SP-treated material at an intensity of 6.4A (6 psi) had the least microhardness effect on the treated material.

4.4.2. Laser Shock Peening-Effect on Microhardness

The work-hardening impact of the LSP can be recognised from the depth profile of the microhardness profile produced (Figure 4.22). Test results of the Vickers microhardness test for laser shock peening processing are shown in Figure 4.22.

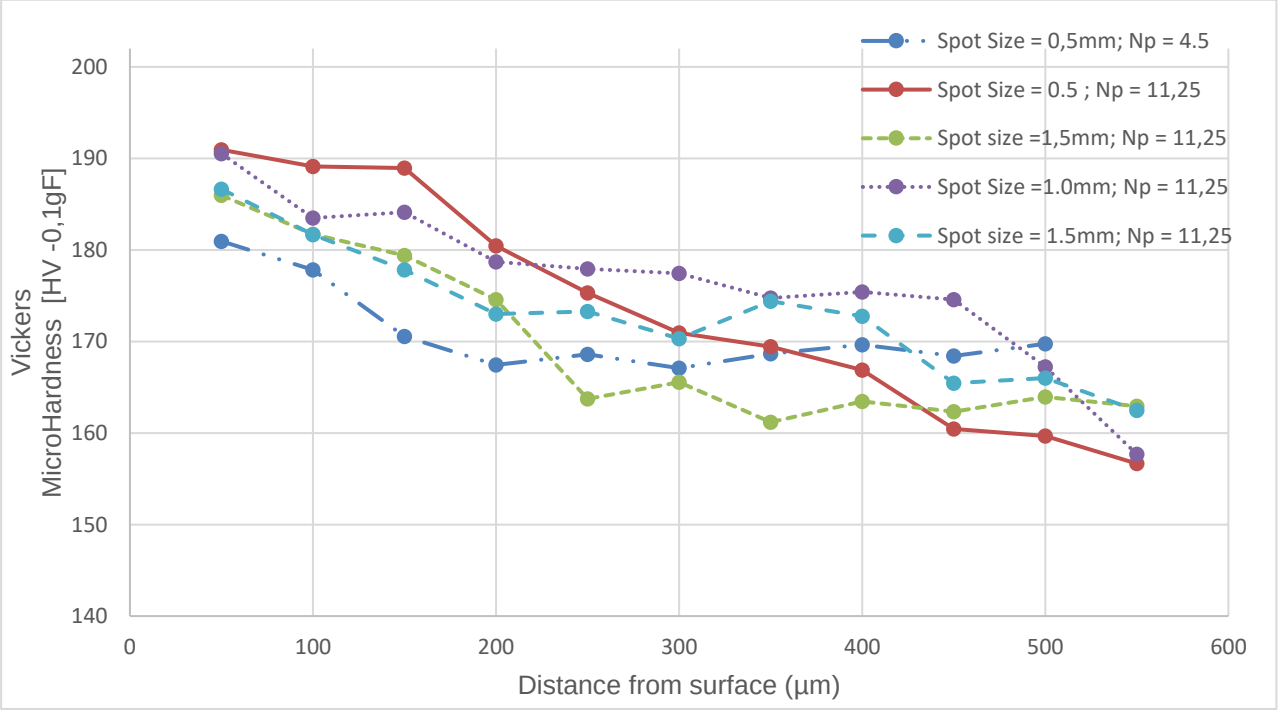

Figure 4-22. Microhardness depth profile for various laser shock peening parameters

It can be observed that all laser shock peening treatment produced microhardness near the surface of the material. Below the surface of the specimen, the microhardness effect decreased with increasing

distance from the surface. The microhardness values from the treated material also varied with spot sizes and pulse-density parameters. At a spot size of 0.5 mm and pulse density of 11.25 pulse/mm^2, the LSP produced maximum microhardness values. The LSP specimen near-surface hardness improved to between 190-180 HV compared to the baseline of 150 HV found on untreated surfaces. The LSP specimens near-surface hardness improved to 191 HV (11.25 pulse/mm^2), 181 HV (4.5 pulse/mm^2) and at constant spot size of 0.5 mm. But, the LSP specimens near-surface hardness improved to 191 HV (SS = 0.5 mm), 186 HV (SS = 1.5 mm) at (11.25 pulse/mm^2). The microhardness values decreased with increasing spot size (SS) at a constant pulse density (Np).

4.5. Summary

The results of the RS profile for the LSP treated metallic material are summarised in Table 4.4.

Table 4.4 RS field results of LSP treated AA7075 metallic material

Variable Parameter	Constant Parameters	RS Profile		
		Value of Compressive RS at surface	**Zero-Depth (*i.e. the depth at which compressive stress turn to tensile***	**Figures**
Spot Size ↗	Coverage, PI	↘	↗	4-5 & 4-6
Coverage ↗	Spot Size, PI	↗	Little change	4-7 & 4-8
Np ↗	Spot Size, PI	→	↗	_4-9
Np ↗ and SS ↗	PI	Changes	↗	_4-10

From the above the larger the SS the more tensile the RS close to the surface. An increase in the SS parameter results also in the an increase in the depth to which residual stresses are compressive, i.e. the zero-depth.

CHAPTER FIVE

5. Discussion

5.1. Introduction

In this chapter a discussion of the results obtained from the experimental results and observations of the SP and LSP-treated metallic material are discussed. From the results, the beneficial effect of the mechanical surface treatment, using SP and LSP on AA7075-T651 material can be deduced.

5.2. Shot Peening Results

Test results of the SP intensity effect on residual stresses, surface roughness, microstructure, and microhardness were analysed. It was found that the compressive RS in the treated material was induced in the material due to SP treatment. The induced compressive RS results increased the surface roughness of treated material when compared to untreated surfaces. However, no microstructural changes were observed in the cross-sectional area of the SP-treated samples when compared to untreated material. Microhardness tests revealed increased microhardness of the material when compared to untreated samples.

5.2.1. Residual Stress of Shot Peened Material

Figure 5.1 shows the effect of power intensity on peak compressive RS and the depth of the RS using SP.

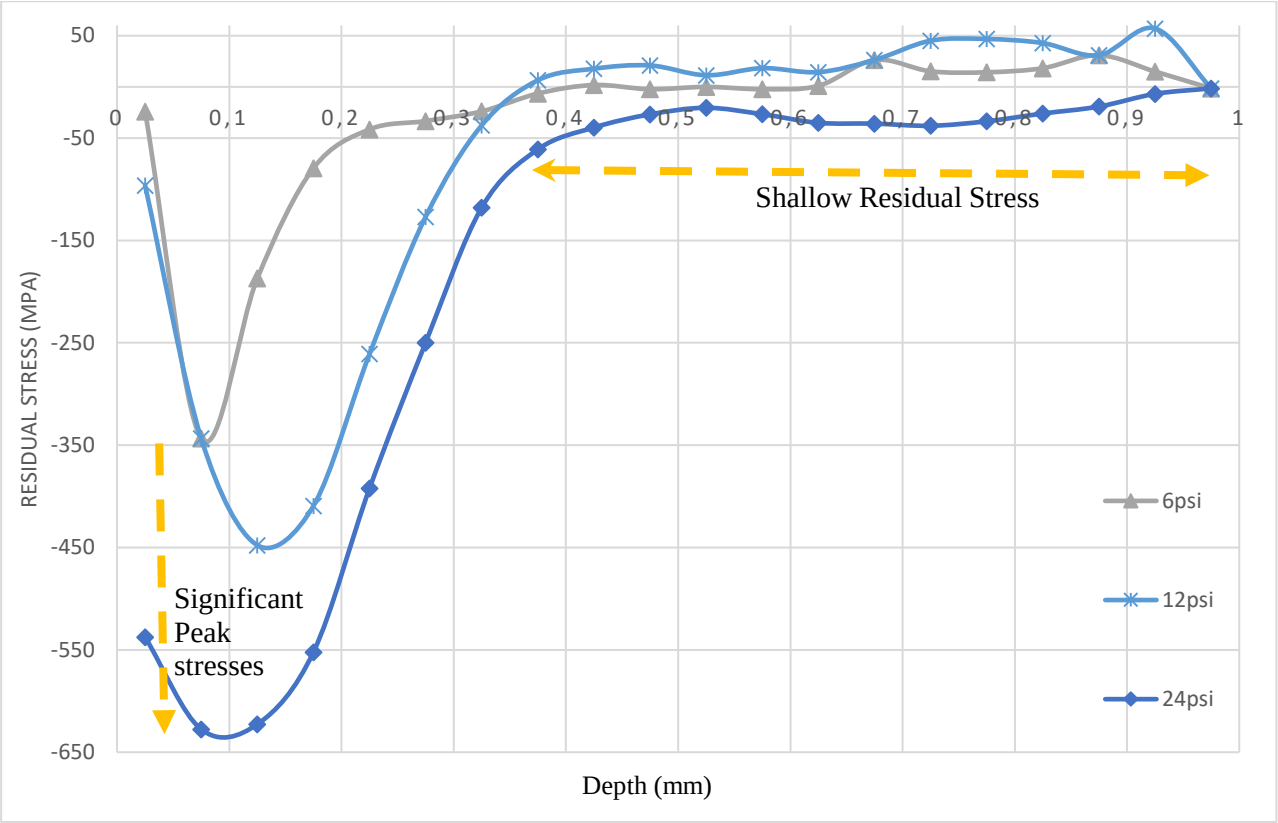

Figure 5-1. Shot Peening at different power intensities

The residual stress level obtained in the material increased with the degree of the SP (intensity). This was shown in the results of 6.4A (at 6 psi), 10A (at 12 psi) and 14.3A (at 24 psi). It was also seen that the degree of the SP intensity determined the resultant compressive RS produced.

5.2.2. Surface Roughness of Shot Peened Material

The SP treatment resulted in uneven surfaces of treated material compared to untreated material. This was due to significant modification of the surface topography compared to untreated material as shown in Table 5.1.

Table 5.1 Surface Roughness obtained for different SP processing treatments using SP on AA7075

Sample	**Processing parameters**			**Surface (µm)**	**Roughness**
	Pressure (psi)	**Intensity (A)**	**Coverage (%)**	**Ra**	**Rz**
Untreated	-	-		0.066	3.046
Sample 1 Parameters	6	6.4	100	3.09	4.65
Sample 2 Parameters	12	10	100	3.94	4.02
Sample 3 Parameters	24	14.3	100	1.50	1.01

Notes. *Peening shot size used is S230 (CCW28).

These undulations were more pronounced in higher intensity SP-treated material. This may be attributed to higher pressure duration produced by SP which resulted in the generation of higher dislocation motion. Except for SP intensity of 14.3A intensity (at a pressure of 24 psi), the surface roughness, at equivalent coverage condition, increased linearly with the power intensity (Table 5.1). The surface roughness of the SP-treated material was found to be a function of the peening intensity, i.e., the lesser the peening intensity, the lower the surface roughness of the material surface. This is in agreement with observations made by Gibson et al. [166].

5.2.3. Microstructure of Shot Peened Material

Metallographic examinations were performed on the cross-section of the SP-treated specimens and on untreated specimens. Micrographic photos were taken at a range between 200X and 2000X magnification. From the results, it was observed that SP treatment induced modification of the surface of the SP-treated specimens (shown in Figure 4.15). However, the results were not conclusive about the deformation mechanism causing alteration of the material surface. There was no evidence of microstructural changes of the SP-treated samples. Furthermore, there were no other new phases after SP treatment.

5.2.4. Microhardness of Shot Peened Material

Effect of SP on the microhardness of the material is linked to its microstructure. Microhardness of the material can thus be changed by microstructural modifications such as plastic deformation. In the SP-treated material, the SP-induced plastic deformation may have increased the hardness of the surface layer. It was observed that the power intensity correlated with the size of microhardness values produced in the material. Higher power intensity produced significant compressive RS which were the highest at an intensity of 14.3A (at peening pressure of 24 psi) amounting to a maximal value of -628 MPa at 75 µm. Furthermore, varying power intensity resulted in varying residual stress profiles at constant SP intensity (Figure 5.2).

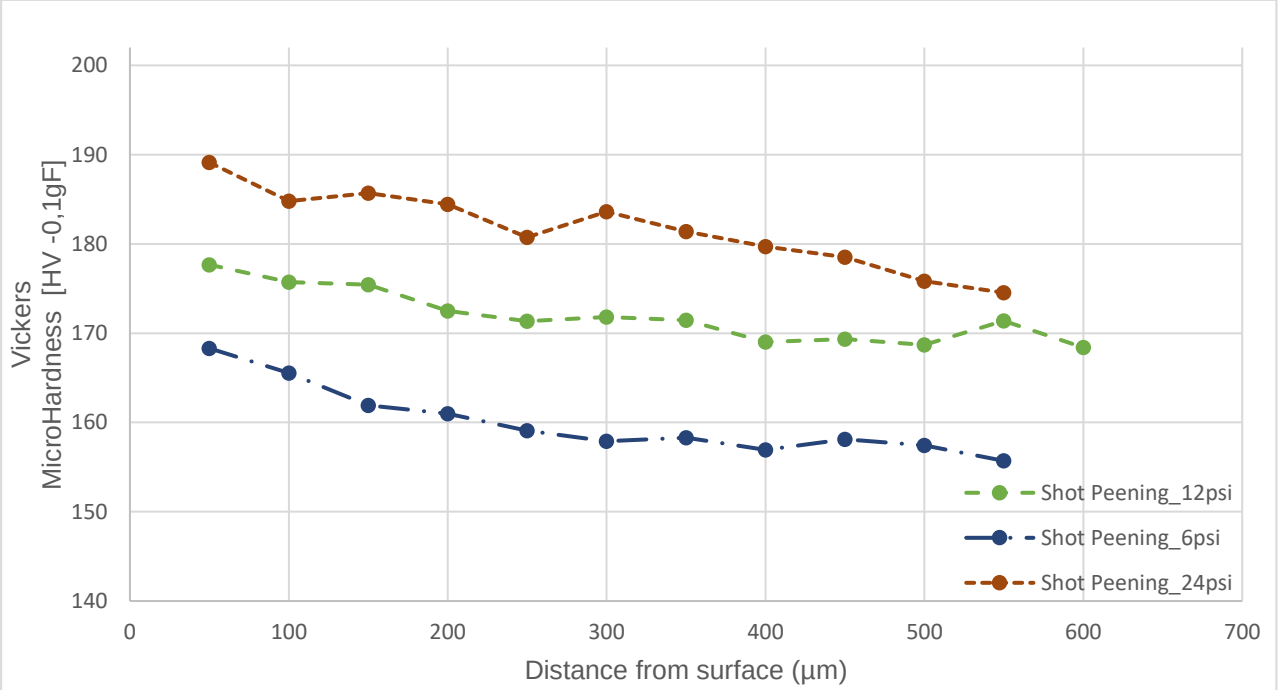

Figure 5-2. Microhardness depth profile for various shot peening parameters

This may be attributed to microstructural changes from fine microstructure to coarse microstructure as the power intensity increased. Scattering was also observed from Vickers microhardness values obtained using SP processed samples. These may be attributed to grain orientation and dislocation densities in the near-surface layer. In Figure 5.2, the depth of the hardened layer in the SP-treated samples was also deeper than that of the plastic deformation layer. The hardening effect in the SP-treated areas may be due to compressive RS induced in the material.

Microhardness increased with SP power intensity as shown in Figure 4.18. This may be attributed to a stream of shots producing increased kinetic energy which resulted in SP intensity reaching greater depths. This is in agreement with observations made by Lu et al. [167].

5.3. Laser Shock Peening Processing

Test results of the LSP intensity effect on residual stresses, surface roughness, microstructure, and microhardness were also analysed. It was found that compressive RS in the LSP-treated material was induced in the material. The induced compressive RS also resulted in increased surface roughness when compared to untreated surfaces. There were no observable microstructural changes due to the LSP treatment on the cross-section of the material. Microhardness test results revealed an increased microhardness of the material when compared to untreated samples.

5.3.1. Residual Stress of Laser Shock Peened Material

Figure 5.3 illustrates the effect of varying spot sizes at a constant pulse density (11.25 pulse/ mm^2) and constant power intensity 3 GW/cm^2. Decreasing the spot size (SS) resulted in higher compressive peak stresses (Figure 5.3). Peak compressive stress increased from sample No. 9 (Coverage = 40%, SS=1.5 mm) to sample 13 (Coverage =40%, SS=0.5 mm) from 215 MPa to 322 MPa respectively.

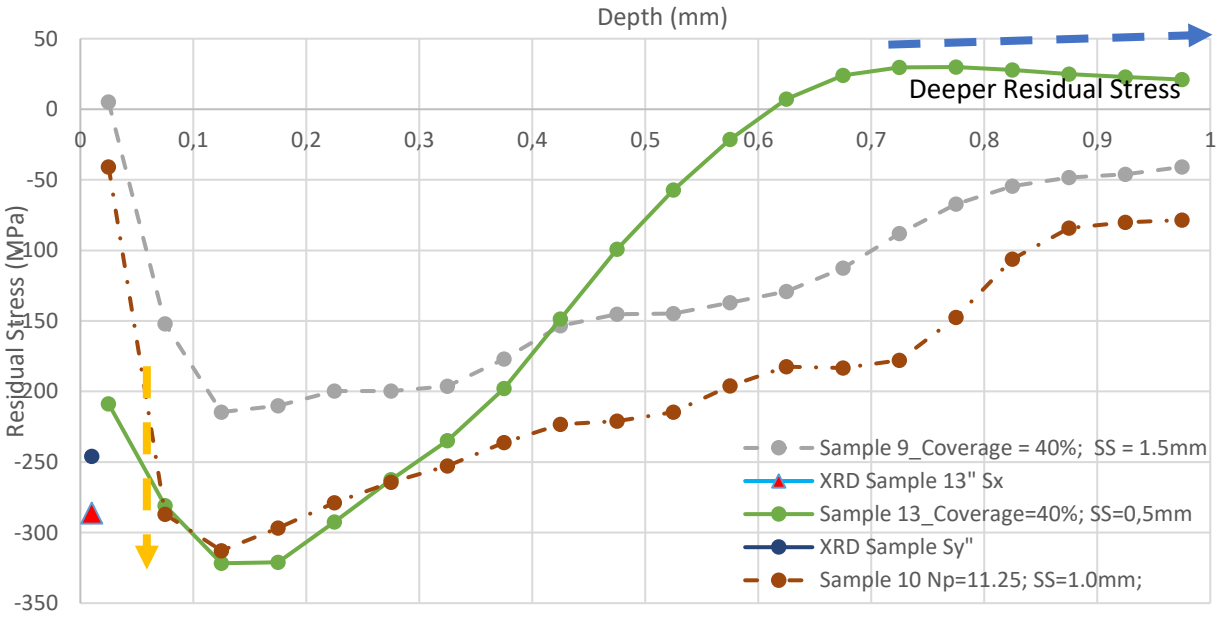

Figure 5-3. LSP results at different spot sizes and constant power intensity and pulse density

Figure 5.3 also shows that with the increase in the laser focused spot diameter, the depth of undulations produced could be varied. Furthermore, that the 0.5 mm spot size generated higher compressive RS compared to those of 1.0 and 1.5 mm. This may be attributed to the mechanical effect of the waves resulting in high strain hardening with higher pulse densities. Similar observations were obtained by Kalainathan et al. [136], Sanchez-Santana [93] and Gujba [40]. It has been suggested that the larger SS were ideal for deeper compressive zones [168]. Larger SS were stated to show better uniformity and coverage due to overlapping of the spots compared to smaller spot sizes [168]. From the above, it can be said that the SS depends on the residual stress profile, uniformity, and coverage. Similar observations were made in the literature [40].

5.3.1.1. Effect of the Spot Size and Coverage on Depth Residual Stress Distribution

From the results, it was observed that reducing spot size (SS) at constant coverage increased the in-depth RS in the material. Similar observations were made in previous studies [40]. There is a discernible correlation between the spot size and the associated compressive stress level produced. Figure 5.4 shows a generalised RS distribution.

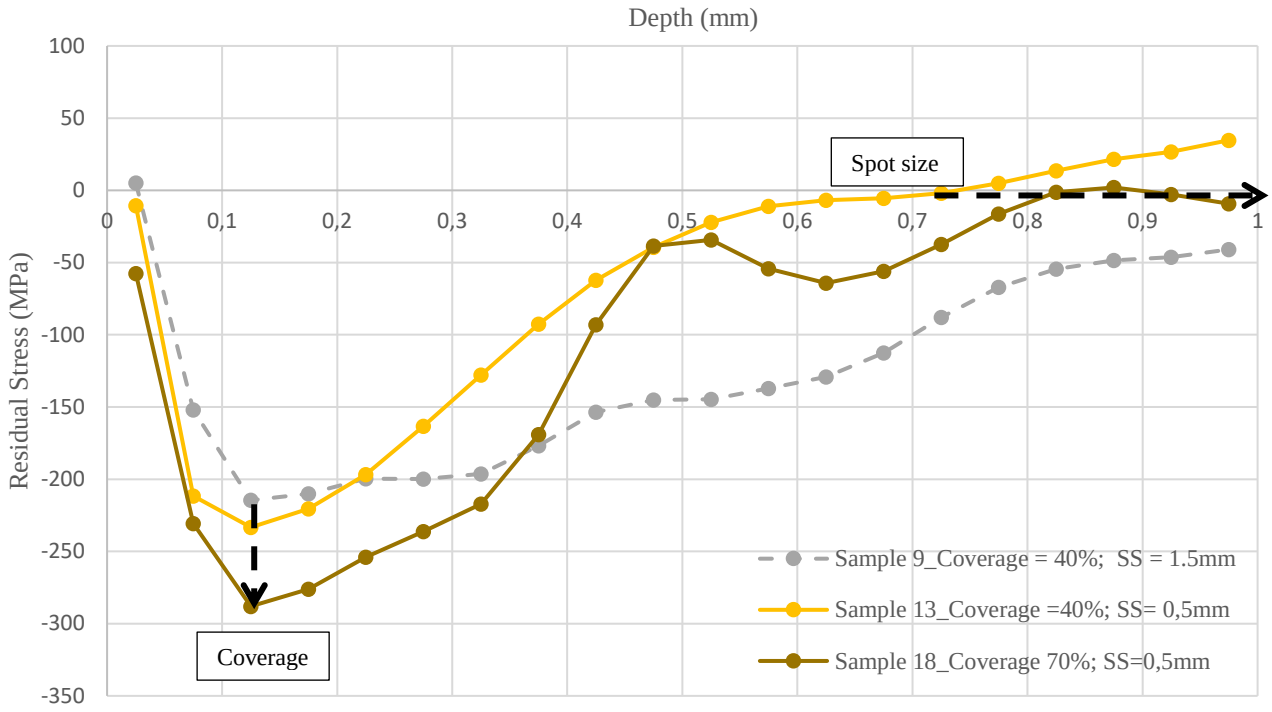

Figure 5-4. The Effect of increasing spot size and coverage on RS distribution behaviour

In Figure 5.4, increasing the spot size results in enlarged compressive peak. This is attributed to the power intensity and spot size inverse proportionality relationship. The power intensity causes the entire RS profile to become more compressive and increases the anisotropy. However, the increase in spot size led to a decrease in zero-depth. This may be attributed to the relationship between the spot size and penetration depth. A similar observation was made in the literature [40]. Furthermore, large spot sizes result in high tensile stresses close to the surface. The increase in the SS parameter also results in the an increase in the depth to which the residual stresses are compressive. Similar observations were made in literature [87]. This was attributed to spherical front observed in smaller spots. These attenuates through the depth at a smaller rate in comparison to a bigger spot. It was stated that a smaller spot diameter/ or spot size produced spherical shock wave expansion at the attenuated rate of $1/r^2$ while for larger spot diameters an attenuated rate of 1/r was observed. Montross et al. [87] contended that less attenuation behaviour resulted in further propagation into the material in large spot diameters. Higher compressive stresses, associated with smaller spots, were attributed to the inverse proportionality of power intensity and spot size given in Equation 4.

5.3.2. Surface Roughness of Laser Shock Peened Material

In LSP-treated samples, the surface roughness was found to increase with an increase in spot size (SS) at constant coverage. The phenomenon observed on the surface of the laser treated surface resulted in roughened surfaces and enhanced material properties such as hardness [40]. Table 5.2 shows the effect of varying LSP parameters.

Table 5.2 Surface Roughness obtained for different laser shock peening treatments using LSP on AA7075

Sample	**Processing parameters**			**Surface (µm)**	**Roughness**
	Np	**Spot Size (mm)**	**Coverage (%)**	**Ra**	**Rz**
Untreated	-	-		0.066	3.046
Sample 1 Parameters	11.25	1.5	80	2.01	5.5
Sample 2 Parameters	1.23	1.5	40	1.78	6.32
Sample 3 Parameters	11.25	1.0	70	1.59	5.54
Sample 4 Parameters	5	1.5	70	1.72	5.89
Sample 5 Parameters	4.5	0.5	70	1.46	6.25

Notes: Power was maintained at 3GW.

It was found that the surface roughness of treated material was a function of the spot size (SS), i.e., the lesser the spot size (SS), the higher the energy imparted to the material, and thus the higher roughness of the surface.

5.3.3. Microstructure of Laser Shock Peened Material

From the microstructural analysis of LSP-treated samples, it was observed that the laser treated samples had similar microstructure to untreated samples. There were no microstructural changes nor distortions observed in treated material. Similar observations were obtained by Ruschau [126],

Fribourga [130] and Vukelić [131]; however, in this research surface melting was observed on the LSP-treated material. This may be attributed to the absence of a protective coating or ablative coating during LSP-treatment. It could further be attributed to higher thermal effects which caused surface melting and re-solidification. The melted surfaces occurred a few microns below the surface of the metallic material. The microstructural features, as manifested through melting of the exposed surface, were found to be dependent on the LSP parameters. For example, the depth of grain modification seems to depend on the spot size of the LSP. This was also observed by Sano [48]; however, Fribourga [130] did not evidence the melting effect on the LSP-treated material.

Fribourga [130] observed the substantial development of precipitate dissolution across the structure of the LSP-treated samples as shown in Figure 4.11 – 4.13. Fribourga [130] concluded that the LSP processing could be referred to as a purely thermal process [130] as he did not detect melting nor changes in grain structure. Fribourga [130] concluded that the process involved changes in precipitate microstructure. However, this observation contradicted results obtained by Zhang [84] and Clauer [129]. They found that microstructural changes were attributed to plastic deformation due to high strain rates estimated to reach magnitudes of 10^6 s^{-1} [63]. Zhang [84] and Clauer [129] contended that the strain rates were sufficient to change the microstructure near the metal surface [169]. It is usually assumed that at these high strain rates deformation twinning was prevalent compared to a deformation slip [169]. The likelihood of deformation twinning is encouraged by compressive loading resulting from the LSP processing [169]. In this study, no evidence of refined microstructure was observed, unlike previous studies [40].

5.3.4. Microhardness of Laser Shock Peened Material

Figure 4.14 (a), (b) and (c) show images from the SEM of the material after treatment. In the LSP-treated samples, the Vickers microhardness value increased with an increase in the laser power. This was expected because of microstructural changes, from fine microstructure to coarse microstructure, as the power intensity increased. This may be due to plastic deformation resulting in dislocation movement and multiplication. Similar observations were made in the literature [26, 120, 136].

Figure 5.5 shows the results of the microhardness depth profile for various laser shock peening parameters.

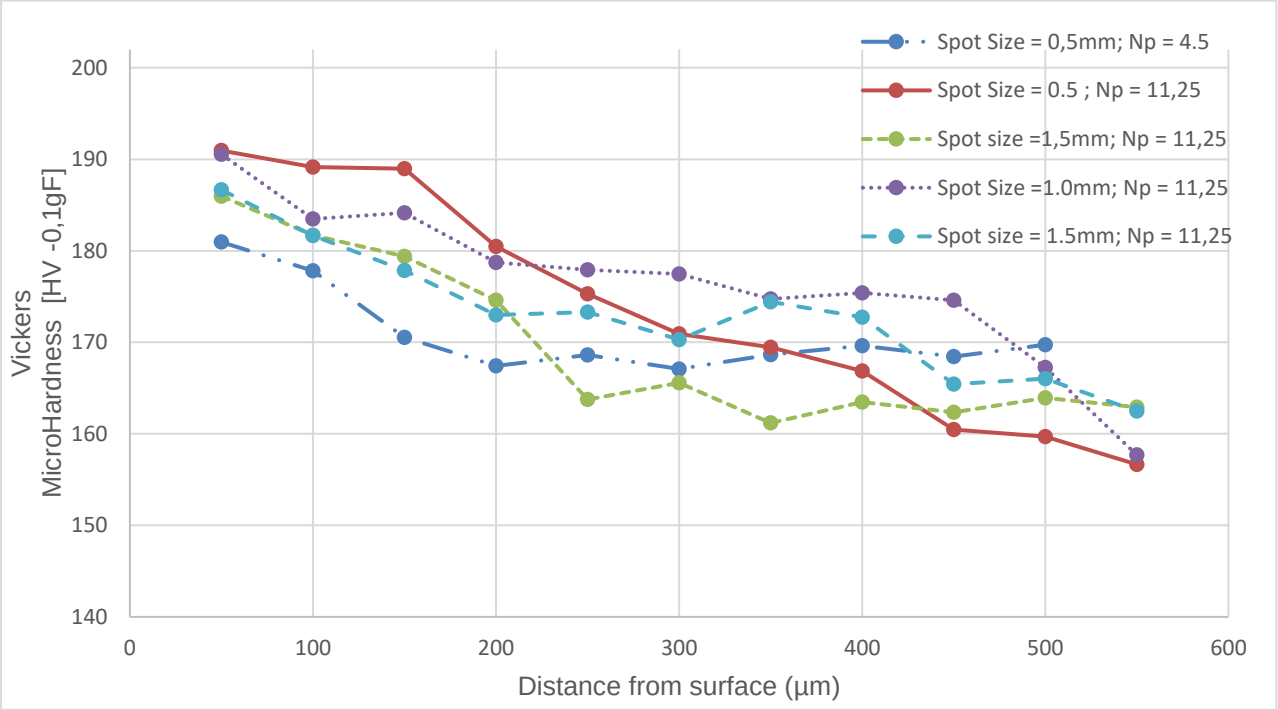

Figure 5-5. Microhardness depth profile for various laser shock peening parameters

In LSP-treated material, reducing pulse density (Np) at constant spot size (SS) resulted in lower microhardness values. When the pulse density increased, the depth of the compressive RS induced also increased. The number of laser impacts resulted in the increased depth of the hardened layer in the metallic material. These observations were confirmed by Clauer et al. [26]. They attributed this to microstructural deformation caused by dislocation of grains near the treated surfaces. The Vickers microhardness measurements were associated with the scattering effect. This may be attributed to grain orientation and dislocation densities in the sample. Similar observations were made in the literature [105]. The laser shock peening direction promotes dislocation formation on the Vickers measurement scatter [79, 105]. This scatter was consistent with previous works on aluminium alloys after LSP treatments [120, 170].

The influence of the LSP processing on properties of LY12CZ aluminium alloy was studied [171]. It was also found that material hardness increased with laser intensity. Furthermore, it is clear from Figure 5.2, Figure 5.5 and Figure 4.19-4.20 that the depth of the hardened layer is deeper than that

of the plastic deformation layer. This is in agreement with observations made by Lu et al. [167] and Montross et al. [87]. The hardening effect in laser treated areas may be attributed to the presence of compressive RS. This mechanical modification generated work-hardening of treated surfaces as observed in a previous study [120].

5.4. Comparison between Shot Peening and Laser Shock Peening

A comparison between the SP and LSP process is carried out in this section. The focus will be on the effect of residual stress, surface roughness, microstructure, and microhardness between these two processes. The impact of varying SP intensity and the LSP parameters will also be discussed.

5.4.1. Residual Stress of Shot Peening and Laser Shock Peening

In Figure 5.6, the results of the SP-treated sample with the LSP-treated samples are shown in Figure 5.6.

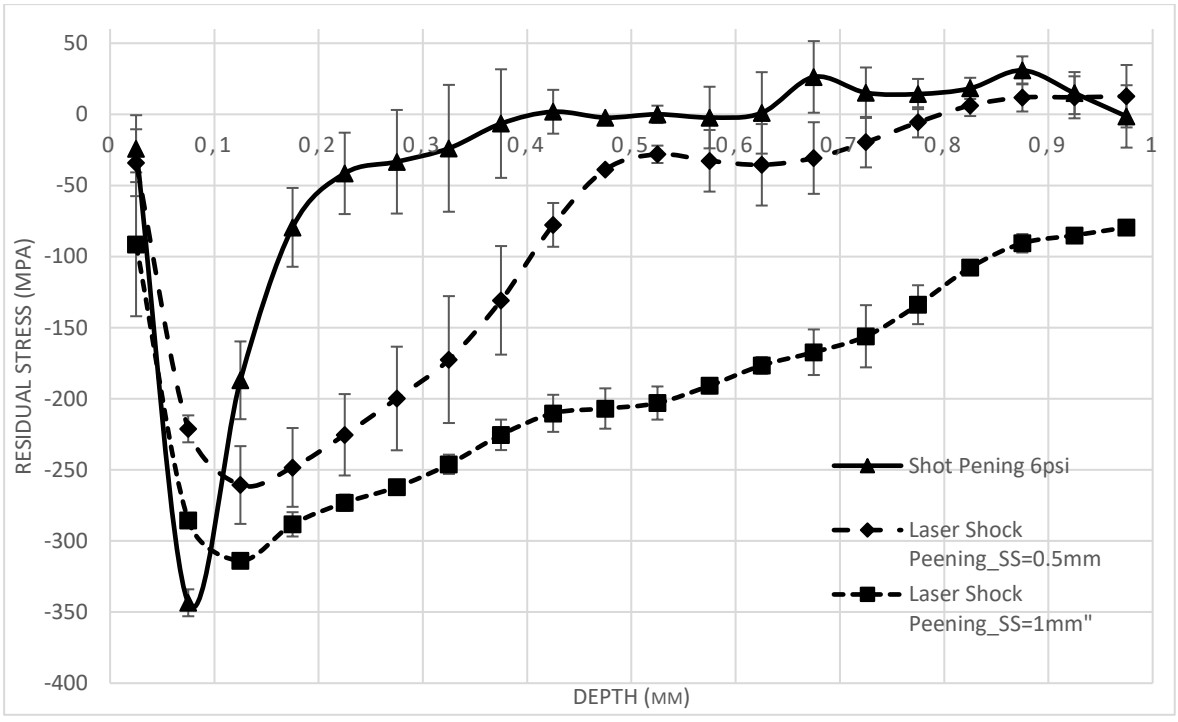

Figure 5-6. Comparison of Residual Stress Fields Induced by Shot Peening and Laser Shock Peening. The error bars representing the standard deviation of the compressive RS data at each depth. Each point marker is obtained from the statistical average of three tests at each LSP intensity.

In Figure 5.6, the SP produces deeper compressive RS compared to the LSP-treated samples combined. At peening intensity of 6.4A (at a pressure of 6 psi), the SP treatment produced higher

compressive stress levels (at -343MPa) compared to laser treated samples. However, these compressive RS levels for the SP were highest and spanned the depth range of 0.50 mm and were better when compared to those produced by LSP treatment (reached -260 MPa and -314 MPa for SS (0.5 mm) and SS (1 mm) respectively). This phenomenon was also evidenced in the literature [106, 172].

However, the LSP-treated samples produced deeper compressive RS compared to the SP-treated material. The SP-treated material in-depth compressive RS reached a depth of 0.4 mm compared to the LSP-treated sample at an in-depth height of 0.8 mm at SS (0.5 mm) and much higher for the SS (1 mm). Furthermore, the compressive RS produced by LSP had uniform magnitudes. Similar observations of deep compressive RS were previously reported for other material [32, 173]. The peak stresses due to SP increased with the increase in power intensity. For process parameters used in this research, the SP-treated material was found to induce higher near-surface compressive RS and higher degree of work-hardening compared to the LSP. However, the LSP impacted greater depth of the surface layer. This was unlike compressive RS produced by SP which were limited to a depth of less than 1 mm.

5.4.2. Surface Roughness of Shot Peening and Laser Shock Peening

The LSP-treated material produced smoother surface finish compared to SP-treated material. In SP treated material the surface roughness increased (Figure 4.19). This may be attributed to higher pressure duration produced by SP resulting in the generation of higher dislocation motion compared to the LSP-treated samples. This is in agreement with observations by Peyre [120].

In the LSP-treated samples, the surface roughness was found to increase with an increase in spot size (SS) at constant coverage. Except for SP intensity of 14.3A (at a pressure of 24 psi), the surface roughness, at equivalent coverage condition, increased linearly with power intensity. In the LSP, the surface roughness of treated material was found to be a function of the spot size (SS), i.e., the lesser the spot size (SS), the higher the energy imparted to the material, and thus the higher the roughness of the surface. This is in agreement with observations made by Gibson et al. [166]. Sample curvature

is an important parameter in the evaluation on the effect of the treatment on the fatigue life of the component. This is also the case in thick components similar to those used in this research.

5.4.3. Microstructure of Shot Peening and Laser Shock Peening

In both the SP and LSP, no microstructural changes were observed in treated material. Besides, the modified surface finish in SP and LSP treated material, there were no conclusive results about changes to their grain structures. No changes to microstructural phases were detected on the SP and LSP-treated material.

From the microstructural analysis of SP and LSP-treated samples, it was observed that the laser treated samples had similar microstructure as untreated samples. There were neither microstructural changes nor distortions observed in treated material. Furthermore, there was no evidence of refined microstructure in both the SP and LSP; this is contrary to a previous study [40].

5.4.4. Microhardness of Shot Peening and Laser Shock Peening

Figure 5.7 shows a comparison between the microhardness of the SP and LSP-treated.

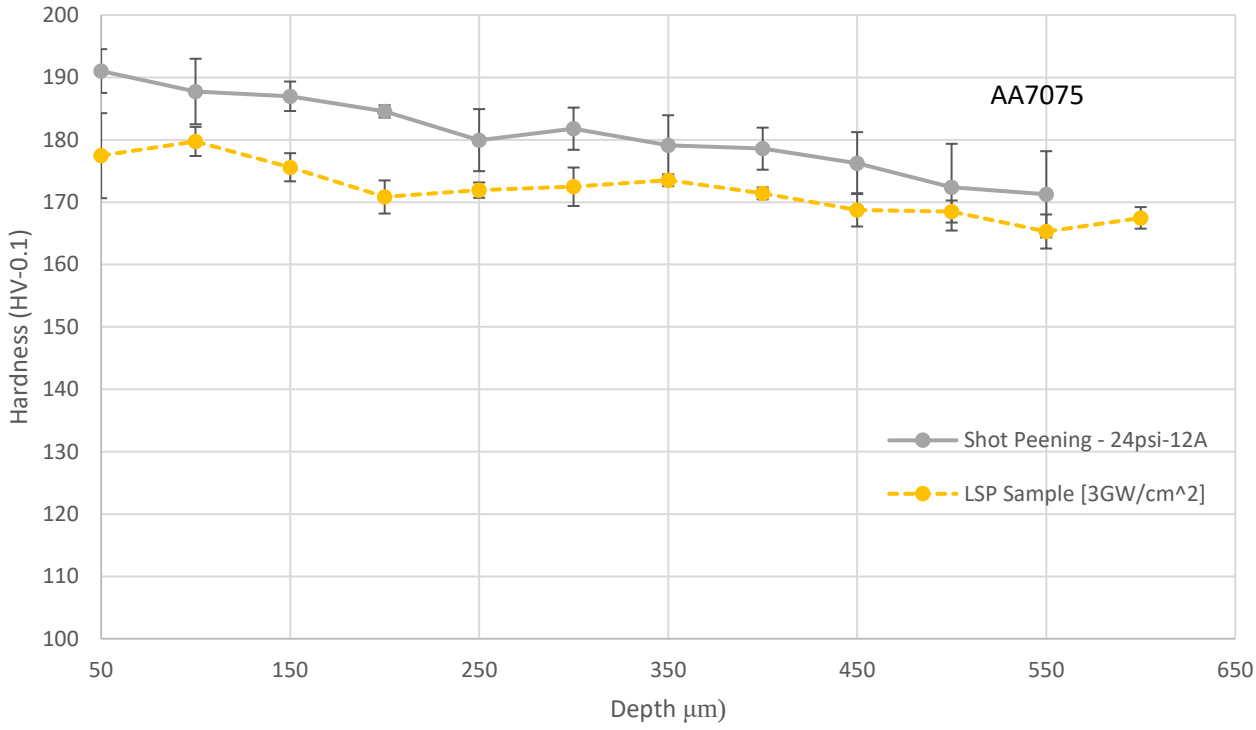

Figure 5-7. Vickers microhardness using 100gf on AA7075-T651 SP and LSP-treated respectively

The SP-treated sample produced slightly higher hardness measurement compared to the LSP-treated sample. Both hardness values decreased with increasing depth from the surface and levelled off at some point in the subsurface of the treated material. The melting phenomenon observed on the surface of the LSP treated surface resulted in roughened surfaces and enhanced material properties such as hardness. The microstructural features were found to be dependent on the LSP parameters; this was similar to a previous study [40].

5.4.5. Summary

The residual stress level obtained in the SP treated material increased with the degree of the SP (intensity). The SP intensity also increased the surface roughness and the microhardness of the treated material. However, no noticeable change was observed on the microstructure of treated material.

An increase in power intensity of the LSP treated material caused the entire RS profile to become more compressive and increases the anisotropy. An increase in SS of LSP treated material caused a decrease in the surface RS but increased the depth of the compressive state. Increasing the coverage percentage overlap) caused an increase in the RS at the surface, but little change through the depth of the sample.

The coverage (percentage overlap) also resulted in an increase in anisotropy. However, the coverage (percentage overlap) stayed constant with the SS variation.

Surface roughness is an important factor in determining the fatigue life of the component. Surface roughness increases with the power intensity of the treated samples.

Sample curvature is an important parameter in the evaluation on the effect of the treatment on the fatigue life of the component. This is also the case in thick components similar to those used in this research.

6. CONCLUSIONS

The effect of the SP and LSP on residual compressive stresses, surface roughness, microstructure, and microhardness of AA7075-651 was experimentally examined and the following conclusions can be made. The experimental results confirmed that both the SP and LSP-induced compressive RS in the AA7075-T651 material. In SP processing, compressive RS produced varied with power intensity. The highest compressive RS produced was -627 MPa using 24 psi power intensity. The cumulative effects of high-density dislocation arrangement which can be produced by work-hardening and compressive RS can improve the mechanical properties of materials.

It was further observed that the LSP processing produced better compressive RS compared to SP processing. These were found to be deeper than 1 mm in LSP and lesser in the SP-treated material. The highest induced compressive RS were -350 MPa using SS of 0.5 mm and at a pulse density (Np) of 5 pulse/cm^2. It was shown that both the SP and LSP were effective surface treatments techniques to improve the properties of the AA7075-T651 alloy.

The SP-treated samples produced higher on surface roughness compared to that from LSP-treated samples. Surface roughness in SP treated samples increased with the SP intensity. In LSP treated samples, the surface roughness produced increased with spot size.

There were no noticeable changes to the microstructure of both SP and LSP-treated samples using the SEM. However, considerable modifications to surfaces of both SP and LSP treated samples could be seen. The Vickers microhardness revealed that both SP and LSP treatment resulted in microstructural changes of the AA7075-T651. The microhardness of near-surface of the AA7075-T651 material can be improved by SP and/ or LSP processing techniques. It was found in both processes that the microhardness gradually decreased with increasing distance from the surface of the material.

7. RECOMMENDATIONS

The following future studies are recommended. A comparative study using different SP and LSP parameters and varying coverage must be undertaken. This will help in improving understanding of the impact of these changes on compressive RS measurement, surface roughness, microstructure, and microhardness.

The relationship between power intensity and compressive RS were analysed. It was concluded that there could be a relationship between the two parameters. However, the results were limited to three power intensity parameters, i.e., 6 psi, 12 psi and 24 psi. Future studies should be conducted at lower power intensity values to better understand this relationship.

SP and LSP-treated samples were analysed using the IHD stress measurement technique supplemented with the laboratory XRD technique. However, the XRD technique suffers from depth penetration limitations of the x-ray beam. This is particularly problematic when trying to characterise below surface stress distribution or compressive RS in treated material. Future research must be carried out to analyse incremental depth analysis of compressive RS using XRD and incremental layer removal by electropolishing to supplement stress results from IHD. Using both techniques could be useful in measuring the effectiveness of mechanical treatment due to the SP and/ or LSP at various phases of an aircraft's life.

The relationship between the SP intensity and surface roughness is understood. However, the effect of the SP shot size on surface roughness is less understood. It is postulated that increasing shot sizes for hard material improves the mechanical properties of the material. However, no evidence was found in this research using a soft material such as aluminium alloys.

The qualitative analysis of the microstructure for SP and LSP-treated material using SEM did not yield satisfactory results. Future research must be conducted to understand the effect of each

processing technique on the microstructure of the material. For example, quantitative analysis using a transmission electron microscope (TEM) may help in better understanding the dislocation mechanics of each mechanical treatment.

Furthermore, the SP and LSP techniques have beneficial results on treated samples; however, there has been no evidence of studies investigating the effect of both techniques on treated samples. This research will ensure a better understanding of the combined effect of both SP and LSP techniques in treated samples.

References

1. Montross, C., T. Wei, and L. Ye, *Laser shock processing and its effects on microstructure and properties of metal alloys: A review.* Int J Fatigue. , 2006. **24**: p. 1021–1036.
2. Rodopoulos, C.A., J.S. Romero, and S.A. Curtis, *Effect of Controlled Shot Peening and Laser Shock Peening on the Fatigue Performance of 2024-T351 Aluminium Alloy.* ASM International, 2003. **12**: p. 414-419.
3. Abdullahi, K.G., Mamoun, M, *Laser Peening Process and Its Impact on Materials Properties in Comparison with Shot Peening and Ultrasonic Impact Peening.* Materials, 2014. **7**: p. 7925-7974.
4. Fuchs, H.O., Stephens, R.I., *Metal Fatigue In Engineering*. 1980: John Wiley & Sons.
5. NASA. n.d. [cited; Available from: http://techreports.larc.nasa.gov/ltrs/PDF/2001/tm/NASA-2001-tm210843.pdf.
6. Wang, Q., J, ed. *Encyclopedia of Tribology*. ed. Q. Wang, J and Y. Chung. Vol. 1. 2013, Springer Link: Boston, MA.
7. Metal Improvement Company. *Metal Improvement Company: Shot peening*. n.d. [cited; Available from: http://www.metalimprovement.com.
8. Vasu, A., *Influence of Curved Geometrics on the Fatigue Life of Laser Peened Components*. 2014, Wright State University.
9. Wohlfahrt, H., R. Kopp, and O. Vohringer, *Shot peening: science technology application.* Bremen: DGM Informationsgesellschaft, , 1987.
10. Champaigne, J., *Shot peening: theory and application*. 1991, MI: IITT-International.
11. Schulze, V., *Modern mechanical surface treatment.* Weinheim: John Wiley & Sons, Wiley-VCH Verlag GmbH & KGaA, , 2006.
12. Curtis, S., et al., *Analysis of the effects of controlled shot peening on fatigue damage of high strength aluminium alloys.* International Journal of Fatigue, 2003. **25**(1): p. 59-66.
13. Berns, H. and Weber, L. *Influence of Residual Stresses on Crack Growth.* Impact Surface Treatment. Elsevier, 1984.
14. Everett, R.A., et al. , *The effect of shot and laser peening on crack growth and fatigue life in 2024 Aluminium Alloy and 4340 Steel.* NASA/ TM-2001-210843, 2001.
15. Lincoln, J.W. and Yeh, H.C. *Treatment of High-Cycle Vibratory Stress in Rotorcraft Damage Tolerance Design," in Application of Damage Tolerance Principles for Improved Airworthiness of Rotorcraft*. in *RTO Meeting Procedures, RTO MP-24.* . 2000. Corfu, Greece.
16. Ferreira, J.A.M., Boorrego, L.F.P., and Costa, J.D.M., *"Effects of Surface Treatments on the Fatigue of Notched Bend Specimens,"*. Fatigue, Fract. Engng. Mater., Struct., (1996). **19**(1): p. 111-117.
17. Chu, J.P., et al., *Laser-Shock Processing Effects on Surface Microstructure and Mechanical Properties of Low Carbon Steel.* Materials Science and Engineering, 1999. **A260**: p. 260-268.
18. Soady, K.A., *Life assessment methodologies incorporating shot peening process effects: mechanistic consideration of residual stresses and strain hardening Part 1 – effect of shot peening on fatigue resistance.* Material Science and Technology, 2013. **29**(6).
19. *Shot Peening Applications*. 7th ed. n.d.

20. Bagherifard, S. and Ghelichi, R. *Experimental and numerical analysis of surface nanostructured materials obtained by high energy shot peening*. 2009.
21. White, R.M., *J.Appl. Phys.34.* 1963: p. 2123-2124.
22. Fairand, B.P., et al. , *Laser Shock Induced Microstructural and Mechanical Property Changes in 7075 Aluminium.* Journal of Applied Physics, 1972. **43**(9): p. 3893.
23. Ford, S.C., et al. , *Investigation of Laser Processing - Executive Summary.* 1981.
24. Hsu, T.R., *Applications of the Laser Beam Technique to the Improvement of the Metal Strength.* Journal of Testing and Evaluation, 1973. **1**(6): p. 457.
25. Mazumdar, J. *The State-of-the-Art of Laser Materials Processing. Interdisciplinary Issues in Materials Processing and Manufacturing*. in *presented at The Winter Annual Meeting of The American Society of Mechanical Engineers. Boston*. 1987.
26. Clauer, A.H., Holbrook, J.H. and Fairand, B.P. *Effects of laser induced shock waves on metals. In Shock Waves and High Strain Rate Phenomena in Metals*. 1981, New York, NY, USA: Plenum Publishing Corporation, .
27. Gibbons, J.F., et al., *Laser and Electronn-Beam Solid Interactions and Materials Processing*. 1981, New York: Elsevier North Holland, Inc.
28. Ready, J.F. *Laser Processing - The First 20 Years. Proceedings of the First International Laser Processing Conference*. 1981. Anahem, California.
29. Ding, K. and Ye, L. *Three-dimensional dynamic finite element analysis of multiple laser shock peening processes.* Surface Engineering, 2003. **19**(5): p. 351-358.
30. Ballard, P., *Residual stresses induced by rapid impact-applications of laser shocking*. 1991, Ecole Polytechnique: France.
31. Celland, C., et al *Experimental Analysis of Nano and Engineering Materials and Structures*. 2007. Netherlands: Springer.
32. Nalla, R.K., et al., *On the influence of mechanical surface treatments - deep rolling and laser shock peening - on the fatigue behavior of Ti-6Al-4V at ambient and elevated temperatures.* Mater Sci Eng., 2003. **A355**: p. 216-230.
33. Spanrad, S., Tong, J, Mater. Sci. Eng. A528, 2011: p. 2128-2136.
34. Rodopuolos, C.A., *et al.*, Mater. Sci. Eng. Perform, 2003. **12**: p. 414-419.
35. Rubio-Gonzalez, C., *et al.*, Mater. Sci. Eng. A 386, 2004: p. 219-295.
36. Hatamleh, O., Int. J. Fatigue, 2009. **31**: p. 974-988.
37. Heckenberger, U.C., *et al.*, Int. J. Struct. Integr., 2011. **2**: p. 22-33.
38. Fabbro, R., et al. , *Physics and applications of laser-shock processing.* J Laser Appl., 1998(10).
39. Zhang, H. and Yu, C. *Laser shock processing of 2024-T62 aluminum alloy.* Materials Science and Engineering, 1998. **257A**: p. 322–327.
40. Gujba, A. and Medraj, M. *Laser Peening Process and Its Impact on Materials Properties in Comparison with Shot Peening and Ultrasonic Impact Peening.* Materials, 2014. **7**(12): p. 7925.
41. Ding, K. and Ye, L. eds. *Laser Shock Peening: Performance and Process Simulation*. Cambridge: Woodhead Publishing, . 2006.
42. Razavi, R.S. and Gordani, G.R. *Laser Surface Treatment of Aluminium Alloys*. 2011.
43. Tenaglia, R.D. and Clauer, A.H. *Bend bar quality control method for laser shock peening*, in *Google Patents*. 2004.

44. Chen, H., Kysar, J.W. and Lawrence, Y.Y. *Characterization of plastic deformation induced by micro-scale laser shock peening.* J Appl Mech: T ASME, 2004. **71**: p. 713–723.
45. Peyre, P., Merrien, P. and Lieurade, H.P. *Laser induced shock wave surface treatment for 7075-T7351 aluminium alloys.* Surf Eng., 1995. **11**(1): p. 47–52.
46. World_of_lasers. *Laser _history*. n.d. [cited; Available from: http://www.worldoflasers.com/laserhistory.htm.
47. Land_laser. *Laser_Process_diagram*. n.d. [cited 07 July 2017.; Available from: : http://www.land-laser.com/laser.asp.
48. Sano, Y., Mukai, N. and Obata, M. *Laser peening without coating: process, effects and applications*. in *Conference on Shot Peening*. 2008. Tokyo.
49. Kalainathan, S., Sathyajith, S., Swaroop, S. , *Effect of laser shot peening without coating on the surface properties and corrosion behavior of 316 L steel.* Opt. Lasers Eng. , 2012. **50**: p. 1740–1745.
50. Hu, Y.X, Chumming, G. and Yao, Z. *Investigation on the non-homogeneity of residual stress field induced by laser shock peening.* Surf. Coat. Technol., 2009. **203**: p. 3503–3508.
51. Sano, Y., Obata, M. and Kubo, T. Mater Sci Eng., 2006. **A 417**: p. 334-340.
52. Ochi, Y., Masaki, K, Matsumura, T, *et al.*, in *12th Int. Conf. on Experimental Mechanics (ICEM12)*. 2004: Bari.
53. Sano, Y., Altenberger, I. and Scholtes, B. In *ASME Pressure Vessels and Piping Division Conference (PVP2006)*. 2006a. Vancouver.
54. Adachi, T., Takehisa, H, Nakajima, M, *et al.* In *Conference on Shot Peening*. 2008. Tokyo.
55. Mannava, S. and Ferrigno, S. *Laser Shock Peening for Gas Turbine Engine Vane Repair-General Electric Company.* 1997 (U.S. Patent 5,): p. 675,892.
56. Ivetic, G., *et al., Fatigue in laser shock peened open-hole thin aluminium specimens.* Mater. Sci. Eng. A 534, 2012: p. 573-579.
57. Banas, G. and Lawrence, F.V. *Shot peening vs. laser shock peening. ICSP4* 1990.
58. Torparli, M.B., *Analysis of Residual Stress Fields in Aerospace Materials After Laser Peening*, in *Department of Design, Development, Environment and Materials*. 2012, The Open University.
59. Yee, R.K., Sidhu, K.S, *Innovative laser heating methodology study for crack growth retardation in aircraft structures.* International Journal of Fatigue, 2005. **27**: p. 245-253.
60. Bolis, C., Berthe, L, Boustie, M, Arrigoni, M, Barradas, S, Jeandin, M *Physical approach to adhesion testing using laser-driven shock waves.* . J. Phys. D Appl. Phys., 2007. **40**: p. 3155–3163.
61. Vasu, A., *Influence of Curved Geometrics on the Fatigue Life of Laser Peened Components*. 2014, Wright State University.
62. Braisted, B. and Brockman, B. *Finite element simulation of laser shock peening.* International Journal of Fatigue, 1999. **21**(7): p. 719–724.
63. Peyre, P., Sollier, A. and Chaieb, I. *FEM simulation of residual stresses induced by laser peening.* Eur Phys J Appl Phys., 2003. **88**: p. 83–88.
64. Yang, C.H., et al., *Three-dimensional finite element modelling of laser shock peening process.* Materials Science Forum., 2007. **561- 565**: p. 2261-2264.
65. Hu, Y., Yao, Z. and Hu, J. *3-D FEM simulation of laser shock processing. Surface & Coatings Technology.* 2006. **201**: p. 1426–1435.

66. Singh, G., Grandhi, R.V. and Stargel, D.S. *Modified particle swarm optimization for a multimodel mixed-variable laser peening process.* Structural and Multidisciplinary Optimization, 2010. **42**(5): p. 797-810.
67. Kruusing, A., *Handbook of Liquids-Assisted Laser Processing*, ed. A. Kruusing. Vol. A. 2010: Elsevier.
68. Nobre, J.P., Kornmeier, M. and Dias, A.M. *Use of the hole-drilling method for measuring residual stresses in highly stressed shot-peened surfaces.* Experimental Mechanics, 2000. **40**(289).
69. Gill, A.S., et al., *High spatial resolution, high energy synchrotron X-ray diffraction characterization of residual strains and stresses in laser shock peened Inconel 718SPF alloy.* J Appl Phys. , 2012. **111**.
70. Rosas, G.G., Rubio-Gonzalez, C, Ocana, J.L, Molpeceres, J.L.O, Porro, J.A, Moreno, W.C, Morales, M, *High level commpressive residual stresses produced in aluminium alloys by laser shock processing.* Applied Surface Science, 2005. **252**: p. 883-887.
71. Niku-Lari, A., Lu, J. and Flavenot, J.F. *Measurement of residual-stress distribution by the incremental hole-drilling method.* Journal of Mechanical Working Technology, 1985. **11**(2): p. 167-188.
72. Sticchi, M., et al., *A parametric study of laser spot size and coverage on the laser shock peening induced residual stress in thin aluminium samples*. The Journal of Engineering. 2015.
73. Vishay_Precision_Group. *Strain Gage Rosettes: Selection, Application and Data Reduction*. n.d. [cited 2018 22 May]; Available from: http://www.digikey.co.il/Web%20Export/Supplier%20Content/Micro-Measurements_1033/PDF/MicroMeasurement-strain-gauge-rosettes.pdf.
74. Zaroog, O.S., Ken, Y, W, and Manap, A.N.A. *Current and Challenges of Residual Stress Measurement Techniques.* Impact Factor, 2012. **3**: p. 358.
75. Cullity, B. and Stock, S.R. eds. *Elements of X-Ray Diffraction*. 2nd ed. 1980, Addison-Wesley: Reading, Massachusetts.
76. Vink, T.J., et al., *Stress, strain, and microstructure of sputter-deposited Mo thin films.* J. Appl. Phys, 1991. **70**: p. 4301-4308.
77. Dane, C., Hackel, L, Daly, J, et al., *Laser peening of metals enabling laser technology.* Adv Mater Process, 1997: p. 13–27.
78. Warrendale, P.A., *Surface performance of titanium*, in *The Minerals, Metals & Materials Society*, J.K. Gregory, Rack, H.J, Eylon, D, Editor. 1997. p. 239–51.
79. Peyre, P., et al., *Laser shock processing of materials, physical processes involved and examples of applications.* J Laser Appl 1996. **8**: p. 135.
80. Rankin, J.R., Hill, M.R. and Hackel, L.A. *The effects of process variations on residual stress in laser peened 7049 T3 aluminium alloy.* . Materials Science and Engineering, 2002.
81. Rankin, J.R., Hill, M.R, Hackel, L.A, *The effects of process variations on residual stress in laser peened 7049 T3 aluminium alloy.* Materials Science and Engineering, 2002.
82. Gomez-Rosas, G., et al., *Laser shock processing of 6061-T6 Al alloy with 1064 nm and 532 nm wavelengths.* Appl Surf Sci 2010. **256**: p. 5828–5831.
83. Cellard, C., et al., *Laser shock peening of Ti-17 titanium alloy: Influence of process parameters.* Mater Sci Eng 2012. **A**(532): p. 362–372.
84. Zhang, X.C., Zhang, Y.K. and Lu, J.Z. *Improvement of fatigue life of Ti-6Al-4V alloy by laser shock peening.* Mater Sci Eng. , 2010. **A**(527): p. 3411–3415.

85. Dane, C., L. Hackel, and J. Daly, *Laser peening of metals enabling laser technology.* Adv Mater Process, 1997: p. 13–27.
86. Zhang, Y., You, J. and Lu, J. *Effects of laser shock processing on stress corrosion cracking susceptibility of AZ31B magnesium alloy.* Surf Coat Technol. , 2010. **204**: p. 3947–3953.
87. Montross, C., Wei, T., Ye, L., *et al.*, *Laser shock processing and its effects on microstructure and properties of metal alloys: A review.* Int. J. Fatigue, 2006. **24**: p. 1021–1036.
88. Masse, G. and Barreau, J. *Surface modification by laser induced shock waves.* Surf Eng., 1995. **11**: p. 131–132.
89. Clauer, A.H., Walters, C.T. and Ford, S.C. *The effects of laser shock processing on the fatigue properties of -T3 aluminium Lasers in materials processing*, in *American Society for Metals*. 1983: Metals Park (OH) . p. 7–22.
90. Masse, G., Barreau, J, *Surface modification by laser induced shock waves.* Surf. Eng., 1995. **11**: p. 131–132.
91. Cellard, C., Retraint, D, François, M, Rouhaud, E, le Saunier, D, *Laser shock peening of Ti-17 titanium alloy: Influence of process parameters.* Mater. Sci. Eng. , A 2012. **532**: p. 362–372.
92. Hackel L.A, Hill, M, and Ngoc, T.K *Production Laser Peening pf High Strength Metals*, in *Metal Improvement Company*. n.d.: Livermore, Califonia.
93. Sánchez_Santana, U., Rubio_González, C. and Gomez_Rosas, G. *Wear and friction of 6061-T6 aluminium alloy treated by laser shock processing.* Wear and friction, 2006. **260**: p. 847–854.
94. Schmidt-Uhlig, T., Karlitschek, P, Yoda, M, Sano, Y, Marowsky, G Eur. Phys. J. Appl. Phys., 2000. **9**: p. 235-238.
95. Rubio_Gonzalez, C., et al., Mater Sci Eng A 386, 2004: p. 219-295.
96. Gomez-Rosas, G., Rubio-Gonzalez, C, Ocaña, J.L, Molpeceres, C, Porro, J.A, Morales, M, Casillas, F.J. , *Laser shock processing of 6061-T6 Al alloy with 1064 nm and 532 nm wavelengths.* Appl. Surf. Sci. , 2010. **256**: p. 5828–5831.
97. Maawad, E., Sano, Y, Wagner, L, Brokmeier, H.G, Genzel, *Investigation of laser shock peening effects on residual stress state and fatigue performance of titanium alloys*. n.d., Institute of Materials Science and Engineering: Zellerfeld, Germany.
98. Yang, J.M., Her, Y.C. and Clauer, A.H. Mater Sci Eng., 2001. **A 298**: p. 296-299.
99. Kadhim, A., Salim, E.T, Fayadh, SM, *et al., Effect of Multipath Laser Shock Processing on Microhardness, Surface Roughness, and Wear Resistance of 2024-T3 Al Alloy.* The Scientific World Journal, 2014. **2014**.
100. Tan, Y., et al., *Laser shock peening on fatigue crack growth behaviour.* Fatigue Fract Eng Mater Struct., 2004. **27**: p. 649-656.
101. Clauer, H.A. *Laser shock peening for fatigue resistance in surface treatment of titanium alloys*. in *In The Metal Society of AIME conference (125th Anniversary)*. 1996.
102. Lundberg, M., et al., *Influence of Shot Peening Parameters on Residual Stresses in Flake and Vermicular Cast Irons.* n.d.
103. XiuQuan, C., et al., *Effect of Shot Peening Intensity on Residual Stress Field of 7075 Auminium Alloy* n.d.
104. Vielma, A.T., Llaneza, V. and Belzunce, F.J. *Shot peening intensity optimization to increase the fatigue life of a quenched and tempered structural steel.* 2014. **74**: p. 273-278.

105. Gill, A.S., *A Study of the Effects of Laser Shock Peening on Residual Stress, Microstructure and Local Properties of IN718 Nickel-Base Superalloy*. 2012, University of Cincinnati.
106. Gao, Y.K., *Improvement of fatigue property in 7050-T7451 aluminium alloy by laser peening and shot peening.* Mater Sci Eng. , 2011. **A** (528): p. 3823–3828.
107. Winburn, D.C., *What Every Engineer Should Know About Lasers*. 1987, Marcel Dekker Inc.: New York.
108. Liu, Q., et al. *Spallation-like phenomenon induced by laser shock peening surface treatment on 7050 aluminum alloy*. in *In Proceedings of the Structural Integrity and Fracture International Conference (SIF'04)*. 2004. Brisbane, Australia: The University of Queensland: Brisbane.
109. Alang, N.A., Razak, N.A. and Miskam, A.K. *Effect of Surface of Roughness on Fatigue Lofe of Notched Carbon Steel.* 2011.
110. Nishitani, H. and Imai, R. Trans. JSME, 1983. **(A) 49-442**: p. 693–698.
111. Taylor, D. and Clancy, O.M. *The Fatigue Performance of Machined Surfaces.* Fatigue Fract Engng Mater Struct., 1991. **14**: p. 329-336.
112. Arola, D. and Williams, C.L. *Estimating the Fatigue Concentration Factor of Machined Surfaces.* Int. J. of Fatigue, 2002. **24**(9): p. 923-930.
113. *Surface Roughness Measurement, Bulletin No. 1984, Mitutoyo.*
114. Luong, H. and Hill, M.R. *The effects of laser peening on high-cycle fatigue in 7085-T7651 Aluminum alloy.* . Mater Sci Eng. **A 2008**(477): p. 208–216.
115. Sharp, P.K., Clark, G, *The Effect of Peening on the Fatigue Life of 7050 Aluminum Alloy.* Defence Science & Technology Organisation, Victoria, Australia, 2001.
116. Cao, Z., Xu, H. and Zou, S. *Investigation of surface integrity on TC17 titanium alloy treated by square-spot laser shock peening.* Chin J Aeronaut 2012. **25**: p. 650–656.
117. Martinez, S.A., Sathish, S. and Blodgett, M.P. *Residual stress distribution on surface-treated Ti-6AI-4V by X-ray diffraction.* Exp Mech. , 2003. **43**: p. 141–147.
118. Lu, J., Luo, K. and Zhang, Y, *Surface Integrity of LY2 Al Alloy Subjected to Laser Shock Processing*. Chapter 2. Vol. 179 2013, Berlin, Germany: Springer.
119. Lu, J., Luo, K. and Zhang, Y. *Surface Integrity of LY2 Al Alloy Subjected to Laser Shock Processing*. 2013. Berlin, Germany: Springer.
120. Peyre, P., Fabbro, R. and Merrien, P. *Laser shock processing of aluminium alloys. Application to high cycle fatigue behaviour.* Mater Sci Eng 1996(A 210): p. 102–113.
121. *http://www.purdue.edu/rem.rs/sem.htm. Accessed November 2018.* [cited.
122. Kusalamwardi, H. and Kusuma, G. *Influence of Shot Peening on the Surface Microstructure of Leaf Spring.* n.d.
123. Thomas, M., et al., *The effect of shot peening on the microstructure and properties of a near-alpha titanium alloy following high temperature exposure.* Acta Mater., 2012. **60**(13-14): p. 5040-5048.
124. Clauer, A.H., Fairand, B.P. and Wilcox, B.A. *Laser shock hardening of weld zones in aluminium alloys.* Metall Trans A. , 1977. **8**: p. 1871–1876.
125. Gerland, M. and Hallouin, M. *Effect of pressure on the microstructure of an austenitic stainless steel shock-loaded by very short laser pulses.* Journal of Materials Science, 1994. **29**: p. 345–351.
126. Ruschau, J., et al., *Fatigue crack nucleation and growth rate behavior of laser shock peened titanium.* Int J Fatigue. , 1999. **21**: p. 199–209.

127. Luo, K.Y., Wang, C.Y, Li, Y.M., *et al., Effects of laser shock peening and groove spacing on the wear behavior of non-smooth surface fabricated by laser surface texturing. .* Appl. Surf. Sci., 2014(313): p. 600–606.
128. Srinivasan, S., Garcia, D.B., Gean, M.C., *et al., Fretting fatigue of laser shock peened Ti-6Al-4V.* Tribol. Int. , 2009. **42**: p. 1324–1329.
129. Clauer, A.H. and B.P. Fairand. *Interaction of laser-induced stress waves with metals*. in *ASM Conference Applications of Lasers in Materials Processing*. 1979. Washington DC.
130. Fribourga, G., Deschampsa, A, Brécheta, Y, Mylonasb, G, Labeasb, G, Heckenbergerc, U, Perezd, M, *Microstructure modifications induced by a laser surface treatment in an AA7449 aluminium alloy.* Materials Science and Engineering, 2011. **A 528**: p. 2736–2747.
131. Vukelić, S., Kysar, J.W. and Yao, Y.L. *Grain boundary response of aluminum bicrystal under micro scale laser shock peening.* Int. J. Solids Struct. , 2009. **46**: p. 3323–3335.
132. Vickers_Microhardness_Test, *Indentec Hardness Testing Machines, Limited, West Midlands, DY9 8HX, Zwick/Roell.*
133. Guo, Y. and Caslaru, R. *Fabrication and characterization of micro dent arrays produced by laser shock peening on titanium Ti-6Al-4V surfaces.* J. Mater. Process. Technol., 2011. **211**(729–736): p. 729–736.
134. Montross, C., Florea, V. and Swain, M. *The influence of coatings on subsurface mechanical properties of laser peened 2011-T3 aluminum.* J. Mater. Sci., 2011. **36**: p. 1801–1807.
135. Amar, H., et al., *Influence of the microstructure and laser shock processing (LSP) on the corrosion behaviour of the AA2050-T8 aluminium alloy.* Corros. Sci., 2011. **53**: p. 3215–3221.
136. Kalainathan, Sathyajith, S., S. and Swaroop, S. *Effect of laser shot peening without coating on the surface properties and corrosion behavior of 316 L steel.* Opt Lasers Eng 2012. **50**: p. 1740–1745.
137. ICAO. *Aircraft decommisioning and dismantling: A global airline view*. 2014 [cited; Available from: https://icao.int/Meetings/EnvironmentalWorkshops/Documents/2014-GreenTechnology/5_Rotger-IATA.pdf.
138. Vohringer, O. *In: Wohlfahrt H, Kopp, R, Changes in the State of the Material by Shot Peening. In Int Conf On Shot Peening 3*. 1987.
139. Altenberger, I. and Scholtes, B. *Improvement of Fatigue Lifetime of Mechanically Surface Treated Materials in the Low Cycle Fatigue Regime" in Surface Treatments IV*. 1999. Southampton, UK: WIT Press.
140. Dorr, T., Wagner, L, *"Fatigue Response of Various Titanium Alloys to Shot Peening" in Surface Treatments IV"*, ed. C.A. Brebbia, Kenny, J.M 1999, Southampton, UK: WIT Press. 349-57.
141. Pangborn, R.N., Weissmann, S *"Prediction of Fatigue Life by X-Ray Diffraction Methods,".* Fatig. Eng. Mater., 1979. **1**: p. 363-69.
142. Wagner, L., Lütjering, G, *"Influence of Shot Peening on the Fatigue Behaviour of Ti-Alloys in Shot Peening"*. 1981, New York, NY,: Pergamon Press. 453-60.
143. Ali, A., et al., *The effect of controlled shot peening on the fatigue behaviour of 2024-T3 aluminium friction stir welds.* International Journal of Fatigue, 2007. **29**(8): p. 1531-1545.
144. Prevey, P., Hornbach, D, Mason, P, *Thermal residual stress relaxation and distortion in surface enhanced turbine engine components*, in *In Proceedings of the 17th Heat Treating*

Society Conference and Exposition and the 1st International Induction Heat Treating Symposium. 1998, ASM International Materials Park, OH, USA.
145. Karunesh, G. and Manjunath, Y. J, *Determination of mechanical properties of Aluminium Alloy 7075 reinforced with Aluminium oxide (Al203).* International Journal of Engineering Research, 2016. **5**(6): p. 1129-1254.
146. Dif, R., Bès, B, Ehrström, J.C, Sigli, C, Warner, T, Lassince, P, Ribès, H Master. Sci. Forum 2000. **331**: p. 1613–1618.
147. Evall, J.C., et al., *Engineering Criteria and Analysis Methodology for the Appraisal of Potential Fracture Resistant Primary Aircraft Structure.* Wright Research and Development Center, 1972. **Report AFFDL-TR- 72-80**.
148. *Guide to Engineering Materials (GEM 2002), Adv. Mater. Process., Vol 159 No.12), 2001*.
149. Gariépy, A., Miao, H. and Lévesque, M. *Peen forming.* Comprehensive Materials Processing, 2014. **3**: p. 295-329.
150. *SAE standard J442, Test strip, holder and gage for shot peening, SAE International, 2008.*
151. *SAE standard J443, Procedures for using standard shot peening test strip, SAE International, 2003.*
152. Glaser, D., et al., *Laser Shock Peening on a 6056-T4 Aluminium Alloy for Airframe Applications.* Advanced Materials Research, 2014. **891-892**: p. 974-979.
153. Wan, S. and Xu, Q. *Parallel-Kinematic Nanopositioning Stages Based on Roberts Mechanism*, in *In: Ru C., Liu X., Sun Y. (eds) Nanopositioning Technologies. Springer, Cham*. 2016.
154. Fitzpatrick, M.E., et al., *Determination of Residual Stresses by X-ray Diffraction*. 2005: Middlesex, UK: National Physics Laboratory.
155. Luo, Q. and Jones, A.H. *High Precision Determination of Residual Stress of Polycrystalline Coatings using Optimised - XRD Sin^2ψ Technique.* Surface and Coatings Technology, 2010. **205**: p. 1403-1408.
156. BSI. *BD EN 15305: Non-destructive Testing — Test Method for Residual Stress analysis by X-ray Diffraction*. 2008.
157. ASTM_XRD, in *ASTM Standard Test Method for Determining the X-Ray Elastic Constants for Use in the Measurement of Residual Stress Using X-Ray Diffraction Techniques, ASTM International, in: E1426-94*
1998: West Conshohocken, PA.
158. ASTM_XRD_Alignment, *ASTM Standard Test Method for Verifying the Alignment of X-Ray Diffraction Instrumentation for Residual Stress Measurement, ASTM International, in: E915-10*. 2010: West Conshohocken, PA.
159. Noyan, I.C. and Cohen, J.B. *Residual Stress Measurement by Diffraction and Interpretation.* 1987.
160. *British Standard. "Assessment of surface texture; methods and instrumentations". In British Standard: 1134.* 1988.
161. Metallographic_Aluminium_Etchants. *Metallographic Aluminium Etchants: Aluminium Alloys*. 2018 [cited; Available from: http://www.metallographic.com/Etchants/Aluminum%20etchants.htmhttp://www.metallographic.com/Etchants/Aluminum%20etchants.htm.
162. Graff, W.R. and D.C. Sargent, *A new grain-boundary etchant for aluminium alloys.* Metallography, 1981. **14**: p. 69–72.

163. Tamadon, A., et al. *Development of Metallographic Etchants for the Microstructure Evolution of A6082-T6 BFSW Welds*. 2017 [cited; Available from: file:///C:/Users/kenosi.mokolobate/Downloads/metals-07-00423.pdf.
164. ASTM_Vickers_Hardness, *Standard Test Method for Vickers Hardness of Metallic Materials, ASTM International, in: E92-82*. 2003.
165. The_Aluminium_Association, *International Alloy Designations and Chemical Composition Limits for Wrought Aluminum and Wrought Aluminum Alloys*. 2015, Tech. rep. The Aluminium Association.
166. Gibson, G.J., et al., *Influence of shot peening on high-temperature corrosion and corrosion-fatigue of nickel based superalloy 720Li.* Materials at High Temperatures, 2016. **33**(3): p. 225-233.
167. Lu, J.Z., et al., *Grain refinement of LY2 aluminium alloy induced by ultra-high plastic strain during multiple laser shock processing impacts.* Acta Materialia, 2010. **58**: p. 3984-94.
168. Ganesh, P., et al., *Studies on laser peening of spring steel for automotive applications.* Opt. Lasers Eng., 2012. **50**: p. 678–686.
169. Mahajan, S. and D.F. Williams, *Deformation twinning in metals and alloys* Int. Metall. Rev., 1973. **18**: p. 43.
170. Ocaña, J.L., Morales, M. and Molpeceres, C. *Experimental assessment of the influence of irradiation parameters on surface deformation ans residual stresses in laser shock processed metallic alloys* Applied Surface Science, 2004(238): p. 501-5.
171. Shujuan, D., et al., *Effects of laser shock processing on material's properties.* Transitions of Nonferrous Metals Society of China 1997. **7**: p. 120-4.
172. Vazquez, J., C. Navarro, and J. Dominguez, *Experimental results in fretting fatigue with shot and laser peened Al7075-T651 specimens.* International Journal of Fatigue, 2012. **40**: p. 143-153.
173. Shepard, M.J., et al. in *Proceedings of the Sixth National HCF Conference*. 2001. Jacksonville, FL.
174. Hatamleh, O., *A comprehensive investigation on the effects of laser and shot peening on fatigue crack growth in friction stir welded AA 2195 joints.* . Int. J. Fatigue 2009. **31**: p. 974–988.
175. Hill, M.R., Dewald, A.T, Rankin, J.E, Lee, M.J, *Measurement of laser peening residual stresses.* J. Mater. Sci. Technol., 2005. **21**: p. 3–9.
176. Wang, F., Yao, Z, Deng, Q, *Experimental study on laser shock processing of brass.* J. Univ. Sci. Technol. Beijing Miner. Metall. Mater., 2007. **14**: p. 529–532.
177. Bugayev, A.A., Gupta, M.C, Payne, R *Laser processing of Inconel 600 and surface structure.* Opt. Lasers Eng., 2006. **44**: p. 102–111.
178. Liao, Y., Suslov, S, Ye, C, Cheng, G,, *The mechanisms of thermal engineered laser shock peening for enhanced fatigue performance.* Acta Mater., 2012. **60**: p. 4997–5009.
179. Sealy, M.P., Guo, Y.B, *Surface integrity and process mechanics of laser shock peening of novel biodegradable magnesium-calcium (Mg-Ca) alloy.* . J. Mech. Behav. Biomed. Mater., 2010. **3**: p. 488–496.

APPENDIX A

Studies conducted using different LSP processing parameters in several metallic materials [40] in Table 0.1.

Table 0.2 Studies using LSP processing parameters on different metallic materials with commentary

Sample	Power density (GW/cm^2)	Pulse duration (ns)	Sacrificial coating	Overlay used	Thickness (cm)	Comments
Ti-6Al-4V	5	10	Al Foil	Water	0.10	Improved fatigue strength by 22.2% and 41,7% for one and two successive laser shocks respectively when compared untreated sample.
Ti-I7 [91]	3,6,9	9, 27	Al	Water	0.1 - 0.9	LSP parameters had influence on the RS profile. But no observed influence on roughness. Minimum effect on work hardening and large effect on hardness due to the compressive stresses induced.
Al2024 T3 [100]	5	18	Black paint	Water	0.25	LSP-treated specimens displayed resistance to fatigue crack growth for various notch geometries as compared to untreated specimens.
AA2195 [174]	5	18	Al	Water		Reduced fatigue crack growth rate of stir welded joint due to LSP treatment compared to SP. The reduced crack growth comparable with unwelded material.
316L SS [49]	2.5	10	No coating	Water		The potentiodynamic polarisation investigation showed improvement in corrosion potential (*Ecorr)* and corrosion current density (*Icorr*) with increase in laser pulse density LPwC specimen showed 30%-40% increase in microhardness than peened specimen.

Sample	Power density (GW/cm^2)	Pulse duration (ns)	Sacrificial coating	Overlay used	Thickness (cm)	Comments
Cu 15 μm (Chen, 2007)	6	10	Black paint	Water		The microscale laser dynamic forming (μLDF) showed that, materials are strengthened due to refined grains and large dislocation density which were dominant in the microstructure.
Alloy 22 [175]	10	25	Al	Water		Slitting method was used to establish a relationship between LSP parameters and RS on flat coupons. While contour method measured the spatial RS on critical geometrical features.
Al2024-T351, Al2024-T851, AA7075-T631, AA7075-T73 (Clauer et al., 1977)		20-30	Black paint	Quartz or water	0.1-0.3	Laser shocking of these alloys increased hardness of the under-aged 2024-T351 but no effect on AA7075-T851 and AA7075-T651 or the over-aged AA7075-T73. The AA7075-T3 produced the largest increases in tensile strength. Laser shocking resulted in significantly decreased Fatigue crack propagation rates.
Brass H62 [176]	1000, 2000, 3000 Pulses/cm^2	10		Water		Higher pulse LSP resulted in higher the microhardness, wear resistance and roughness. No observable features in the microstructure after LSP.
AA2024 AA60061-T6	2.5 and 5 respectively	8	N/A	Water	0.5	LSP surface RS level is much higher than that achieved by conventional

Sample	Power density (GW/cm^2)	Pulse duration (ns)	Sacrificial coating	Overlay used	Thickness (cm)	Comments
						Shot Peening and deeper penetration.
Al2024-T3 [98]	5	18	Black paint	Water	0.25	LSP-treatment technique improved the fatigue performance of the Al alloys having various notch configurations.
Inconel 600 [177]	$10J/cm^2$	12	-	Water Jacket		LSP resulted in tilted column microstructure due to overlapping of laser spots during scanning. Spherical nanoparticles with 60nm diameter were observed as a result of laser ablation.
4140 Steel [178]	3	5	Al	BK7 Glass		WLSP and DSA showed improved fatigue life due to enhanced cyclic stability of compressive RS, the stability and reliability were attributed to the enhanced dislocation pinning effect associated with the WLSP and DSA process.
2204 Duplex SS (Rubio-Gonzalez et al., 2011)	900, 1600 2500 pul/cm^2	8	No	Water		Higher residual stresses were observed with higher pulse density. Untreated specimens showed less crack growth rate resistance compared to LSP-treated specimens.
Fe-3%Si (Clauer, Fairand, Wilcox, 1977)	0.1-1	25-200	Pb	Quartz		Laser shocking showed that quartz plus lead overlay gave the most deformation for given power density. The deformation occurred by slip and twinning mechanism.

Sample	Power density (GW/cm^2)	Pulse duration (ns)	Sacrificial coating	Overlay used	Thickness (cm)	Comments
						Most of the samples showed surface melting for 200 ns pulses.
Mg-Ca [179]	78	5 to 7	Black paint	Water		Sequential peening showed an increase in the tensile pile up region up to 50% which was considered applicable for orthopaedic applications.
AZ31BMg	5	23	AA7075	Water		Sub-grain sizes of 5.8μm were obtained after four laser impacts. The RS near the surface increased with number of impacts. LSP showed retardation to SCC crack initiation and propagation.
Al2024-T3 [99]	6.36-12.73	10	Black paint	Water	0.2	LSP is an effective surface treatment technique to improve microhardness and wear resistance of Al2024-T3. They found that microhardness increased with the increase in laser energy and thus LSP treatment.

Note. Adapted from "Laser Peening Process and Its Impact on Materials Properties in Comparison with Shot Peening and Ultrasonic Impact Peening" by A. Gujba, and M Medraj, 2014, *Materials Science Journal, 7* (12), 7925.

APPENDIX B

Different residual stress testing methods [67] in Table 9.

Table 0.1 Compressive residual stress Testing methods

Technique	Restriction to Materials	Penetration	Spatial Resolution	Accuracy	Comments
Synchroton Diffraction (Hard X-rays)	Crystalline	>500μm, 100μm for aluminium	20 μm	$\pm 10x10^{-6}$ *	Triaxial stress, access difficulties. Laboratory based and specialised facility [74].
X-Ray Diffraction	Crystalline	5 μm(Ti), 50 μm (Al)	20 μm depth, 1mm Lateral	±20**	Combined often with layer removal for greater depth. Limited to measurement of small components [74].
Neutron Diffraction	Crystalline	4 mm. (Ti), 25 mm (Fe), 200 mm (Al)	500 μm	$\pm 50x10^{-6}$ *	Non-uniquely determined Stress field [67]. Laboratory based and specialised facility [74].
Hole Drilling	None	Approx., 1,2xhole Diameter	0,05 of thickness	±50**	Flat surface needed (for strain gauges) semi destructive. Simple and quick to use but has limited resolution and sensitivity [74].
Curvature/ Layer Removal	None	0.1-0.5 of thickness	0,05 of thickness		Stress field not uniquely determined
Slitting (crack compliance)	None	N/A	<50 μm		Semi destructive, flat surfaces required
Surface contour	None	N/A	1 mm Depth		Cheap and simple, suits well for welds, destructive
Ultrasonic	Metals. Ceramics	>10 cm	5 mm	10%	0,5-10 Mhz
Magnetic	Magnetic	10 mm	1 mm	10%	Microstructure sensitive
Raman/ Fluorescence/ Birefringence	Ceramics, Polymers	<1 μm	<1μm approximately	50**	Inapplicable directly to metallic materials (Feasible when proper coating is used)

Note. * Strain; ** MPa. Adapted from "Handbook of Liquids-Assisted Laser Processing," by A Kruusing, 2010, Volume. A, Elsevier.

APPENDIX C

INSPECTION CERTIFICATE OF THE 7075 ALUMINIUM ALLOY

INSPECTION CERTIFICATE № 14.11094

EN 10204 - 3.1

Certified by Russian Register

Consigner: KAMENSK URALSKY METALLURGICAL WORKS JOINT STOCK COMPANY
5, Zavodskaya Str., Kamensk Uralsky, Sverdlovsk Region, 623405, Russia Tel: (3439) 39 52 22 Fax: (3439) 39 50 68

Consignee: NK Cutting cc	Quantity, pcs.*: 19 Net Weight, kg.: 240
Contract No.: V3419-S P.O. No.: PO119620 Article No: -	S.O. No.: V3419 Lot No.: 3 Package No.: 342569
Description of Goods: Rectangular bars	Requirements on the Products:
Grade of Product: 30X50 / Dimensions, inch/mm: 3000	Material conforms to quality of alloy: 7075 T6511 Product conforms to all requirements of: EN573-3,EN755-1,2,5

Mechanical Properties

The Condition of Tested Standards	Lot No.	Cast No.	Quantity smple	Tensile Strength MPa min	Tensile Strength MPa max	Yield Strength (0,2% offset) MPa min	Yield Strength (0,2% offset) MPa max	Elongation, % min	Elongation, % max	Hardness, HB
Required				560.0	-	500.0	-	7.0	-	-
-	32803	2-2895	1	588.0	588.0	532.0	532.0	10.0	10.0	-

Chemical Composition, %

Element	Silicon Si	Iron Fe	Copper Cu	Manganese Mn	Magnesium Mg	Chromium Cr	Nickel Ni	Zinc Zn	Titanium Ti	Zirconium Zr
Required	0.4	0.5	1.2-2.0	0.3	2.1-2.9	0.18-0.28	-	5.1-6.1	0.2	-
Contents	0.08	0.27	1.5	0.06	2.4	0.22	-	5.7	0.05	-

Element	Ti+Zr	Na	Tin Sn	Bismuth Bi	Plumbum Pb	Mn+Cr	Ca	Other Elements Each	Other Elements Total	Al
Required	-	-	-	-	-	-	-	0.05	0.15	remainder
Contents	-	-	-	-	-	-	-	0.05	0.15	remainder

Other Tests

Method	Macro-structure	Micro-structure	UT	Electro-conductivity	SCF	Contents H2 of metals cm3/100gr
Result	-	-	-	-	-	-

On behalf: OAO KUMZ

Date: 18.04.14

Inspector: K.V.Zyryanova

Inspection Department Engineer: N.V. Alekhina

Form № QAD/3-001,Revision 01

APPENDIX D

Intensity of shot peening, type of test piece and arc HT [10]

Intensity of shot peening (Almen degree)	Type of test piece	Arc. HT in mm
4 N		0.10
6 N		0.15
8 N	N	0.20
16N		0.40
18N		0.45
6A		0.15
8 A		0.20
10 A	A	0.25
20 A		0.50
24 A		0.60
7 C		0.18
9 C		0.23
11 C	C	0.28
21 C		0.53
23 C		0.58

0.1 mm A = 4A
0.1 mm C = 4C
0.1 mm N = 4N

APPENDIX E

HOLE DRILLING MACHINE SPECIFICATIONS

Technical specifications of the MTS3000 system: alignment-drilling tool

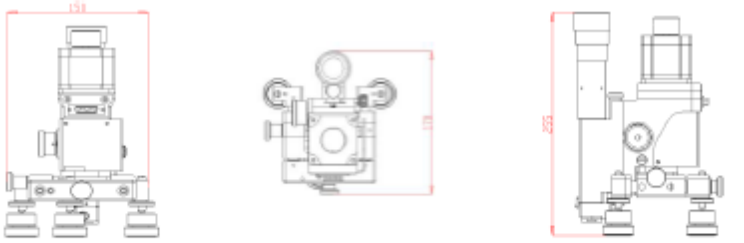

Dimensions (height, width and length) without dial gages	mm	270 x160x175
Weight	kg	4.6
Maximum turbine speed	RPM	400,000
Acoustic emission (at 1 meter)	dBA	76
Max turbine feed pressure	bar	5
Drilling resolution	µm	5
Drilling speed range	mm/min	0.03 to 1
Vertical lift (fast/manual)	mm	60
Vertical lift (slow with motor)	mm	6
Horizontal movement (x;y)	mm	7 -10
Height adjustment of feet	mm	60

Technical specifications of the MTS3000 system: electronic control system

Dimensions (height, width and length)	mm	140 x 245 x 220
Weight	kg	5.4
Grid power supply	Vac	90 - 264 (50 - 60Hz)
Compressed air max. input pressure	bar	6

APPENDIX F

Hardness Test Results Shot Peening at 12 psi (14.3A intensity)

Sample - 12 psi	TEST 1			TEST 2 Sample - 12 psi				TEST 3 Sample 12 psi			
Sample	Distance from the surface	D1	D2	Sample	Distance from the surface	D1	D2	Sample	Distance from the surface	D1	D2
176,84	50	0,0326	0,0321	166,88	50	0,0337	0,033	165,7	50	0,0335	0,00334
173,31	100	0,0304	0,0332	164,38	100	0,0307	0,0355	163,59	100	0,0335	0,0338
174,19	150	0,0357	0,0286	157,07	150	0,0311	0,0378	159,61	150	0,0323	0,0359
171,41	200	0,0363	0,0351	156,18	200	0,0321	0,0368	158,48	200	0,0321	0,0363
173,98	250	0,0321	0,0332	153,22	250	0,0319	0,0377	158,39	250	0,0325	0,0359
169,63	300	0,0321	0,0321	154,19	300	0,0332	0,0362	155,17	300	0,0327	0,0366
168,79	350	0,0311	0,0316	153,4	350	0,0338	0,0358	155,72	350	0,0348	0,0342
169,62	400	0,0326	0,0337	155,48	400	0,0337	0,0354	154,36	400	0,0349	0,0344
169,63	450	0,0321	0,0321	155,66	450	0,0343	0,0347	153,73	450	0,0354	0,034
168,32	500	0,0332	0,0332	155,41	500	0,0346	0,0345	156,77	500	0,035	0,038
164,18	550	0,0321	0,0332	155,41	550	0,0357	0,0334	150,5	550	0,0361	0,0327

Hardness Results of the LSP Sample

Sample 8 LSP	Distance from the surface	D1	D2	Sample 8 LSP	Distance from the surface	D1	D2	Sample 8 LSP	Distance from the surface	D1	D2
186,65	50	0,0299	0,0309	170,37	50			175,32	50	0,0326	0,0324
181,66	100	0,0333	0,0306	181,09	100			176,45	100	0,0321	0,0327
177,84	150	0,033	0,0316	176,43	150	0,321	0,0327	172,51	150	0,0307	0,0349

172,99	200	0,0324	0,0313	167,09	200	0,0335	0,0332	172,41	200	0,0329	0,0326
173,29	250	0,0335	0,0319	172,18	250	0,0323	0,0333	170,31	250	0,0328	0,0332
170,31	300	0,0325	0,0335	176,83	300	0,0322	0,0325	170,27	300	0,0318	0,0342
174,41	350	0,0327	0,0325	173,92	350	0,0332	0,0321	172,2	350	0,0325	0,0332
172,76	400	0,0334	0,0322	170,77	400	0,033	0,0329	170,69	400	0,0323	0,0336
165,45	450	0,0335	0,0335	171,99	450	0,0321	0,0331	168,86	450	0,0324	0,0339
166,01	500	0,0335	0,0335	169,53	500	0,0335	0,0327	169,96	500	0,0325	0,0336
162,48	550	0,0336	0,0339	168,99	550	0,0324	0,0338	164,41	550	0,0335	0,0337
				169,21	600	0,0333	0,0329	165,75	600	0,0325	0,0344